Experimental Determination and Prediction of Drag Coefficient of Newtonian Fluids Flowing Over Solid and Hollow Objects

Saroj Kumar Samantaray

Department of Chemical Engineering

National Institute of Technology Rourkela

Experimental Determination and Prediction of Drag Coefficient of Newtonian Fluids Flowing Over Solid and Hollow Objects

Dissertation Submitted in partial fulfilment of the

Requirements of the Degree of

Master of Technology (Research)

in

Chemical Engineering

by

Saroj Kumar Samantaray

(Roll No.: 614CH3006)

based on research carried out

Under the supervision of

Prof. Basudeb Munshi

August 2017

Department of Chemical Engineering

National Institute of Technology Rourkela

Department of Chemical Engineering

National Institute of Technology Rourkela

August 21, 2017

Roll Number: *614CH3006*
Name: *Saroj Kumar Samantaray*
Title of Dissertation: *Experimental Determination and Prediction of Drag Coefficient of Newtonian Fluids Flowing Over Solid and Hollow Objects*

We the below signed, after checking the dissertation mentioned above and the official record book (s) of the student, hereby state our approval of the dissertation submitted in partial fulfillment of the requirements of the degree of *Master of Technology (Research)* in *Chemical Engineering* at *National Institute of Technology Rourkela*. We are satisfied with the volume, quality, correctness, and originality of the work.

_____
Basudeb Munshi
Supervisor

_____
Pradip Chowdhury
Member, MSC

_____
Braja Gopal Mishra
Member, MSC

_____
Debayan Sarkar
Member, MSC

_____
Mrs. Abanti Sahoo
Chairperson, MSC

_____
Indra Vir Singh
External Examiner

_____
Raghubansh Kumar Singh
Head of the Department

Department of Chemical Engineering

National Institute of Technology Rourkela

Prof. Basudeb Munshi

Associate Professor

August 21, 2017

Supervisors' Certificate

This is to certify that the work presented in the dissertation entitled *Experimental Determination and Prediction of Drag Coefficient of Newtonian Fluids Flowing Over Solid and Hollow Objects* submitted by *Saroj Kumar Samantaray*, Roll Number 614ch3006, is a record of original research carried out by him under our supervision and guidance in partial fulfillment of the requirements of the degree of *Master of Technology (Research)* in *Chemical Engineering*. Neither this dissertation nor any part of it has been submitted earlier for any degree or diploma to any institute or university in India or abroad.

Basudeb Munshi

Declaration of Originality

I, *Saroj Kumar Samantaray*, Roll Number *614CH3006* hereby declare that this dissertation entitled *Experimental Determination and Prediction of Drag Coefficient of Newtonian Fluids Flowing Over Solid and Hollow Objects* presents my original work carried out as a doctoral student of NIT Rourkela and, to the best of my knowledge, contains no material previously published or written by another person, nor any material presented by me for the award of any degree or diploma of NIT Rourkela or any other institution. Any contribution made to this research by others, with whom I have worked at NIT Rourkela or elsewhere, is explicitly acknowledged in the dissertation. Works of other authors cited in this dissertation have been duly acknowledged under the sections "Reference" or "Bibliography". I have also submitted my original research records to the scrutiny committee for evaluation of my dissertation.

I am fully aware that in case of any non-compliance detected in future, the Senate of NIT Rourkela may withdraw the degree awarded to me on the basis of the present dissertation.

August 21, 2017

NIT Rourkela

Saroj Kumar Samantaray

Acknowledgment

I would like to express my profound and heartfelt gratitude to my supervisor Dr. Basudeb Munshi for his invaluable supervision and endless encouragement throughout this work. His able knowledge and expert guidance with unswerving patience fathered my work at every stage. Without his warm affection and support, the fulfillment of the task would have been very difficult.

I express my sincere thanks to Prof. Animesh Biswas, Director, NIT Rourkela for creating healthy environment in the campus and giving freedom to use the facilities available in the institute for this study.

I express my sincere thanks to Prof. R.K.Singh, Head, Chemical Engineering Department and members of Master Scrutiny Committee (MSC) Prof. (Mrs.) A. Sahoo, Prof. P. Chowdhury, Prof. B. G. Mishra, Prof. D. Sarkar, and all the faculty members of Chemical Engineering Department for their suggestions and constructive criticism during the preparation of the thesis.

I would like to extend my sincere thanks to Prof. Soumya Sanjeeb Mohapatra for his valuable remarks and constructive criticism throughout this work.

I am very much thankful to Dr. Akhilesh P. Khapre, Devendra M. Ghodki, Satya Sundar Mohanty, Sangram Patil, Arvind Kumar, Miss. Lily, Swarna, Sherya, Vikash, Akash, Mihir, Adarsha Sir, Mantra Sir, Manoj Sir, Sambit Sir, Soumya Sir, Ashutosh Sir, Swati Madam and Asit Sir and all other my dear friends for their cordial support, valuable information and guidance, which helped me in completing this task through various stages.

Last but not the least, I would like to express my gratitude to Badanana Dr. Kamdev Samantaray and his family for unconditional support, caring and believing me since the death of my parents.

I am grateful to the Lord Jagannath for guiding me through these years and achieving whatever I have achieved until date.

Jai Jagannath.

Saroj Kumar Samantaray

Abstract

Drag offered by fluid medium on submerged object is subject of intense research as needed in multiple process and solid handling applications. In spite of this, the literature remains silent on some critical problems. Catering the issues and limitations in literature is the main motivation of this work. Movement of sphere along inclined plane is involved in numerous applications. Nevertheless, a few published articles are available to deal with this for a limited scope of diameter ratio and angle of inclinations, θ. In the prospective of extending this work for broader range of diameter ratio and tube inclinations, this study encompasses diameter ratio 0.09 to 0.37 and channel inclination 10°-90°. The terminal velocity shows an increasing trend (reverse of the available experimental data) with d/D ratio. It also increases with θ due to increase in downward force. The drag coefficient, C_D, is reported as a function of Re, d/D and θ. C_D also shows the reverse trend with d/D ratio. The dependency of $C_D Re$ on fluid viscosity and θ are expressed in terms of the developed correlations. The variation of C_D with the inverse of Re is studied graphically to find out the flow regimes of the experimental data which are at laminar or early state of transition flow. The experimental C_D values are validated with numerically calculated data using Ansys Fluent v15.0 for both vertical and inclined channels. The close agreement with experimental results confirms the applicability of the used numerical approximation.

Like, solid object, hollow objects are also involved in numerous industrial processes but, no single research article is available in literature to explain the fluid dynamic interaction for hollow particle. Hence, here the fluid dynamic behavior of flow over hollow frustum and cylinder are studied in terms of terminal velocity and drag coefficient in both vertical and inclined channel. Like sphere, the predictive equations are also developed for each tube

inclination for the hollow objects. The numerical prediction using Ansys Fluent is employed to predict the drag coefficient for above mentioned hollow objects and an excellent agreement is observed while comparing with experimental drag coefficients.

In spite of having the experimental results for conical shaped particle, the numerical study still untouched in open sources. In view of this, the effect of blockage ratio i.e. diameter ratio of cone, d, and flow channel, D on the drag coefficients of Newtonian fluid flow over cone is studied numerically by solving the *CFD* equations in Ansys FLUENT. The drag coefficients (C_D) as a function of Reynolds number (Re) and d/D are reported for the range of Re: 0.01-30000 and d/D: 0.0015-0.9. The C_D values are obtained higher for confined flow (high d/D) than unconfined flow. The variations of angle of separation and its effect on the drag coefficients are examined and justified. The comparative studies among the drag coefficients of sphere, cylinder and cone, are carried out in terms of wall effect, re-circulation length and slope of axial velocity profile. The observations revealed the following order of C_D : cylinder>cone>sphere. The hydrodynamic interactions between wall and fluid medium are presented with the help of velocity contour plots. The simulated results presented herein for unconfined flow are in good agreement with the literature data. Furthermore, the variation of drag coefficient due to change of shape the particle from cone to cylinder are also studied to enrich the literature and for industrial applications.

Keywords: Drag Coefficient, Terminal Velocity, Reynolds Number, Wall effect, Frustum, Sphere, Cone, Inclined Channel

Contents

4. NEWTONIAN FLOW OVER HOLLOW FRUSTUM IN VERTICAL AND INCLINED PLANE: AN EXPERIMENTAL OBSERVATION FOR TERMINAL VELOCITY AND DRAG COEFICIENT

List of Figures

List of Tables

Nomenclature

A	Projected area (m^2)
C_D	Drag coefficient
$C_{D\infty}$	Unbounded flow drag coefficient
CS	Corn syrup
D	Diameter of flow channel(mm)
d	Diameter of particle(mm)
do	Outer diameter of hollow frustum (mm)
di	Inner diameter of hollow frustum (mm)
F_B	Buoyancy force (N) (Chapter 1)
F_B	Body force (N) (except Chapter 1)
F_D	Drag force(N)
F_g	Gravitational Force (N)
F_R	Solid –Solid resistance (N)
G	Percentage of Glycerin in aqueous solution
g	Acceleration due to gravity(m/s^2)
P	Pressure
R	Bottom radius of particle(mm)
r	Top radius of particle (mm)

Re	Reynolds number based on V
Re_∞	Reynolds number based on V_∞
u	Velocity of fluid,(m/s)
V	Terminal velocity (m/s)
V_∞	Unbounded terminal velocity(m/s)

Greek Symbols

θ	Angle of separation(Degree) (Chapter 6)
θ	Angle of inclination (Degree) (except Chapter 6)
ρ_S	Density of solid (kg/m^3)
ρ_F	Density of fluid (kg/m^3)
μ	Kinetic viscosity(Pa. s)

CHAPTER 1

INTRODUCTION TO FLOW OVER AN OBJECT AND DRAG COEFFICIENT

Introduction

Force exerted by the fluid on the solid surface in the direction of flow is called the drag force. The condition for the existence of the drag force is the relative velocity between the submerged body and fluid. It is usually expressed in term of drag coefficient, C_D a dimensionless number. It is an important parameter used for designing the fixed and fluidized bed reactors, processing of large food particles, and pneumatic and hydraulic conveying of particles [1]. It is also an essential parameter for determining the settling behavior of solid particles in liquids frequently countered in chemical blending, mineral processing, powder sintering and other solid handling process. Because of this, it is important to estimate the drag coefficient of a particle. A particle falling or rolling in the liquid medium under the influence of gravity will accelerate until the resistance forces comprised of buoyancy force and drag force do not balance the gravitational force. At the balanced condition of the forces, particles move with constant velocity called the settling velocity or terminal velocity. Volumes of correlations were developed for the estimation of drag coefficient as a function of any flow parameter, especially Reynolds number [4].Owing to the wide range of application, it is a subject of intense research since many decades.

1.1. Terminal Velocity and Drag Coefficient

As mentioned above, movement of particle through a liquid medium observes three forces, I: Gravitational force (F_g), which acts downward, II: Buoyant force (F_B), which acts parallel with the gravitational force but in opposite direction, and III: The Drag force (F_D), which acts in upward direction and it is always towards pressure applied by the fluid on the particle [1]. When a particle is allowed to move in fluid, the object accelerates from zero to a maximum velocity. The drag force and buoyancy forces will maintain equilibrium with weight, and the particle will settle with a consistent or terminal velocity. The free body diagram is shown in Fig.1.1.
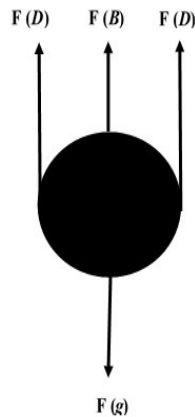
Fig.1.1 Free body diagrams of an object falling in quiescent fluid medium [1]

The net drag force on a solid body depends on two resistive forces called viscous or friction drag and pressure or form drag. For a moving object in a fluid medium, pressure drag, C_P and the viscous drag, C_F appears due to the total applied pressure on the object and the shear force (produced by the viscous force) distribution on the body along the flow direction, shown in Fig.1.2. The schematic diagram of flow over a streamline body and component of drag force is presented in Fig.1.2.
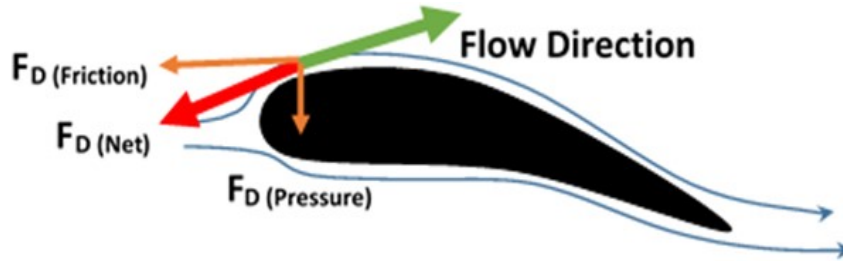
Fig.1.2. Flow over a streamline body [3]

At equilibrium (i.e. when the particle moves with a terminal velocity), the force balance equation can be written as,

$$F_g = F_B + F_D \tag{1.1}$$

$$m_p g = \left(\frac{m_p}{\rho_p}\right)\rho_F g + \frac{1}{2}\, C_D \rho_F V^2 A \tag{1.2}$$

$$C_D = \frac{mg(1 - \frac{\rho_F}{\rho_p})}{0.5 A V^2 \rho_F} \tag{1.3}$$

Where, ρ_p is the density of particle, m_p is the mass of solid particle and the the g is the acceleration due to gravity. Eq. (1.3) is widely used to evaluate the drag coefficient irrespective of the shape of the solid body.

1.2. Variation of Drag Coefficient with Reynolds Number, (*Re*)

Drag coefficient is not identical always; it varies with flow speed, object size, fluid density and fluid viscosity, terminal velocity and a characteristic length scale of the object [4].Hence, these flow parameters are incorporated into a dimensionless quantity called the Reynolds number, *Re*. The drag coefficient is a function of Reynolds number, which gives

importance insights about the nature of fluid flow i.e. laminar, transition and turbulent flow. It is a relative measurement of inertial to the viscous force of stream flow. The mathematical expression is

$$Re = \frac{\rho_F V d}{\mu} \tag{1.4}$$

Based on Reynolds number, fluid flow is categorized into three regions namely, I. Laminar Zone ($Re \leq 2300$); II: Transition Zone ($2300 \leq Re \leq 4000$); III: Turbulent Zone ($Re \geq 4000$). The drag coefficient is high at low Reynolds number i.e. in the laminar zone and found to decrease with Reynolds number owing to the prominent effect of the viscous force over inertial force. However, when this region is finished, transition zone starts; here the impact of Reynolds number on drag coefficient is diminished. In the turbulent zone, high terminal velocity leads to very low drag coefficient, and it becomes independent of *Re* at the higher range of Reynolds number. Thus, the drag coefficient and Reynolds number are reciprocal to each other, especially in laminar zone. The variation of C_D-*Re* is shown in Fig.1.3 for smooth sphere and smooth
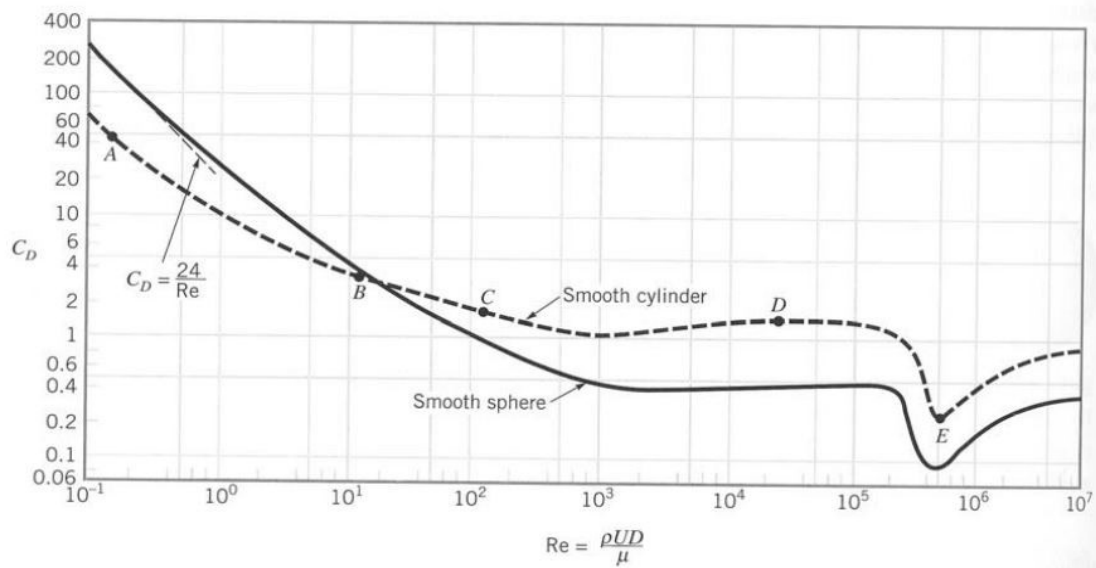
Fig.1.3. Drag Coefficient as a function of Reynolds number of sphere and cylinder [2]

Fig.1.3 shows that, at low Reynolds, number C_D varies linearly with *Re*. A sudden change is observed at point E. This is due to the reduction in the size of the wake and the pressure on the object. Drag coefficient affected largely by the geometry. Hence the C_D-*Re* curve is not identical to all system of consideration.

1.3. Drag Coefficient Experienced by Regular Shaped Body

(a) In Vertical Channel

The pioneering works of Clift et al. [1], Chhabra [4]; Khan and Richardson [5]; Uhlherr and Chhabra [6] included the drag coefficient of the spherical body. Similar kinds of studies for solid cylindrical objects were carried out by Unnikrishnan and Chhabra [7 & 8], where they developed the predictive correlations for the drag coefficient and discussed the effect of walls on the drag coefficient. Along with the experimental work, a majority of the theoretical analysis for sphere and cylinder is available in the Krishnan and Kaman [9] and Chakraborty et al. [10]. The effect of the wall on the drag coefficient was discussed theoretically in Nitin and Chhabra [11] and Munshi et al. [12]. Apart from this, Chhabra [13], Sharma, and Chhabra [14] reported some qualitative insights for cone and non-spherical particle respectively.

(b) In inclined Channel

In numerous processes, the particles may be sliding or rolling over the inclined planes. For example, the flow of fluid in inclined packed and fluidized beds, dredging underwater silt and gravel, and storage in large containers, etc. As compared to vertical channel, quite a few works were reported on the flow over solid objects especially for non-spherical particles in an inclined channel. Carty [15] first reported it for a spherical particle in the smooth inclined plane.

5

Subsequently, Garde and Sethuraman [16] also repeated the same experiment of Carty [15] in both smooth and rough inclined planes. Jan and Chen [17] and Chhabra et al. [18] also communicated the similar kind of observations for Newtonian fluid flow in both the smooth and rough inclined planes. Chhabra and Ferreira [19] and Jalal and Ganji [20] developed a set of equations for the terminal velocity and drag coefficient for the inclined channel using numerical analysis. In all the above-discussed literature, C_D-Re empirical equations were developed.

1.3. Origin and Objective of the Work

As discussed in proceeding paragraphs, a number of qualitative efforts have been made to accord the fluid dynamic interaction for all regular shaped particle like a sphere, cylinder, and disk. Comparatively, sphere and solid cylinder draw maximum attention. Falling or rolling of the solid object along inclined plane encounters in many industrial processes. However, quite a few research was carried out to study the solid-fluid interaction in an inclined plane in terms of settling velocity and drag coefficient with a restricted scope of particle diameter to channel diameter ratio and angle of inclination i.e. $\leq 30^0$. In the literature, angle independent C_D-Re correlations were proposed for incline flow channel which creates the ambiguity for real life application. Several kinds of hollow particles are used in chemical process industries, especially as a packing material. In spite of having abundant published literature on the hydrodynamics of fluid flow over solid particles, no attempts were made earlier in regards to the estimation and reporting of the terminal velocity and drag coefficient of any hollow object. Numerical analysis of flow over regular shaped particles are now available considering many aspects, but, no numerical study was communicated in regards to flow over conical particle and the surrounding effects on drag coefficient. The variation of drag coefficient as flow geometry changes from cone-to-cylinder is still unattempted.

Based on the above gap in existing literature following objectives are opted in the present study

- Experimental findings of the terminal velocity and drag coefficient for Newtonian fluid flow over a sphere in an inclined channel having a wide range of diameter ratio and angle of inclination. Development of the angle dependent predictive equations of the drag coefficient. Theoretical validation of the drag coefficient with experimental results.

- Experimental findings of the terminal velocity and drag coefficient for Newtonian fluid flow past a hollow frustum and hollow cylinder in both vertical and inclined channels with a broad range of diameter ratio and angle of inclination. Empirical model development for drag coefficient for each angle of inclination as a function of diameter ratio and Reynolds number. Theoretical validation of the drag coefficient with experimental results.

- Prediction and analysis of the drag coefficient of the cone using flow models available in Ansys Fluent v15.0.

- To find and analyze the effect of change of the shape of the solid particle from cone to the cylinder on the drag coefficient.

1.4. Organization of Thesis

The thesis is divided into seven chapters. Introduction chapter is the very fast chapter, which pronounces the brief introduction to flow over a solid object, drag coefficient, Reynolds number, flow separation, etc. It also includes the motivation and objective of the present work. An extensive literature survey on many aspects of flow over several kinds of solid objects including both experimental and theoretical work is discussed in **Chapter 2**. **Chapter 3**

7

describes the Newtonian flow past a sphere in an inclined plane for a wide scope of diameter ratio and angle of inclination, and it reveals the effect of the wall and confined boundary on terminal velocity and drag coefficient. The effect of diameter ratio and tube inclination on terminal velocity and a drag coefficient of Newtonian fluid flow over hollow frustum and circular cylinder in both vertical and inclined plane is discussed in **Chapter 4** and **Chapter 5** respectively. **Chapter 6** embodies the flow over the conical object and the effect of the finite and infinite boundary on drag coefficient through numerical investigation. A set of comparison among cone, sphere, and cylinder in terms of re-circulation length, the angle of separation, wall effect, etc. are also discussed. The variation of drag coefficients for the transition of solid geometry from cone-to-cylinder is studied numerically and discussed here. **Chapter 7** includes the overall conclusions of the present research output and scope of future work.

CHAPTER 2

LITERATURE REVIEW

Introduction

The resistance on a body in a fluid medium; is a quantity of central interest for numerous designing applications. Over the years, a substantial amount of studies were proposed to quantify the resistance or drag observed by the body or conversely, the net force required to travel in fluid medium through experimental and theoretical investigations. A class of solution with a qualitative description of flow nature under several flow condition is now accessible for a regular shaped object like a sphere, cylinder, and circular disk, etc. Before presenting the findings and the observations of present work, it is necessary and informative to discuss the earlier studies and the conclusion drawn by past researchers.

Compared to other, the sphere has received maximum attention. Most of the studies have attempted to devise a model for prediction of drag coefficient as a function of Reynolds number for several flow regime. In accordance to this, abundance empirical equations were proposed based on experimental results are listed in Table 2.1. However, a comprehensive discussion on this is available in the book or article of Clift et al. [1], Chhabra [4], Khan and Richardson [5] for a spherical particle in the Newtonian and non-Newtonian fluid. In the line of this, for cylinder and circular disk, a good number of experimental and numerical studies were conducted. The relevant literature to this study are appended below.

Table 2.1

C_D-*Re* relationship

Cheng [21]	$C_D = \frac{24}{Re}(1 + 0.27Re)^{0.43} + 0.47(1 - exp(-0.04Re^{0.38}))$	$Re < 10^6$
Brown and Lawler [22]	$C_D = \frac{24}{Re}(1 + 0.15Re)^{0.681} + \frac{0.407}{1 + 8710Re^{-1}}$	$Re < 2*10^5$
Clift et al.[1]	$C_D = \frac{24}{Re} + \frac{3}{16}$	$Re < 0.01$
	$C_D = \frac{24}{Re} + (1 + 0.1315Re^{0.82-0.05logRe})$	$0.01 < Re \leq 20$
	$C_D = \frac{24}{Re} + (1 + 0.1935Re^{0.6305})$	$20 < Re \leq 260$
	$C_D = 10^{1.6435-1.1242logRe+0.1558log^2Re}$	$260 < Re \leq 1500$
	$C_D = 10^{-2.4571+2.5558logRe-0.9295log^2Re+0.1049log^3Re}$	$1500 < Re \leq 1.2*10^4$
	$C_D = 10^{-1.9181+0.637logRe-0.063log^2Re}$	$1.2*10^4 < Re \leq 1.4*10^4$
	$C_D = 10^{-4.339+1.5809logRe-0.154log^2Re}$	$4.4*10^4 < Re \leq 3.38*10^5$
	$C_D = 29.78 - 5.3logRe$	$3.38*10^5 < Re \leq 4*10^5$
	$C_D = 0.1logRe - 0.49$	$4*10^5 < Re \leq 10^6$
	$C_D = \frac{0.19 - 8*10^4}{Re}$	$10^6 < Re$
Flemmer and Banks [23]	$C_D = \frac{24}{Re}10^\alpha, \alpha = 0.261Re^{0.369} - 0.105Re^{0.431} - \frac{0.124}{1+log^2Re}$	$Re < 3*10^5$
Turton and Levenspiel [24]	$C_D = \frac{24}{Re}(1 + 0.173Re^{0.657}) + \frac{0.413}{1 + 16300Re^{-1.09}}$	$Re < 2*10^5$

Engelund and Hansen [25]	$C_{D=}\dfrac{24}{Re}+1.5$	$Re < 2 * 10^5$
Khan and Richardson [5]	$C_D = (2.49Re^{-0.328} + 0.34Re^{0.067})^{3.18}$	$Re < 2 * 10^5$
Clift and Gauvin [26]	$C_D = \dfrac{24}{Re}(1 + 0.15Re^{0.687}) + \dfrac{0.42}{1 + 42500Re^{-1.16}}$	

2.1. Wall and Diameter Ratio Effect on Drag Coefficient

In confined flow, the particle flows along flow axis in a flow channel. The wall of the channel applies an additional retarding effect on the terminal velocity of the particle which is called wall effect and can be represented by the wall factor defined as [7&14]

$$f = \frac{V}{V_\infty}\qquad\qquad(2.1)$$

In which V and V_∞ are the terminal velocity of the particle in bounded and unbounded fluids respectively. In Newtonian fluid f, is a function of the ratio of the diameters of free falling particle and flow channel, and Reynolds number.

The presence of the tube wall makes the behaviour of the bounded flow different from the unbounded flow due to three factors (Singha and Sinhamahapatra [27]) which control the spread of the wake, moves the separation point in the downstream site, and changes vortex interaction due to interaction between vortices from the flow wall and solid particles.

The unconfined drag coefficient $C_{d\infty}$ was determined experimentally by many researchers [7& 14] just by finding the drag coefficient as $d/D \to 0$ which are obtained from C_d vs. d/D data of confined flow of the particle.

In the solid handling process, the mixture contains solid particles of different shapes. It is always beneficial for the efficient designer to know the drag coefficient of all possible shaped

particles especially from the simulated data with high accuracy. The simulated drag coefficient and wall effect data are available for spherical, cylindrical and other regular shaped particles. However, it is unavailable for the cone shaped particles.

Uhlherr and Chhabra [6] showed that the drag coefficient of the sphere while falling in cylindrical tubes is affected by both the falling sphere to flow tube diameter ratio and Reynolds number, shown in Fig.2.1. They concluded that at low ($Re \leq 0.5$) and large ($Re \geq 100$) Reynolds numbers the wall factor, f depends only on the diameter ratio. They used the following equation to find directly the unconfined drag coefficient from the logarithmic plot of C_D against Re using diameter ratio as the parameter.

$$C_D Re^2 = \text{Constant} \tag{2.2}$$
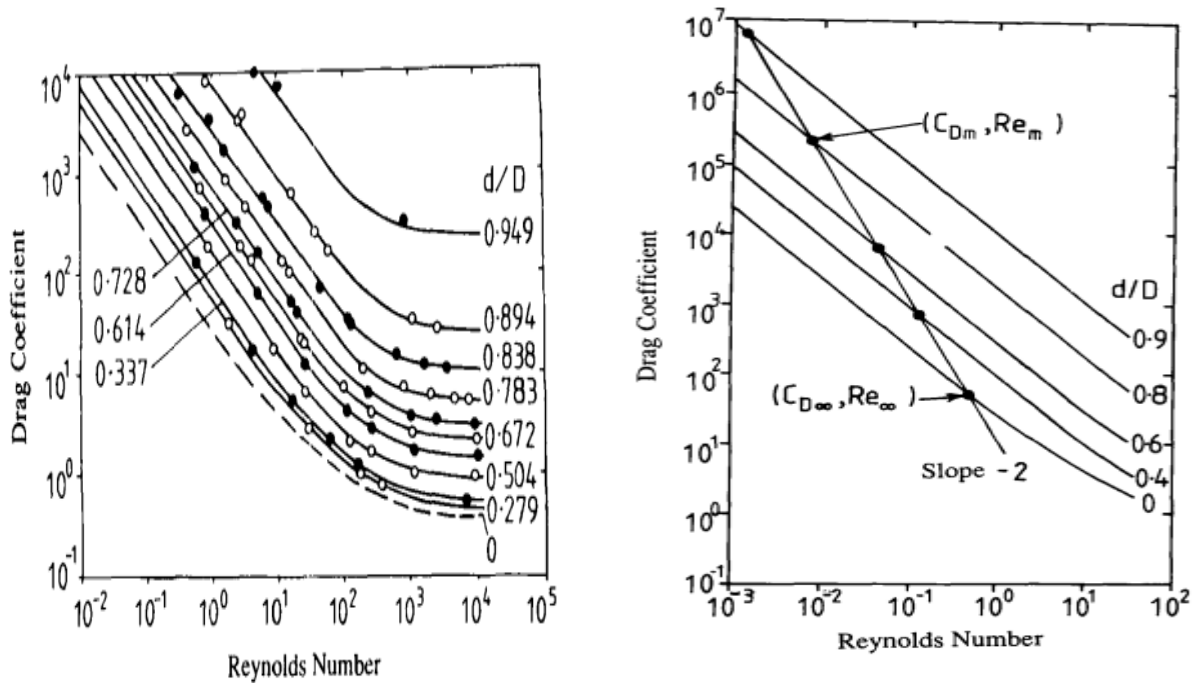
Fig.2.1. Variation of C_D with d/D [6]

Chhabra et al. [28] also examined the wall effect on the terminal velocity of the sphere which settles along the axis of a cylinder filled with Newtonian fluids. According to their observations, the wall factor, *f* changed only with the sphere to flow channel diameter ratio at very low and very high Reynolds number, but it is a function of both the ratio and Reynolds numbers for the intermediate values of these. Many researchers studied the effect of the blockage ratio and Reynolds number on the drag coefficient and wall factors of the particles settling in non-Newtonian fluids [29-33].

Both the hydrodynamics and heat transfer behavior of laminar flow of Newtonian fluid over a hot confined sphere were theoretically studied by Krishnan and Kaman [9]. They showed that the wall effect is predominant at lower particle Reynolds number, and the accuracy of the prediction of wall effect became better at higher blockage ratio and Reynolds number. Stalnaker and Hussey [34] studied the wall effect due to the transverse motion of long length and short diameter cylinder through a Newtonian fluid. The effect of the wall on the dimensionless drag coefficient was categorized into the strong boundary and weak boundary regions. The effect was seen less in the weak boundary zone than the strong region. Unnikrishnan and Chhabra [7] studied the wall effects on the drag coefficient of cylinders falling through different Newtonian fluids with a wide range of viscosity. The ratio of the cylinder to flowing tube radius was varied in the range of 0.08 to 0.4, cylinder length to cylinder diameter from 0.05 to 2 and Reynolds number 0.2 to 180. The unconfined terminal velocity was calculated by extrapolating the experimental terminal velocity versus diameter ratio profile to the ratio value of zero. The work showed the dependency of the terminal velocity and wall factor on the length of the cylinder and wall factor on Reynolds number of low magnitude. Analytical expression of the unconfined drag coefficients given below was developed by them.

$$C_{D\infty} = \frac{17.5}{Re_\infty}(1 + 0.68Re_\infty^{0.43}) \qquad \text{for } 0.0513 \leq L/d \leq 2 \tag{2.3}$$

in which $C_{D\infty}$ and Re_∞ are the drag coefficient and Reynolds number at unconfined terminal velocity, L and d are the length and diameter of the cylinder, and D is the diameter of flow channel.

According to them, for $Re < 30$, the wall factor of the cylinder can be calculated from the sphere wall factor provided the diameter of the sphere is replaced by equivalent volume diameter of the cylinder. Eq. 2.4 was developed by them to calculate the wall factor for $Re > 30$.

$$f = 1 - 0.69\frac{d}{D} \qquad \text{for } Re > 30 \tag{2.4}$$

Chakraborty et al. [10] carried out numerical analysis of the hydrodynamic behavior of Newtonian fluid flow over a circular cylinder confined in a rectangular channel. Reynolds number and the ratio of the cylinder diameter to flow channel width were varied in the range of 0.1 to 200 and 0.05 to 0.66 respectively. They too observed that the drag coefficient decreased with decreasing the diameter ratio and increasing the Reynolds number.

Experimental results on the wall effect and drag coefficient of cone shaped particles settling in both the Newtonian and non-Newtonian fluids was reported by Sharma and Chhabra [14]. The study was carried out for a wide range of system parameters where cone angle was varied in the range of 43° to 93.7°, flow behavior index, n ranges 1 to 0.62 with the consistency index, m $3.73X10^{-3} < m < 4$ Pa s^n , and the ratio of the cone to flow channel diameter varied in the range of 0.148 to 0.4343. The unconfined flow Reynolds number changes between very low to 500. The wall effect, f independent of the apex angle and power law index, was mostly affected by the diameter ratio (linearly varies) and Reynolds number. The study on the wall

factor was not only limited to spherical and cylindrical shaped particles. Chhabra [13] reported the wall factor for a range of non-spherical particles like cubes, parallelepipeds, cylinders, needles, thin plates and circular discs sedimented in stationary Newtonian liquids. The falling tube diameter was varied in the range of 20-100 mm. The wall factor showed to vary with the shape of the particle and size of the fall tube at low Reynolds number. They also developed the correlations for the wall factor with the particle to tube diameter ratio. They showed that all shapes except thin cylinders (L/d > 10) experiences smaller wall effects than a sphere of equal volume. Nitin and Chhabra, and Munshi et al. [11 & 12] solved numerically the effect of the flow channel wall on the total pressure and friction drags of a disk oriented normal to the direction of flow. The study comprised of Reynolds number: 1 to 100 and disk to flow channel diameter ratio: 0.02 to 0.5. The effect of the disk thickness on the wall effect decreased with the Reynolds number.

2.2. Evaluation of Drag Coefficient of Sphere in Inclined Plane

In all above said literature, the sphere does not interact with boundary wall, but there are numerous circumstances, where the sphere is descending along the inclined plane due to the action of gravity while immersed in the Newtonian fluid. The critical examples are long-term storage of household products in suspension form, dredging underwater silt and gravel, and storage in large containers, etc. [15 & 16]. Few more other uses of the rolling of particles on the inclined surface are given in Chhabra et al. [17]. As compared to a normal plane, a less number of open source literature are available in this field. The very first study made by Carty [15] showed the drag in the inclined plane is larger than normal plane due to additional retardation force from inclined plane.

The study included the drag coefficient values for the sphere to channel diameter ratios (*d/D*) in the range 0.003 - 0.055. Following the same trend, Garde and Sethuraman [16] also conducted the experiment but for the range *d/D* of 0.04 to 0.11. However, the experimental outcomes of Carty [15] did not match with the Garde and Sethuraman [16] due to differences in tube length and the diameter ratio.

Jan and Shen [35] studied on the fall of a sphere over a rough inclined (3^0-27^0) surface submerged in a Newtonian fluid. They considered a constant *d/D* ratio of 0.94. Jan and Chen [17] also established a set of C_D-Re relationship for sphere rolling down an inclined plane submerged in an incompressible Newtonian fluid. Experiments were carried out for the limited range of angle of inclination (θ) i.e. $2° \leq \theta \leq 10°$. They demonstrated the effect of the wall on the drag coefficient over the range of *d/D* of 0.22-0.96. The experimental set-up and equation used by [17] as follows
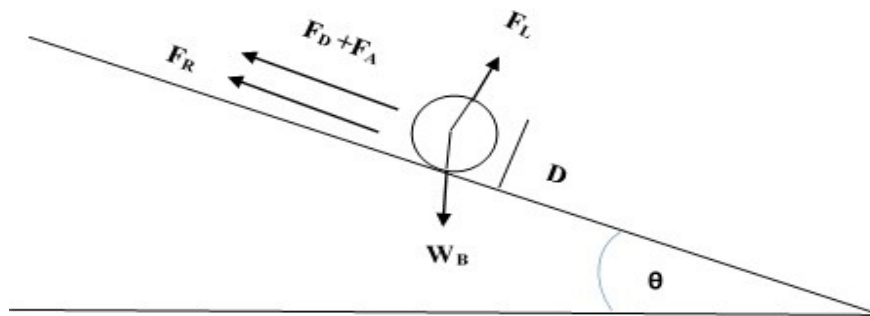
Fig.2.2. Schematic view of Jan and Chen [17] for inclined plane experiment

Their proposed Reynolds number dependent C_D-Re relations are given in Table 2.2.

Table 2.2

C_D - Re correlations [17]

C_D-Re Relationship	Reynolds Number Range
$C_D = \dfrac{322}{Re}$	Re<10
$C_D = 10^{[3.02 - 1.89 \log Re + 0.411 (\log Re)^2 - 0.033 \ \log Re^3]}$	10<Re<20000
$C_D = 0.74$	Re>2000

Chhabra and Ferreira [19] established a simpler correlation, Eq. (2.6) for the C_D-Re valid for

$0.1 \leq Re \leq 10^5$:

$$C_D = \alpha + \frac{\beta}{Re} \tag{2.6}$$

Where α and β are the constants. The mathematical structure of Eq. (2.6) is the same to

equations used for the free fall sphere drag coefficient [36]. With the estimated constants using

the experimental data of Jan and Chen [17], the Eq. (2.6) becomes

$$C_D = 0.861 + \frac{321.906}{Re} \tag{2.7}$$

Chhabra et al. [18] experimentally estimated the drag coefficient for sphere is moving

down a smooth inclined (3º – 30º) plane for a wide range of Reynolds number ($10^{-6} \leq Re \leq 3000$).

The *d/D* was varied in the range of 0.114-0.58. They also developed the empirical relations for

C_D-Re given in Table 4.2.

Table 2.3

C_D - *Re* correlations [18]

C_D-Re Relationship	Reynolds Number Range
$C_D = \dfrac{225}{Re}$	Re<1
$C_D = 1 + \dfrac{235}{Re}$	1<Re<250
$C_D = 1.23 + \dfrac{177.5}{Re}$	Re>250

Jalal and Ganji [20] developed an analytical solution using homotopy perturbation method for the estimation of settling velocity, acceleration and terminal position of the sphere while falling over an inclined surface. They compared successfully the computed homotopy results with the numerical outcomes using 4th order Runga-Kutta method.

2.3. Effect of Polymer on Drag Reduction

Reduction of drag by adding polymer and surfactant in a fluid medium is a subject of intense research for many decades as drag reduction is very vital for many industrial applications. Successfully the drag reduction or drag crisis was achieved for solid particle by adding a small amount of polymer in parts per million (ppm). Polymers are viscoelastic in nature. Hence, the elongation and recovery are time depended called memory effect which leads to a continuous decay of the stress when fluid motion allowed to stop. The extensive elongational viscosity of polymer chain arrangement stabilized the turbulent boundary layer and caused for minimum energy dissipation. This is called drag crisis, and the effect of polymer on drag crisis is mostly notable for the turbulent flow regime [37]. The drag reduction using polymeric additives is a phenomenon that was first reported by Toms [38].The author showed that the addition of small quantities of polymers of high molecular weight in a turbulent flow could reduce

significantly (80%) the friction factor. Later, Lumley [39] defined the drag reduction as the reduction of friction factor of the additives solution with respect to the solvent, measured in the same Reynolds number. Thenceforth, the phenomenon has been extensively studied, due to the great benefit reached in practical applications in several areas of the engineering. Drag reduction additives can be classified into three categories: high and low molecular weight polymers, cationic-anionic-zwitterionic surfactants and fibers. Among these, the most effective drag reducer is the high molecular weight polymers, but their high degradation rate decreases the effectiveness of the recirculation systems. Surfactant additives also suffer from temporary mechanical and thermal degradations, but they have the capability of 'repairing' themselves in the order of seconds [40]. Vlachogiannis .et .al [41] examined the drag reduction effects of these polymers are most effective when the polymers are adaptable with a large structure. In recent past, Khadom et al. [42] demonstrated the impact of polyacrylamide (PAM) as drag decreasing polymer on a stream of raw petroleum in channel lines, and very recently, Tian et al. [43] analyzed that addition of Hydroxypropyl xanthan gum (HXG) increases the drag reducing rate as the concentration of HXG increases. In some cases, it also noticed that the higher amount of polymer causes for higher viscosity magnitude, hence the drag ingresses significantly [37].

CHAPTER 3

WALL EFFECT ON THE TERMINAL VELOCITY AND DRAG COEFFICIENT FOR THE NEWTONIAN FLOW PAST A SPHERE IN INCLINED PLANE

Introduction

The through literature survey showed that the studies on the effect of d/D on the settling velocity and the effect of angle of inclination on both the drag coefficient and settling velocity were performed for a limited range of d/D ratios except two studies [17,18]. In most of the literature, the angle of inclinations was restricted up to 30^0. Hence, this work is concerned to fill the voids in literature and to establish empirical equations to relate the drag coefficient with the Reynolds number for a different angle of inclination i.e. $(10^0\text{-}90^0)$ in a smooth circular tube domain, filled with incompressible Newtonian liquid. The current study includes the effect of d/D ratio on the terminal velocity and drag coefficient for $0.09 \leq d/D \leq 0.37$.

3.1. Physics around the Solid Particle

The falling state of a sphere with all the forces acting on it is shown in Fig. 3.1. The angle of inclination of the cylindrical flow channel is θ. The active forces on the sphere are the drag force (F_D), the net body weight of the sphere (F_B), and solid–solid resistance (F_R) along with the weight of the sphere (w). At equilibrium (i.e. when the particle moves with a terminal velocity), the force balance equation may be written as ,

$$F_B \sin \theta = F_D + F_R \qquad\qquad (3.1)$$

In which the drag force F_D can be expressed as

$$F_D = \frac{1}{2} C_D \rho_F V^2 \pi R^2 \qquad (3.2)$$

F_R becomes zero for smooth plane. The expression of the C_D for the smooth plane finally can, be written as

$$C_D = \frac{4gd}{3V^2} \left(\frac{\rho_S - \rho_F}{\rho_F}\right) \sin\theta \qquad (3.3)$$
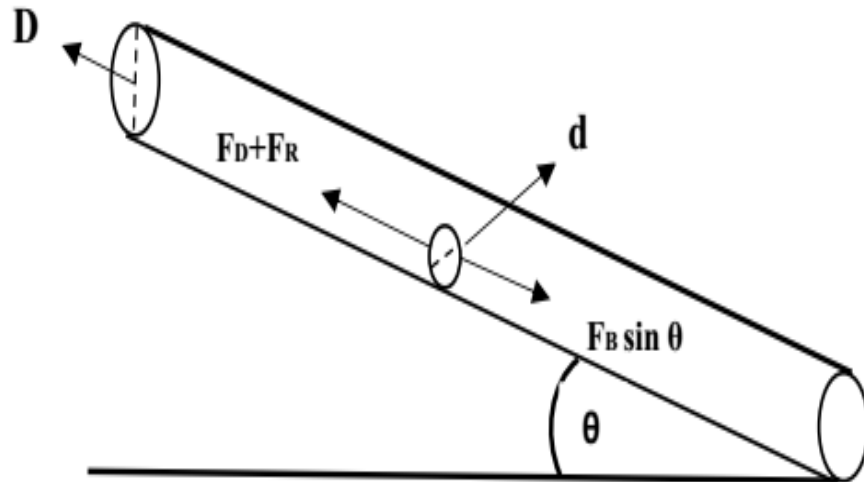
Fig.3.1. Schematic representation of flow over sphere in inclined plane

3.2. Experimental

3.2.1. Materials

The spheres of steel, aluminum and POM (Polyoxometalate) are used with diameters ranging from 3 mm to 11.4 mm and densities from 1420.93 to 9330.02 kg/m^3. The diameters are measured by digital caliper, and the average values are used. The densities are calculated by

mass and volume of the sphere. 1200 mm long perplex tube of diameter 30.1 mm is used as the flow domain for all sphere. In this work, the diameter ratio (*d/D*) is varied by changing only the sphere diameter. Four aqueous solutions of glycerin with different glycerin concentrations and pure glycerin (all are Newtonian) are used as the process fluid. The viscosities and densities of the fluids are measured using Rheometer (Anton Parr, Germany, RheolabQC) and pycnometer, respectively. All the essential physical properties are listed in Table 3.1.

Table 3.1

Physical properties of test fluids at 25^0C

Soln. No.	Fluid	Density (kg/m^{-3})	Viscosity (Pa. s)
1	100% Glycerin	1250.93	0.7533
2	80% Glycerin	1198.34	0.0571
3	70% Glycerin	1167.66	0.024
4	50% Glycerin	1144.81	0.0059
5	35% Glycerin	1121.23	0.003

3.2.2. Experimental Setup and Procedure

A transparent tube of 1200mm length and 30.1 mm diameter is supported on a frame of plywood with a facility of changing the angle of inclination from 10^0 to 90^0. The angles are measured at the fix-end of tube and clamps are hooked at the different angular position. The movable end of the tube is shifted from one angle to other to perform the experiment. The test fluids are loaded 24hrs before the experiment to maintain thermal equilibrium and bubble free condition [17, 19]. The spheres are released using forceps, and a stopwatch is used to note its terminal settling time for the specified section of the tube. The test section was taken sufficiently away from the top end of the flow channel not only to confirm the negligible end effects but also to allow sufficient distance to attain the constant terminal velocity [17]. Each experiment was

repeated for five times and mean settling time is recorded for the calculation of the terminal velocity, in turn, the drag coefficient and Reynolds number.

3.3. Result and Discussion

3.3.1. Variation Settling Velocity (V) with d/D

The estimation of terminal velocity of the spherical is necessary to estimate the drag coefficient of the sphere. In the present work, the terminal velocities are estimated for $0.08 \leq Re \leq 5504$, $0.09 \leq d/D \leq 0.37$ and $10^o \leq \theta \leq 90^o$. The variations of terminal velocity of the sphere with the (*d/D*) ratio for different Newtonian fluids are shown in Fig. 3.2. The angle of inclination of the flow channel θ is used as the parameter. The figure depicts that the measured fall velocity increases with increasing the angle of inclination. It occurs due to increase of the downward force, $F_B Sin\theta$ with increasing the plane inclination. In the figure, the measured fall velocity shows an increasing trend with *d/D* ratio, which contradicts the decreasing trend of the terminal velocity with *d/D* ratio [7, 14]. In the latter case, the *d/D* ratio was varied by changing the flow channel diameter, *D* for a particular sphere diameter, *d*, where the wall effect was reduced due to increase of *D*, which in turn reduces the obstruction to the free fall movement of the body. In the present work, *d/D* is reduced by decreasing the sphere diameter, *d*, which also helps to reduce the wall effect. But at the same time, the weight of the body acting in downward direction decreases with decreasing its diameter, *d*. Overall, the reduction of the body weight supersedes the favorable reduced wall effect, and thus, the terminal velocity increases with increasing *d/D* ratio while sphere diameter *d* is varied keeping *D* as constant. Fig 3.2 also depicts an asymmetric nature of the velocity variation curves at lower θ compared to the monotonically increasing trend at higher angle of inclination.

In the previous work [7, 14], the terminal velocity, V_∞ at infinite domain with zero wall effect was calculated taking $d/D \to 0$. But in the present work, the same treatment results in the negative values of V_∞. It leads to calculate the required diameter of the sphere, $d_{V=0}$ at zero terminal velocity of the sphere when sphere just floats in fluid. $d_{V=0}$ is calculated by substituting the terminal velocity as zero in the fit equation of the velocity of the sphere with (d/D) ratio. The variation of $d_{V=0}$ with the angle of inclination is illustrated in Fig. 3.3. The resistance to flow of sphere increases with increasing the viscosity of the fluid. Thus, $d_{V=0}$ increases with increasing the viscosity of the Newtonian fluid. A zigzag variation of it is observed with the angle of inclination.

The effect of *d/D* ratio on C_D for a different angle of inclination θ is depicted in Fig. 3.4. It shows a decreasing trend for C_D with *d/D* ratio for all θ which is reverse of the observations made by Uhlherr and Chhabra [6]. The physical explanation follows the explanations given above for the terminal velocity.
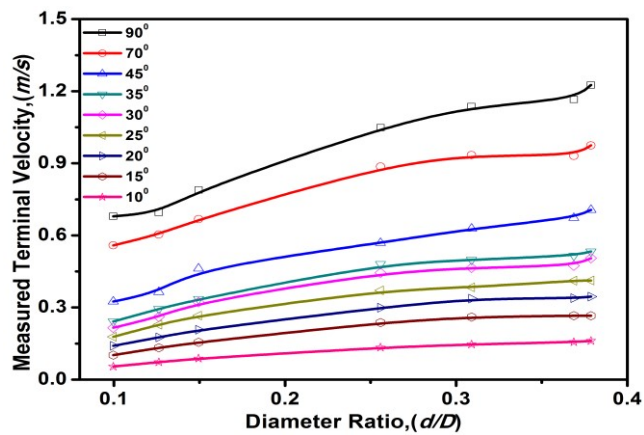
(A)
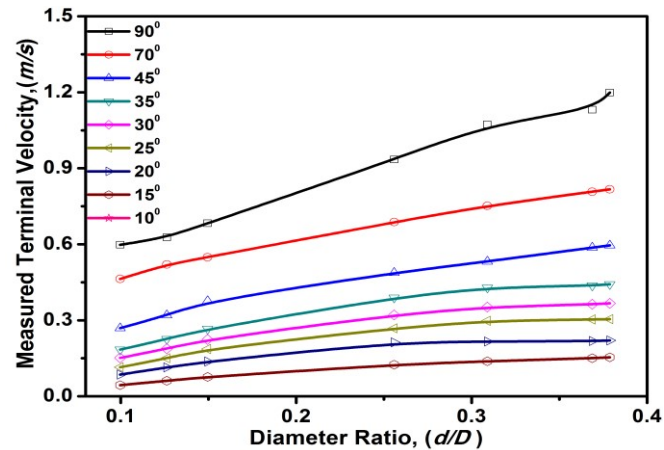
(B)
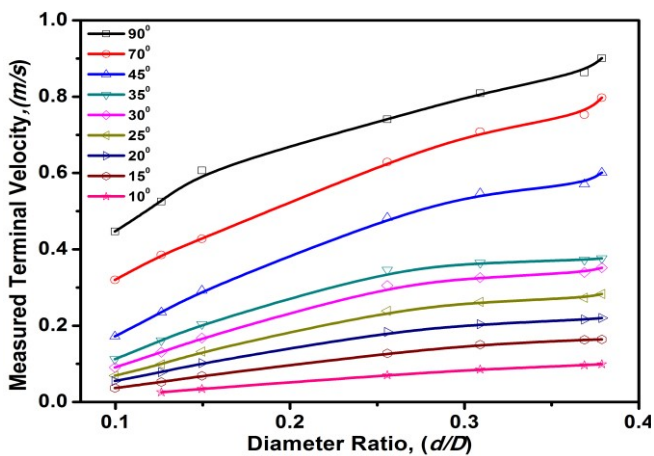
(C)
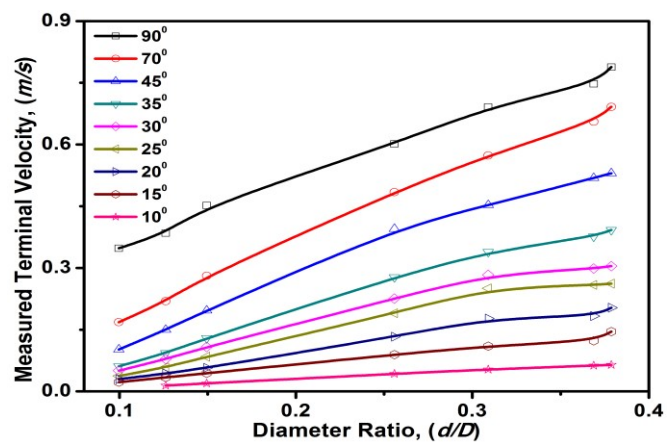
(D)
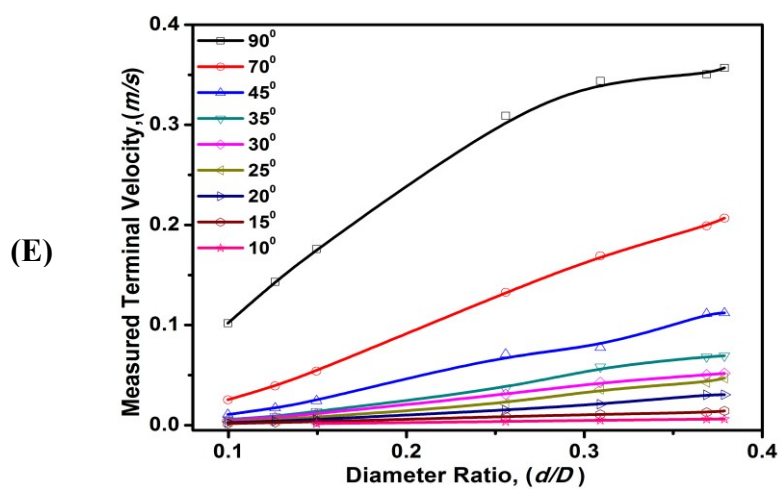
(E)

Fig. 3.2. Variation of measured terminal velocity on diameter ratio (*d/D*) and angle of inclination (θ) in (A) 35% glycerin, (B) 50% glycerin, (C) 70% glycerin, (D) 80% glycerin and (E) 100% glycerin
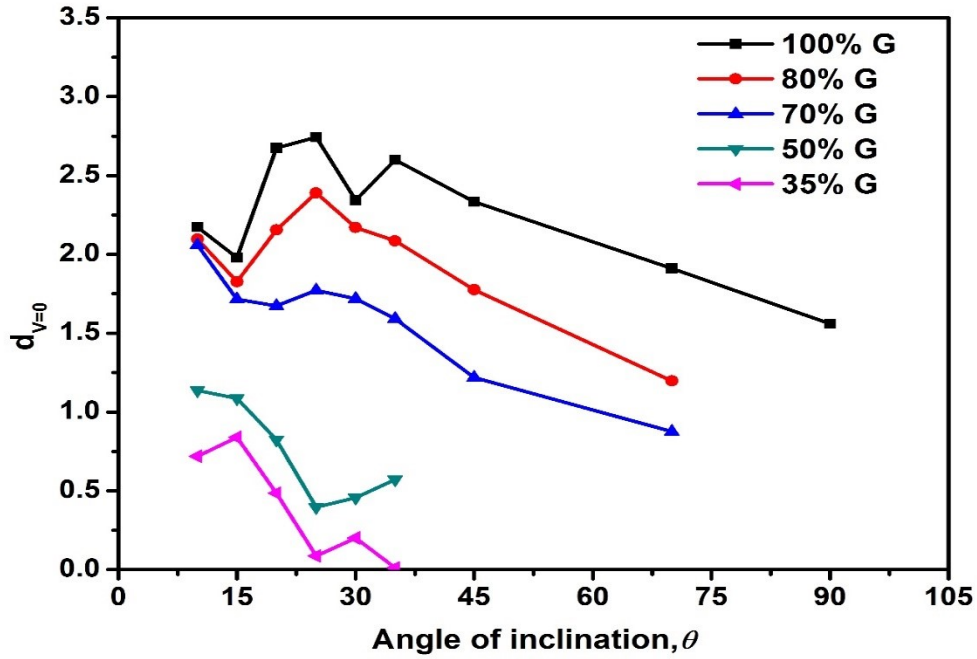
Fig. 3.3. Variation of $d_{V=0}$ with angle of inclination
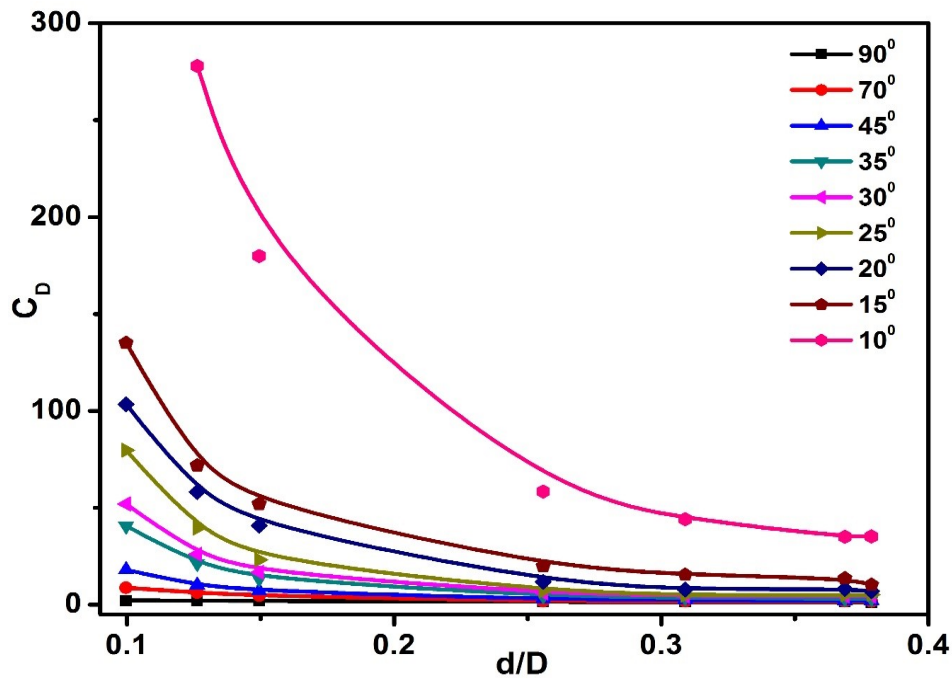
Fig. 3.4. Variation of drag coefficient as function of diameter ratio (d/D) and inclination angle in 80% glycerin solution

3.3.2. C_D-Re relationship

The variations of C_D with Re for a different angle of inclination of the flow channel and, for five Newtonian fluids are shown in Fig. 3.5. It is observed that the drag coefficient decreases with both the angle of inclination and Reynolds number irrespective of the fluid medium.

Hasan [44] developed the following Reynolds number and d/D ratio dependent expression for C_D which is valid for $d/D < 0.707$.

$$C_D Re = 15.717\{1 - (d/D)\}^{-2.5} \tag{3.4}$$

But, the Eq. (3.4) does not include the effect of the angle of inclination on the drag coefficient. The present work has developed the expression of the variation of C_D with Re and (d/D) ratio where the coefficient parameters of the correlation in Eq. (3.5) are a function of the inclination angle, θ. A least-square method is used to find the value of the coefficients i.e. A, B, C and E for a particular n and m values. The best values of the parameters to achieve the regression coefficient $R^2 > 0.99$ are given in Table 3.2. The R^2 vales of Table 3.2 confirm the viability of the correlation for the drag coefficient in Eq. (3.5). The negative values of n and m indicate a decreasing trend of C_D with both Reynolds number and d/D ratios. Similar trend is observed in Fig. 5. In the equation, the variations of A, B, C, E, n and m with θ are given in Table 3.3. The tabulated data shows that the magnitude of E is much lower than A and B and thus, it proves the lesser effect of (d/D) ratio on the drag coefficient than the Reynolds number.

$$C_D = A + BRe^{-1} + CRe^n + E\left(\frac{d}{D}\right)^m \tag{3.5}$$
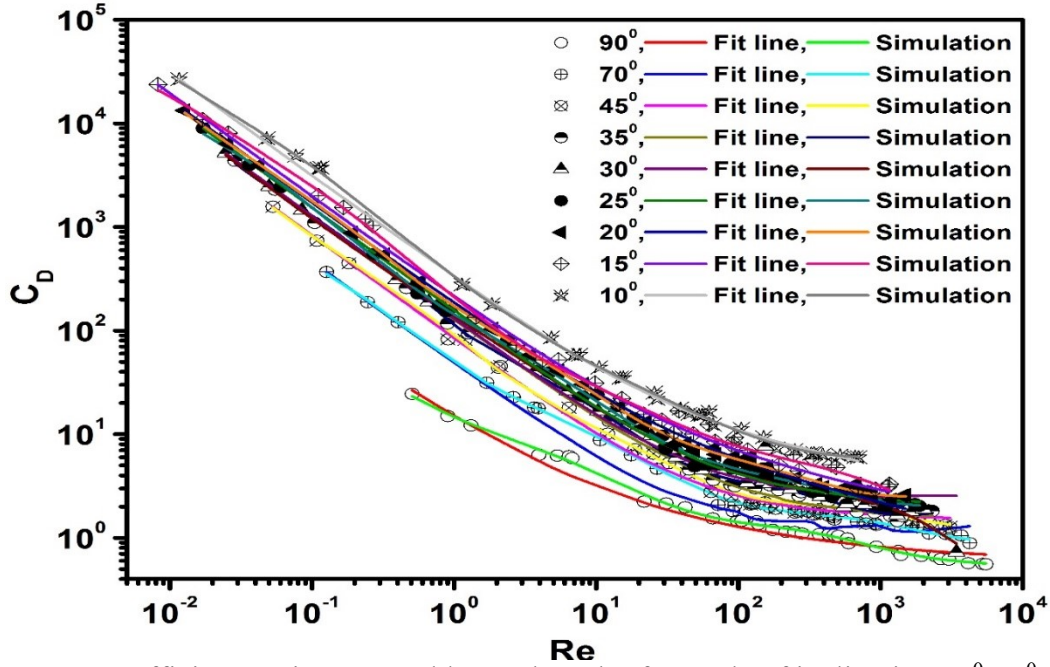
Fig. 3.5. Drag coefficient against Reynolds number plot for angle of inclination 90^0-10^0 with *d/D* in the range of 0.09 – 0.37

Table 3.2

Coefficients of Eq. 3.5 for different angle of inclination

Angle of inclination, θ	A	B	C	E	n	m	R^2
90	0.5641	-10.6782	3.8045	0.0011	-0.4	-0.3	0.99137
70	0.9641	-40.5848	7.1269	0.08	-0.9	-0.3	0.99983
45	0.9693	-83.0075	1.022	0.09	-0.1	-0.05	0.99976
35	1.0245	-125.261	1.652	0.1	-0.2	-0.3	0.99975
30	2.197	-127.042	1.1037	0.0535	-0.4	-0.7	0.99987
25	0.6	-153.788	2.9324	0.0811	-0.1	-0.3	0.99983
20	0.262	-645.549	16.2828	-0.0054	-0.3	-0.7	0.99981
15	0.344	-194.908	18.2269	0.02475	-0.3	-0.5	0.99931
10	0.5417	-309.688	22.9745	0.0295	-0.25	-0.7	0.99843

Table 3.3

Relationships of obtained coefficients with angle of inclination, θ

Coefficients	Fitting line equation
A	$1.717e^{\left(-((\theta-30.51)/3.677)^2\right)} + 4.208 \times 10^{14}e^{\left(-((\theta+483.6)/83.88)^2\right)} +$ $1.11e^{\left(-((\theta-60.45)/33.7)^2\right)}$
B	$-500.6e^{\left(-((\theta-19.77)/0.7143)^2\right)} - 7.32 \times 10^{17}e^{\left(-((\theta+1909)/322.1)^2\right)}$
C	$332.4sin(0.004343 \times \theta + 2.87) + 50.74sin(0.03681 \times \theta + 4.138)$ $+ 3.495sin(0.3052 \times \theta - 4.104)$
E	$0.09512sin(0.02971 \times \theta + 0.2725) + 0.02162sin(0.2072 \times \theta + 1.333)$ $+ 0.03766sin(0.09118 \times \theta - 2.621)$
n	$0.5353sin(0.03662 \times \theta + 2.515) + 0.3073sin(0.1016 \times \theta - 2.965)$ $+ 0.1372sin(0.3318 \times \theta - 5.878)$
m	$0.6398sin(0.006824 \times \theta + 5.511) + 0.2224sin(0.09718 \times \theta - 3.382)$ $+ 0.1028sin(0.298 \times \theta - 4.603)$

According to Eq. (3.4), the product term $C_D Re$ is function of only (d/D) ratio. To examine it, the $C_D Re$ data of the present work are plotted against (d/D) ratio for different tube inclination and fluids in Fig. 3.6. The figure depicts the dependency of $C_D Re$ on the both the angle of inclination and fluid viscosity. The third term in Eq. (3.5) accounts the dependency of C_D on the fluid viscosity. Table 3.2 shows that the magnitudes of C are lower than B in all the cases; it shows that the effect of Re on C_D is higher than the fluids viscosity. Fig. 3.6 also depicts a decreasing variation of $C_D Re$ with (d/D) ratio at higher viscous solution. It occurs due to increase of the terminal velocity of the sphere with decreasing the viscosity of fluid.

A linear variation of C_D with $1/Re$ is observed in Fig. 3.7. It shows that the estimated drag coefficients are in laminar and early transition flow regions. According to Fig. 3.5 $C_{D,}$ have higher values at lower θ for a particular Re. Hence, a decreasing trend of the slope of the C_D vs.

1/Re plots with increasing the angle of inclination, θ of the flow channel is observed in Fig. 3.7. It also shows a redetection of *1/Re* range with θ. It occurs due to increase of the terminal velocity of the sphere with θ in presence of higher gravitational force at higher θ.

(A)

(B)

(C)

(D)

(E)
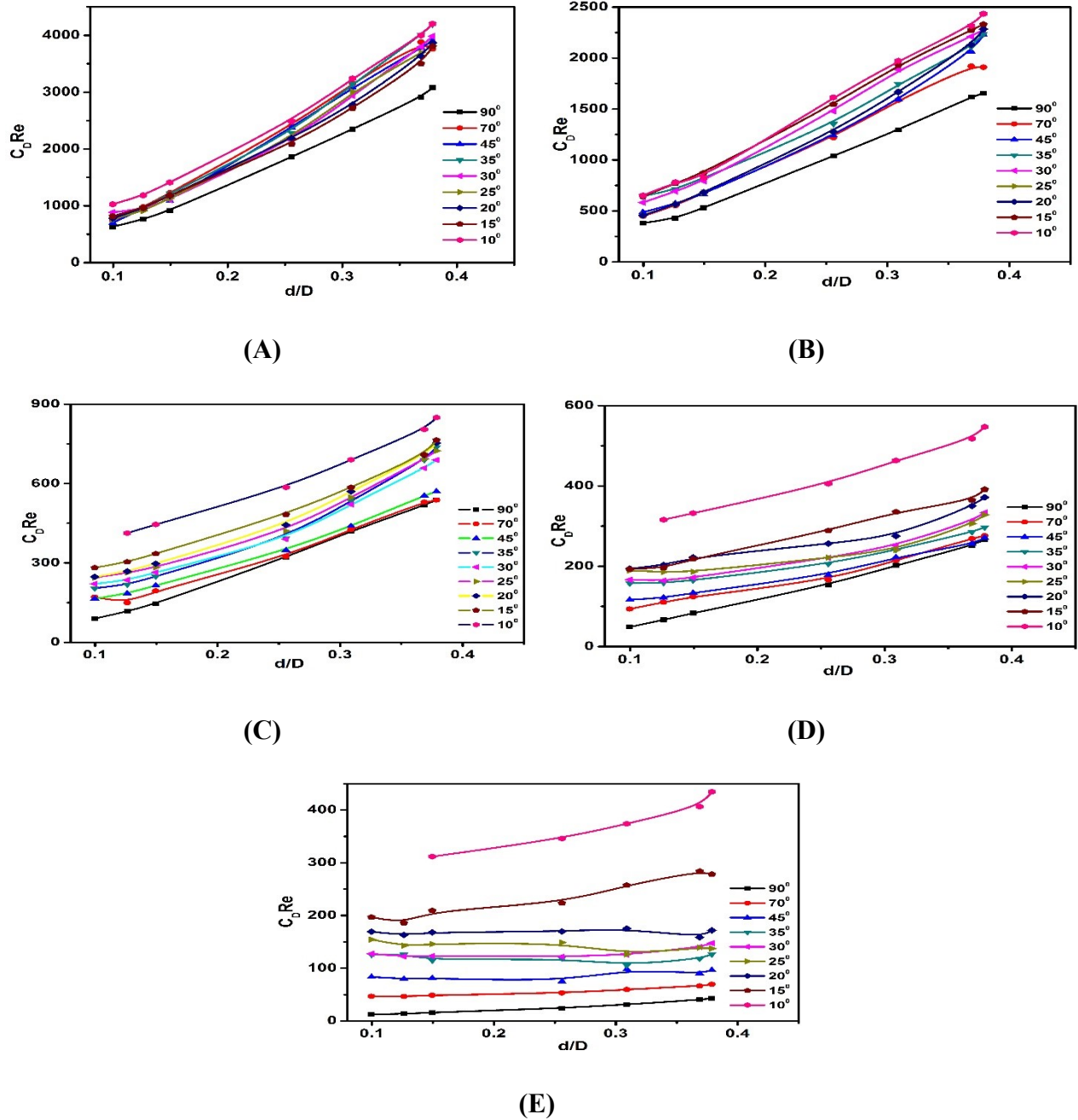
Fig.3.6. Variation of C_DRe with diameter ratio (*d/D*) and angle of inclination (θ) in (A) 35% glycerin, (B) 50% glycerin, (C) 70% glycerin, (D) 80% glycerin and (E) 100% glycerin

31
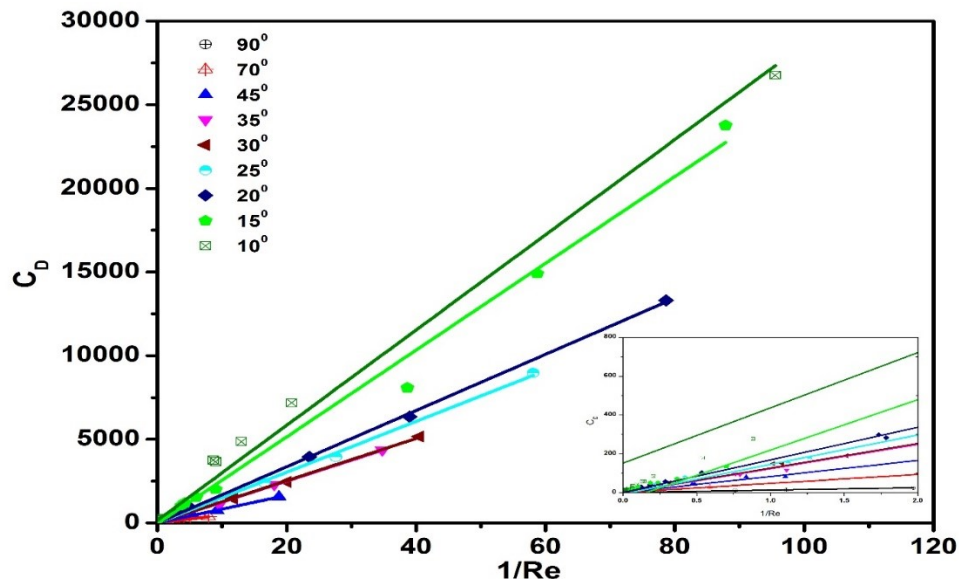
Fig. 3.7. Variation of C_D with inverse Reynolds number for different angle of inclination.

3.4. Prediction of Drag Coefficient through Numerical Approximation

3.4.1. Model Equations and Geometry

In the present study, the experimental data of the drag coefficient are predicted by Ansys Fluent v15.0. The following steady state model equations are used for the incompressible Newtonian fluids under consideration in the present study.

$$\nabla.(\rho u) = 0 \tag{3.6}$$

$$\nabla.(\rho uu) = -\nabla P + \nabla \tau + \rho_F g \tag{3.7}$$

Where ρ_F is the fluid density, u is the velocity of the fluid, P is the pressure, τ is the stress tensor and, g is the acceleration due to gravity.

The meshed geometries prepared in Ansys Workbench are shown in Fig 3.8 (A) and (B) for the vertical and inclined flow channels, respectively. In the vertical channel, the vertically oriented

sphere is placed symmetrically at the center of the channel. However, for the inclined channel, the sphere is placed off-centered at the mid-height of the channel. The exact off-centered location of the sphere is determined by adjusting its position to match the experimental data. In the present study, at all the channel inclinations and diameter ratios, the sphere is kept 0.15 mm away from the wall.

(A)   **(B)**
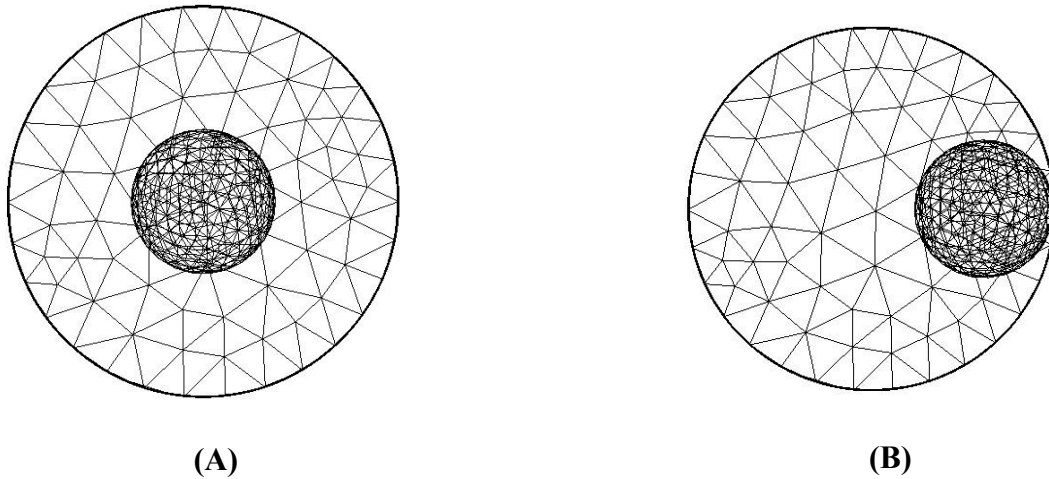
Fig.3.8. Top view of generated mesh for (A) vertical and (B) inclined plane

3.4.2. Boundary Conditions

The inlet velocity in the flow direction is specified as the terminal velocity. The surface is opposite to inlet assigned as pressure outlet boundary with specified zero gauge pressure. The no-slip condition is imposed on channel and sphere. For inclined channel, the acceleration due to gravity is used as *gsinθ*.

3.4.3. Solution Methods

The experimental results are in the range of laminar and early transition zone, hence to achieve the best and consistent results over the ranges of *Re*, various models including laminar flow model available in Ansys Fluent are tested. However, Reynolds Stress Model (RSM) model predicted better, and consistency in results is seen over all the ranges of *Re*. Hence, the predicted drag coefficient using RSM is presented in this work. The default values of the RSM parameters are used in the present study. SIMPLE algorithm and the second order upwind scheme are chosen for the faster convergence and higher accuracy. The convergence criteria are kept 0.00001 for all the flow variables.

3.4.4. Mesh Independency Test

Meshing is very important for the solution purpose and the sensitivity on the mesh quality and quantity affect largely the results. The triangular meshes with fine relevance center and high smoothing are chosen. In order to get fine mesh quality, an additional feature i.e. the *Relevance* is increased with a periodic increase of 10 for automatic refinement of the existing mesh. After 60-relevance center, no further improvements in the results are noticed. The number of nodes and elements are varied along with the diameter ratio. The mesh independency tests are carried out for the optimum grid. In Table 3.4 the changes of C_D values with the grid is given for $Re = 3.914588513$, $d/D=0.37$. This schema is also tested for other Reynolds numbers and d/D.

Table 3.4

Mesh independence test for *Re= 3.91*, *d/D=0.37*, Experimental value =17.62

No. of Elements	No. of Nodes	C_D
15907	71991	15.85
18876	86739	16.22
25051	117526	16.88
32127	153886	17.23
35668	172542	17.43
38421	195241	17.54

3.4.5. Discussion of the Predicted results

The experimental terminal velocity is used as the inlet velocity of the working fluid. The simulation results for all the channel inclinations are compared successfully with the experimentally obtained drag coefficients in Fig.3.5. The velocity counter profile for Re= 0.6 is shown in Fig.3.9. The Fore and aft symmetry for both the vertical and inclined channels confirms the laminar flow behavior of fluid flow over the sphere. The prediction of drag coefficient with negligible errors confirms the viability and applicability of the numerical models available in the Ansys Fluentv15.0 for both the vertical and inclined flow channels.

(A)   **(B)**
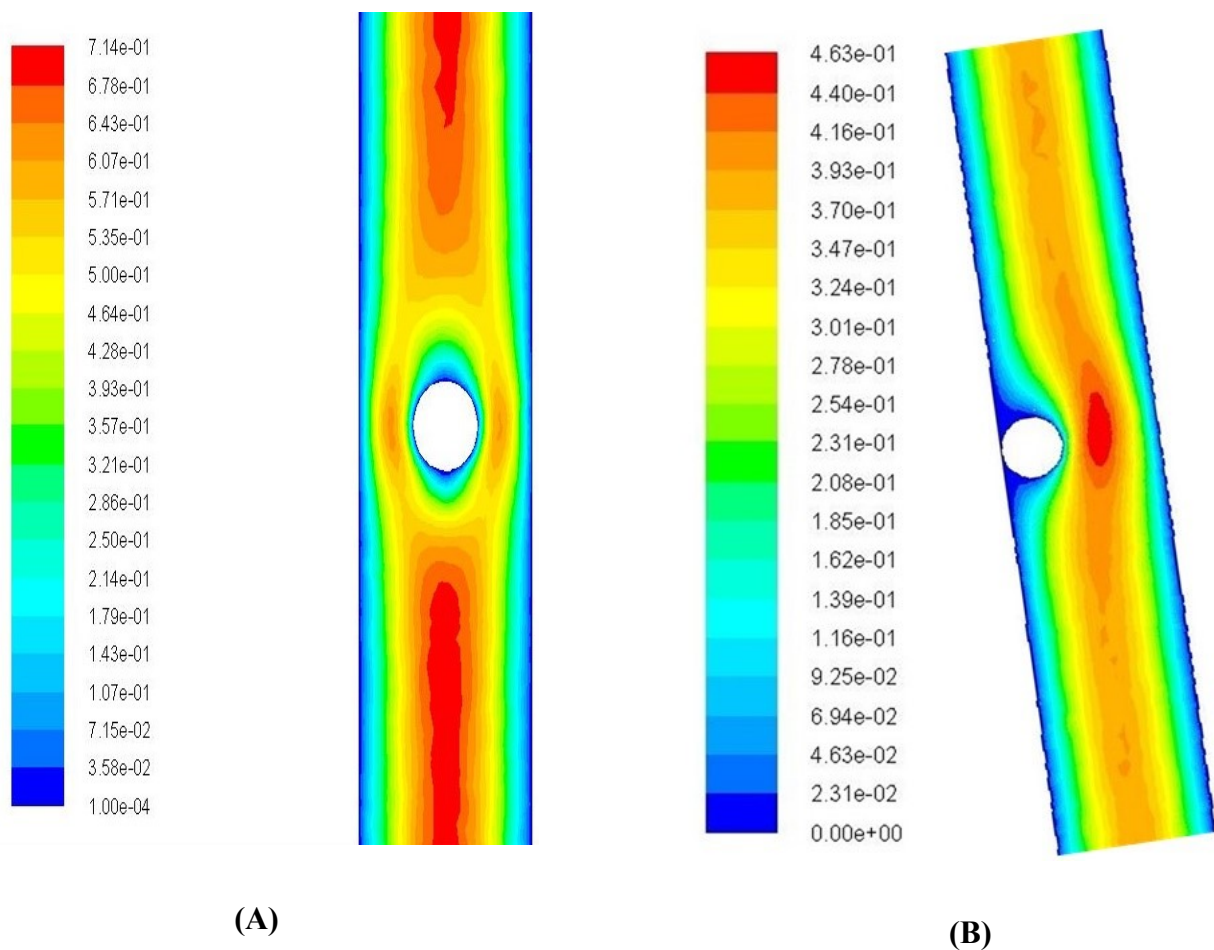
Fig.3.9. Velocity distribution around sphere in (A) vertical plane and (B) inclined plane

3.5. Conclusions

Terminal velocity and drag coefficient of the sphere in vertical; and inclined plane are estimated for a series of the angle of inclination and diameter ratio. The terminal velocity of the falling sphere trend was increased with increasing the *d/D* ratio of the sphere and flow channel. The increasing trend is just opposite of the decreasing trend the drag coefficient of the sphere with increasing the *d/D* ratio. The terminal velocity was increased with increasing the angle of inclination due to increasing the downward body force with the flow channel inclination. The

estimated diameter of the sphere for zero terminal velocity showed dependency on both θ and d/D ratio. The drag experienced by the sphere for the inclined channel was represented by the drag coefficient, which was estimated for $0.08 \leq Re \leq 5504$, $0.09 \leq d/D \leq 0.37$ and $10^o \leq \theta \leq 90^o$. The C_D values were higher for lower angle of inclination due to the decreasing trend of terminal velocity. Appropriate prediction equations for C_D as function of Re, d/D and θ were developed by the least square method. The product of $C_D Re$ showed its dependency on both the angle of inclination and fluid viscosity. It showed a declining trend with the viscosity of solution. The linear variation of C_D with $1/Re$ showed the collected experimental data are in laminar and early transition flow regions. The experimental drag coefficients are numerically predicted using Reynolds Stress Model (RSM) model and observed accuracy for both vertical and inclined plane consideration.

CHAPTER 4

NEWTONIAN FLOW OVER HOLLOW FRUSTUM IN VERTICAL AND INCLINED PLANE: AN EXPERIMENTAL OBSERVATION FOR TERMINAL VELOCITY AND DRAG COEFFICIENT

Introduction

In preceding paragraphs of Chapter, the literature included the drag coefficient data of solid regular shaped body in the vertical and inclined flow channels. To the best of the author's knowledge, no attempt was reported for the drag coefficient due to the flow of Newtonian fluid over any hollow particle. Looking at the usefulness of the hollow particles in process industries, to fill the void and to enrich the existing literature, the present work is undertaken to estimate the drag coefficient of the hollow tapered cylindrical body called hollow frustum (Fig. 4.1, A) flowing in the Newtonian fluid in both the vertical and inclined channels. Pure glycerin and its aqueous solutions are used as the working fluid in the present study.

4.1. Contribution of the work

Based on the literature gaps, the following objectives are adopted for the present work.

- To estimate the effect of the angle of inclination, θ on the terminal velocity and drag coefficient of the hollow frustum, which is still unreported in the open literature.

- To estimate the effect of the inner diameter to outer diameter ratio (*di/do*) of the hollow frustum and the outer diameter of the hollow frustum to the flow channel diameter ratio (*do/D*) on the measured terminal velocity and estimated drag coefficient.

- To develop the correlation for the drag coefficient, C_D as a function of *Re, di/do, do/D* for a different angle of inclination, θ.

4.2. Physics around particle

The schematic representation of the hollow frustum is given in Fig.4.1. When a hollow frustum is moving down in fluid inside an inclined channel, the forces exerting on hollow frustum are drag force (F_D), the net body weight of the hollow frustum ($F_B \sin \theta$), and solid–solid resistance (F_R). The force balance equation at equilibrium is

$$F_B \sin \theta = F_D + F_R \tag{4.1}$$

The expression of drag force is

$$F_D = \frac{1}{2} C_D \rho_F V^2 A \tag{4.2}$$

For smooth plane with F_R zero, the expression of C_D becomes

$$C_D = \frac{mg(1-\frac{\rho_F}{\rho_p})}{0.5AV^2\rho_F} sin\theta \tag{4.3}$$

For vertical channel consideration, Eq. (4.3) is reduced to

$$C_D = \frac{mg(1-\frac{\rho_F}{\rho_p})}{0.5AV^2\rho_F} \tag{4.4}$$

The diameter ratios (*di/do, do/D*) and the angle of inclination are the vital parameters to affect the drag coefficient in inclined plane consideration, hence the total drag coefficient C_D may be written as follows

$$C_D = f(Re, do/D, di/do, \theta) \tag{4.5}$$
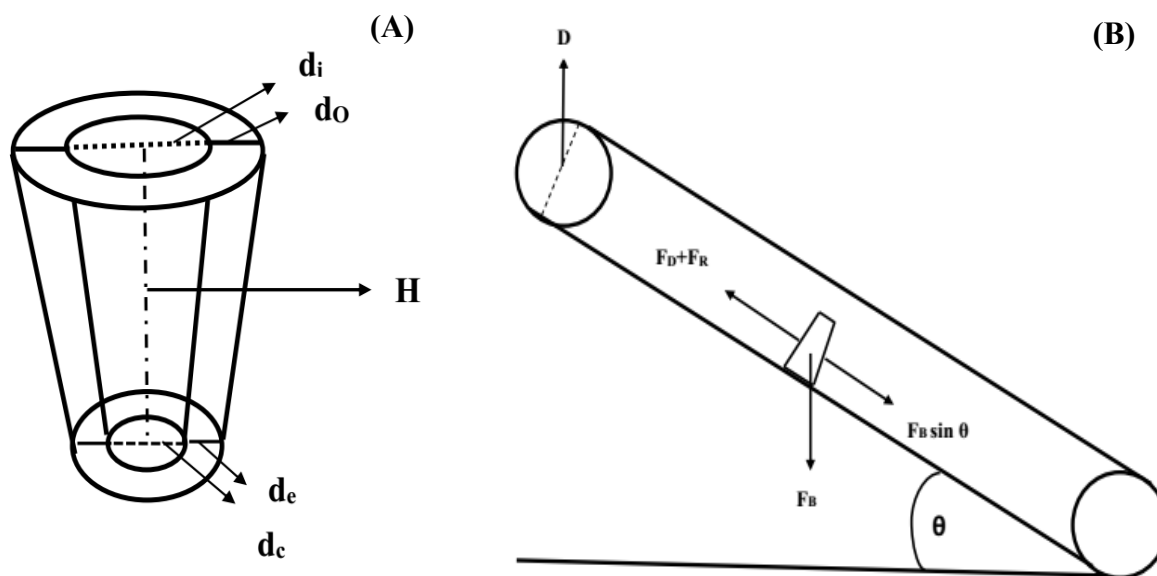
Fig.4.1. Schematic representation of flow over hollow frustum in (A) normal plane and (B) in inclined plane

4.3. Experimental

4.3.1. Materials

Hollow frustums (SS 304L) of different dimension (listed in Table 4.1) and density 7849.46 kg/m^3 are machined in wire EDM (Electrical Discharge Machining) and used as hollow obstacles in 30.1×1200 mm circular Perspex tube. The viscosities of working fluid are measured using Rheometer (RheolabQC, Anton Parr, Germany,), and the densities are estimated by pycnometer. The rheological properties of test fluids are listed in Table 4.2.

Table 4.1. Physical dimensions (all are in mm) of hollow frustum

Sl. No.	d_o	d_i	d_c	d_e	H
1	10	7			
2	10	4			
3	10	3			
4	9	7			
4	9	4	8	2	12
6	9	2			
7	6	4			
8	6	3			
9	6	2			

Table 4.2. Physical properties of test fluids

Soln. No.	Fluid	Temperature (K)	Density (kg/m^3)	Viscosity (Pa.s)
1	100% Glycerin	298	1247.09	0.7433
2	98% Glycerin	298	1241.906	0.4378
3	96% Glycerin	298	1246.723	0.4024
4	94% Glycerin	298	1241.439	0.3044
4	92% Glycerin	298	1236.346	0.2606
6	90% Glycerin	298	1231.172	0.2094

4.3.2 Experimental Setup and Procedure

The inclination angles (90^0-40^0) are varied by rotating the moveable end of the tube around the fixed end. The schematic representation of the experimental setup is shown in Fig. 4.1 (B). The test fluids are loaded in the tube 24hrs before starting the experiment to make the fluid bubble free [17,18]. The test location is taken sufficiently away from the inlet to allow the frustum to reach constant terminal velocity. The hollow frustums are released by forceps and stopwatch is used to measure settling time. Every experiment is repeated for five times and mean settling time is taken for the calculation of terminal velocity followed by Reynolds number and C_D.

4.4. Result and Discussion

4.4.1. Effect of d_o/D and d_i/d_o on measured terminal velocity

Measured terminal velocity is one of the vital parameters for the estimation of drag coefficient and Reynolds number, and it depends on the ratio of the particle and channel diameters [7, 14]. In this study, the particle is hollow; hence, it is believed that the ratio of inner diameter, d_i to the outer diameter, d_o of the hollow frustum may possess some effect on the terminal velocity. Fig. 4.2 represents the variation of the measured terminal velocity of the hollow frustum with d_o/D using di/do as the parameter. The angle of inclination is 90° here. The d_o/D ratio is varied by changing d_o keeping D fixed. For a particular di/do, the increase of do makes the particles heavier. Thus, the terminal velocity of the frustum increases with increasing the d_o/D ratio. The increasing trend of the velocity with d_o/D ratio contradicts the declining trend of it for fixed diameter, d solid spherical, cylindrical and conical [7, 14]. In the latter case, the d/D ratio was increased by reducing the flow channel diameter, D for a particular sphere diameter, d which thus decreased the terminal velocity due to increasing the wall effect on the free falling sphere. In the present study, the d_i/d_o ratio is also an important parameter. The hollow frustum becomes thinner and lighter with increasing the d_i/d_o ratio for a particular d_o. Thus, the terminal velocity as shown in Fig. 4.2 decreases with increasing d_i/d_o.
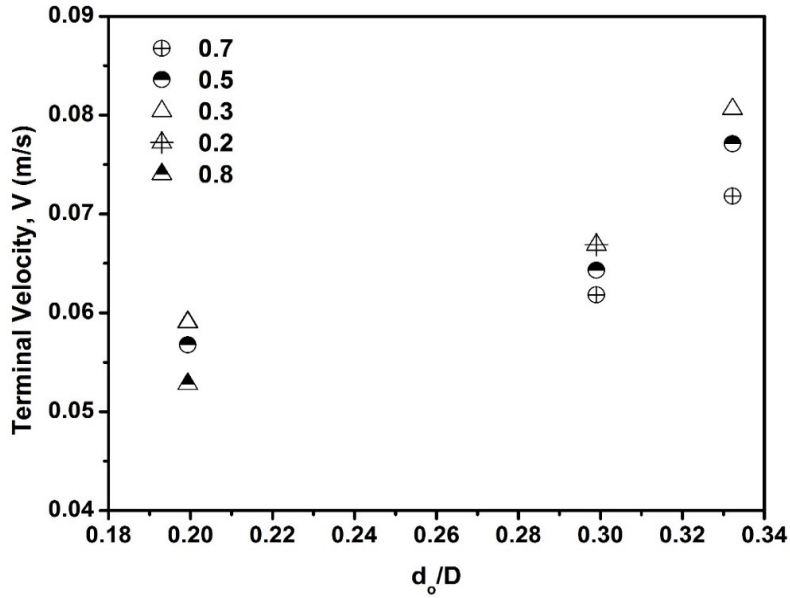
Fig.4.2. Variations of terminal velocity with d_0/D for different d_i/d_o in 100% glycerin and 90^0 angle of inclination

The effect of angle of inclination (90^0-40^0) on the terminal velocity is illustrated in Fig.4.3 for pure glycerin. It shows an increasing trend of the terminal velocity with *do/D* ratio for all the angle of inclinations. The most profound variation of the terminal velocity with the d_o/D ratio is observed for vertical flow channel, and it becomes less with decreasing the angle of inclining. This occurs due to decreasing the effect of body force on the terminal velocity with decreasing the angle of inclination of the flow channel. For other operating fluids, the similar trend is observed.
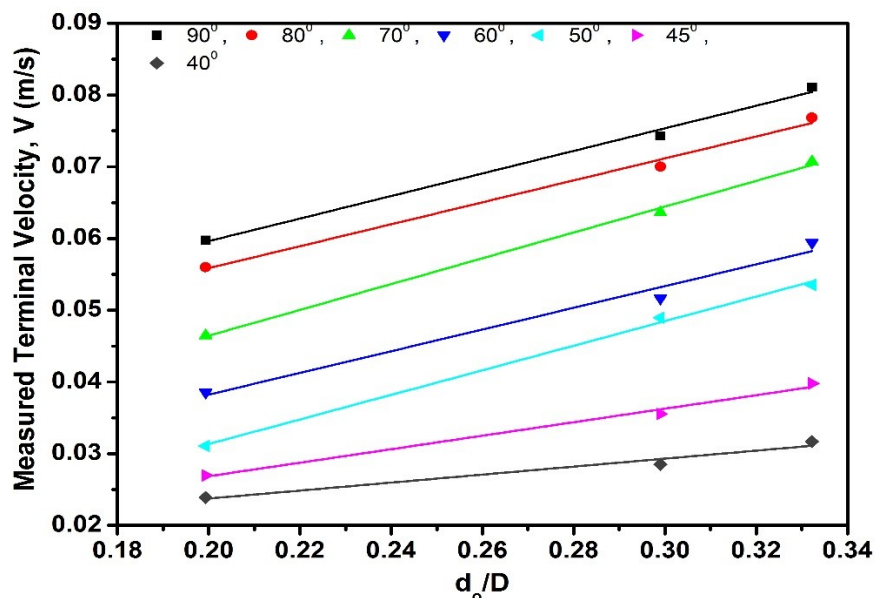
Fig.4.3. Variation of terminal velocity with d_o/D and θ for $d_i/d_o = 0.4$ in 100% Glycerin ($R^2 > 0.99$)

4.4.2. Drag coefficient and Reynolds number relationship

The drag coefficient and Reynolds numbers are calculated from the fundamental properties of the hollow frustum and fluid, and the terminal velocity for different angle of inclination, d_o/D and d_i/d_o. The orientation of the hollow frustum was normal to the flow direction in the 90^0 and horizontal for all other acute angles. Hence, appropriate projected areas and characteristic lengths are considered for the estimation of C_D and Re.

According to Eq. (4.5), the drag coefficient is also a function of Re. The effect of Re on C_D is shown in Fig.4.4. It shows the expected decreasing trend of C_D with Re for all the angles of inclination. The variation of drag coefficient with Reynolds number is matching with the trend obtained by investigators for regular shaped particle [1, 4&5]. The C_D value obtained as the maximum for the vertical orientation of the tube where the orientation of hollow frustum is normal as shown in Fig. 4.1 (A). For the other inclined tubes, the hollow frustum becomes horizontal

shown in Fig.4.1 (B) and thus the drag coefficient increases with decreasing the θ. The highest value at 90^0 is obtained due to normal orientation which gives lesser projected area than other inclined channels.
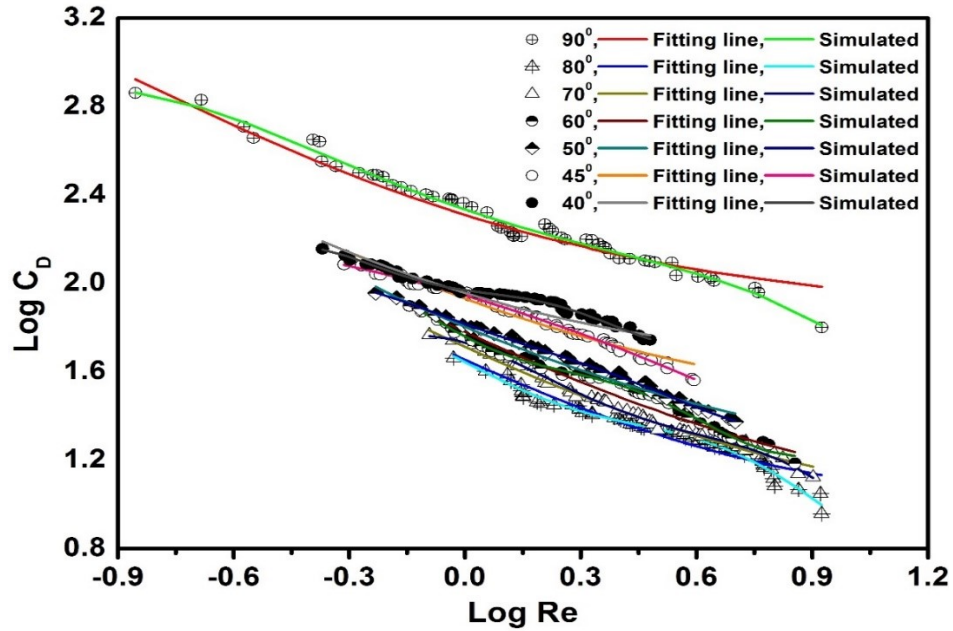
Fig.4.4. Drag coefficient against Reynolds number plot for angle of inclination 90^0- 40^0

For 40º to 80º inclinations, projected areas are same, but as mentioned above the terminal velocity decreases with decreasing the angle of inclination. According to Eq. (4.3) and (4.4) C_D is inversely proportional to V^2. Hence, it increases with decreasing the θ values. The drag coefficient is also inversely varied with the projected area, A, which is the minimum for the normally oriented frustum. Thus, C_D is the maximum for the vertical channel in spite of having the highest terminal velocity.

Hasan [44] developed the following Reynolds number and d/D ratio dependent expression for C_D for spherical particles falling in an inclined channel.

$$C_D Re = 14.717\{1 - (d/D)\}^{-2.4} \tag{4.6}$$

They did not explore any effect of the angle of inclination on the drag coefficient expression. The present work has developed the expression of C_D given in Eq. (4.7) which includes the dependency of it on all the variables like Re, di/do and do/D ratio. The coefficients of the correlation in the equation are also a function of the inclination, θ. A least-square method is used to find the value of the coefficients i.e. A, B, C, E and F for a particular n, m and k values. The estimated parameters with regression coefficient $R^2 \geq 0.97$ are given in Table 4.3. R^2 values closer to 1.0 show the viability of the correlation, Eq. (4.7). The declining trend of C_D with Reynolds number and di/do, do/D ratios leads to negative values of n, m and k. In the equation, the θ dependent A, B, C, E, F, n, m and k with are given in Table 4.4. The tabulated data shows that the magnitude of E and F is much lower than A and B, which shows weak effect of di/do and do/D ratio on the drag coefficient than the Reynolds number and this agrees with the conclusion drawn in [31].

$$C_D = A + BRe^{-1} + CRe^n + E\left(\frac{d_i}{d_o}\right)^m + F\left(\frac{d_o}{D}\right)^k \tag{4.7}$$

According to Eq. (4.6), the product term $C_D Re$ is function of only (d/D) ratio. To examine it, the $C_D Re$ data of different Newtonian fluids are plotted in Fig. 4.5 against (do/D) ratio keeping $di/do = 0.5$. The figure depicts that $C_D Re$ varies with both the fluid viscosity and angle of inclination along with the Reynolds number. Fig. 4.5 portrays a decreasing trend of $C_D Re$ with viscosity in both the angle of inclination owing to well-known inverse relation of terminal velocity with viscosity. The magnitudes of C (stands for viscosity affect in Eq. 4.7) as given in Table 4.3 are lower than B for all the tube inclinations, which confirms the effect of Re is higher on the drag coefficient than the viscosity. The terminal velocity of the hollow frustum decreases with increasing the fluid viscosity and thus, a lesser variation of $C_D Re$ with d_o/D ratio is observed in the figure.

Table 4.3. Obtained coefficients of Eq.6 for different angle of inclination, θ

θ	A	B	C	E	F	n	m	k	R^2
90	0.00641	-100.6782	94.044	1.0002	1.002218	-0.1	-0.03	-0.6	0.97
80	0.1137	-34.9284	9.088	0.012	0.1441	-0.01	-0.1	-0.4	0.978
70	0.1089	-39.2276	11.1669	0.0011	0.4167	-0.1	-0.1	-0.4	0.9932
60	0.1261	-47.7332	12.1739	0.11	0.1184	-0.1	-0.3	-0.6	0.989
40	0.1124	-43.3212	19.9844	0.2246	0.3914	-0.1	-0.4	-0.7	0.993
44	0.1681	-40.8861	34.2011	0.0611	0.0967	-0.1	-0.4	-0.4	0.979
40	0.0061	-47.3412	42.1484	0.0111	0.4427	-0.01	-0.1	-0.2	0.979

Table 4.4. Relationship among the coefficients of Eq. 6 and angle of inclination, θ

Coefficient	Fitting line equation
A	$0.4869e^{\left(-((\theta-47.21)/1.836)^2\right)} + 0.1344e^{\left(-((\theta+67.4)/18.36)^2\right)}$
B	$-49.11e^{\left(-((\theta-41.11)/33)^2\right)} - 7.32 \times 10^{16}e^{\left(-((\theta-404.2)/70.69)^2\right)}$
C	$1.444 \times 10^{42}e^{\left(-((\theta-740.3)/68.61)^2\right)} - 4.976 \times 10^{26}e^{\left(-((\theta+1944)/262)^2\right)}$
E	$1.432e^{\left(-((\theta-94.22)/6.47)^2\right)} - 0.2072e^{\left(-((\theta+43.37)/6.773)^2\right)}$
F	$2.439 \times 10^6 - 3.366 \times 10^6 \cos(0.001679\theta) - 3.614 \times 10^4 \sin(0.001679\theta) + 8.273 \times 10^4 \cos(0.001679\theta) + 1.797 \times 10^4 \sin(0.001679\theta)$
n	$-7.243 \times 10^7 + 9.646 \times 10^7 \cos(-0.0003434\theta) - 1.729 \times 10^6 \sin(-0.0003434\theta) - 2.413 \times 10^7 \cos(-0.0003434\theta) + 8.646 \times 10^4 \sin(-0.0003434\theta)$
m	$3.827 \times 10^9 - 4.102 \times 10^9 \cos(0.0002293\theta) - 8.04 \times 10^7 \sin(0.0002293\theta) + 1.274 \times 10^9 \cos(0.0002293\theta) + 4.019 \times 10^7 \sin(0.0002293\theta)$
k	$1.146sin(0.04742 \times \theta + 0.7786) + 0.7248sin(0.08442 \times \theta + 1.001)$
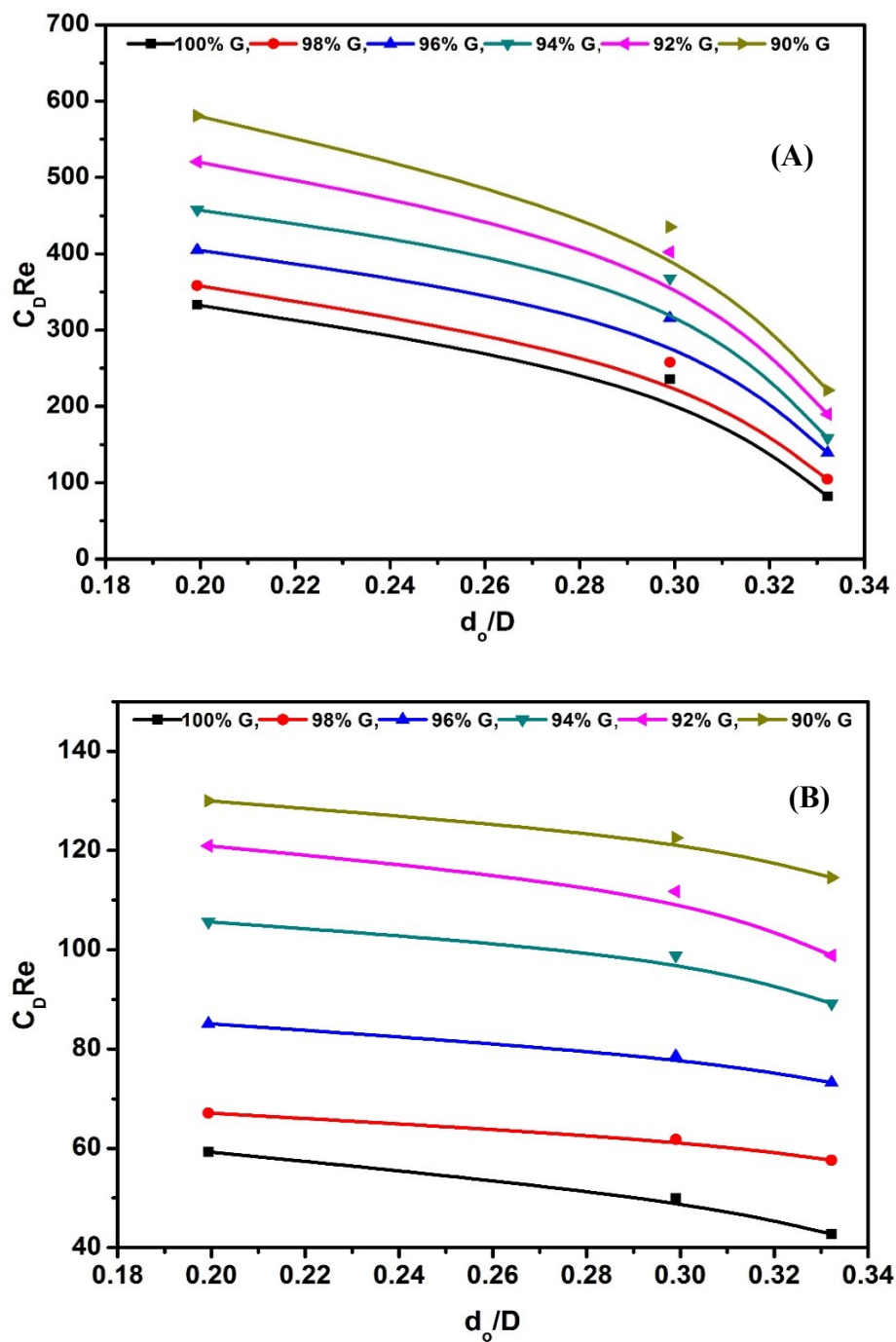
Fig.4.5. Dependency of $C_D Re$ on do/D and the viscosity of fluid for (A) 90^0 and (B) 40^0 angle of inclination at di/do=0.4

The variation of the drag coefficient with $1/Re$ is studied in Fig. 4.6 where all the present drag coefficients are plotted against $1/Re$. The range of $1/Re$ in the figure confirms that all the present experimental data are valid in laminar flow state. The variation is approximately linear especially at lower angles of inclination.
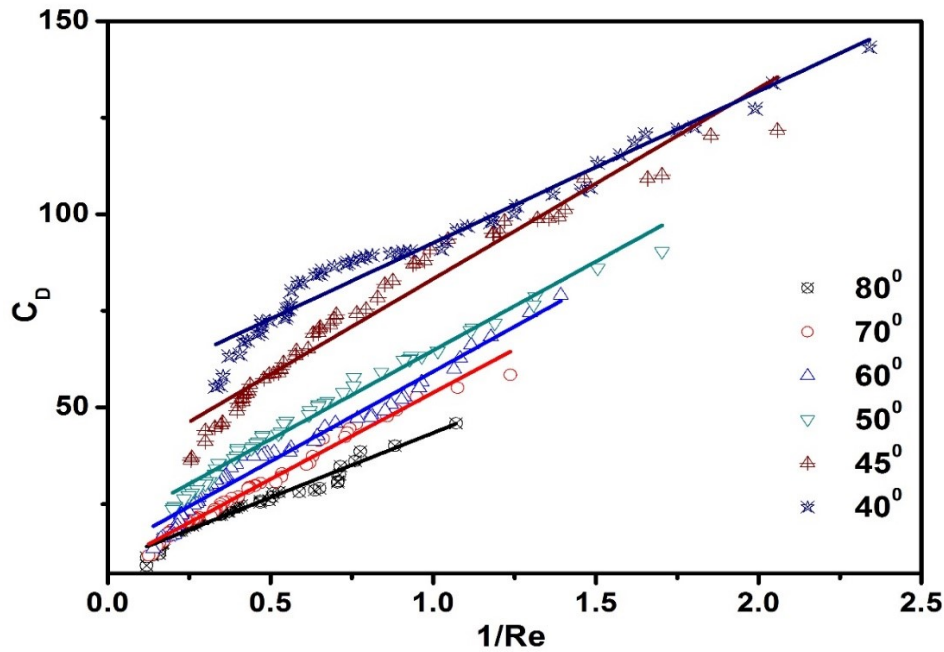
Fig.4.6. Variation of C_D with *1/Re* for different angle of inclination

4.5. Prediction of Drag Coefficient through Numerical Approximation

4.5.1. Model Equations and Geometry

In the present study, the experimental data of the drag coefficient are predicted by Ansys Fluent v15.0. The following steady state model equations are used for the incompressible Newtonian fluids under consideration in the present study.

$$\nabla.(\rho u) = 0 \tag{8}$$

$$\nabla.(\rho u u) = -\nabla P + \nabla \tau + \rho_F g \tag{9}$$

Where ρ_F is the fluid density, u is the velocity of the fluid, P is the pressure, τ is the stress tensor and, g is the acceleration due to gravity.

The meshed geometries prepared in Ansys Workbench are shown in Fig. 4.7 (A) and (B) for the vertical and inclined flow channels, respectively. In vertical channel, the vertically oriented hollow frustum is placed symmetrically at the center of the channel. But for the inclined channel, the horizontal hollow frustum is placed off-centered at the mid-height of the channel. The exact off-centered location of the hollow frustum is determined by adjusting its position to match the experimental data. In the present study, at all the channel inclinations and diameter ratios, the hollow frustum is kept 0.87 mm away from the wall.

(A)

(B)
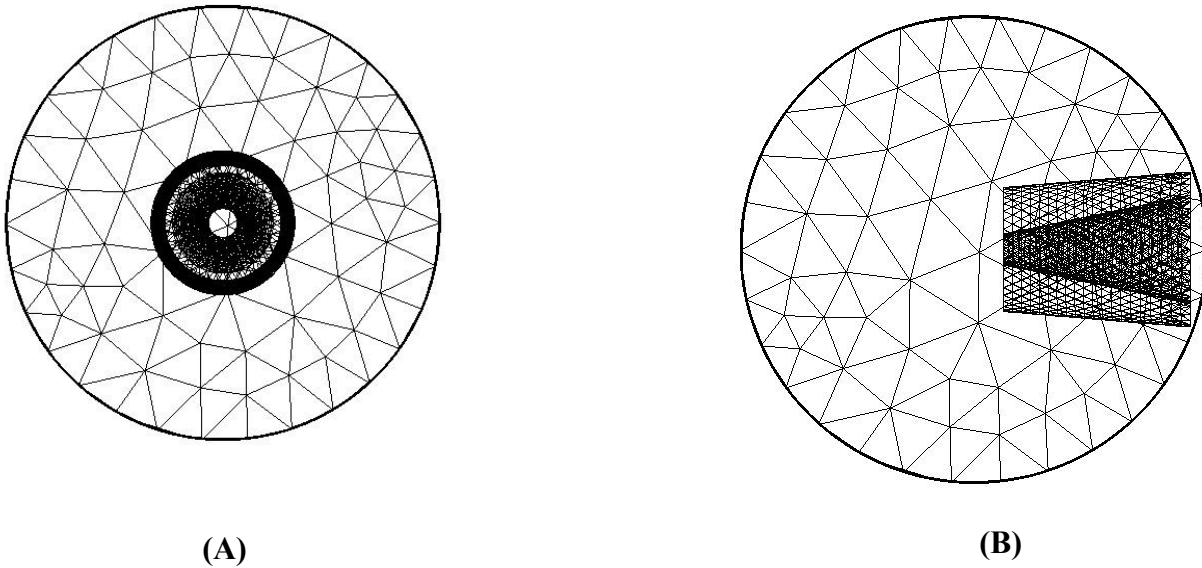
Fig. 4.7. Top view of generated mesh for (A) vertical and (B) inclined plane

4.5.2. Boundary Conditions

The inlet velocity in the flow direction is specified as the terminal velocity. The surface is opposite to inlet assigned as pressure outlet boundary with specified zero gauge pressure. The no-slip condition is imposed on the channel and hollow frustum walls. For inclined channel, the acceleration due to gravity is used as *gsinθ*.

4.5.3. Solution Methods

The experimental results are in the range of laminar and early transition zone, hence to achieve the best and consistent results over the ranges of *Re*, various models including laminar flow model available in Ansys Fluent are tested. Up to Reynolds number 2.84, both the laminar and Reynolds Stress Model (RSM) models predict the experimental drag coefficient equally well, but RSM is found as a better model for higher Reynolds number. Overall, the predicted drag coefficient using RSM is presented in this work. The default values of the RSM parameters are used in the present study. SIMPLE algorithm and the second order upwind scheme are chosen for the faster convergence and higher accuracy. The convergence criteria are kept 0.00001 for all the flow variables.

4.5.4. Mesh Independency Test

Meshing is very important for the solution purpose and the sensitivity on the mesh quality and quantity affect largely the results. The triangular meshes with fine relevance center and high smoothing are chosen. In order to get fine mesh quality, an additional feature i.e. the *Relevance* is increased with a periodic increase of 5 for automatic refinement of the existing mesh. After 85-relevance center, no further improvements in the results are noticed. The number of nodes and

elements are varied along with the diameter ratio. The mesh independency tests are carried out for optimum grid. In Table 4.5 the changes of C_D values with grid is given for Re = 0.359475, do/D= 0.33 and di/do=0.7. This schema is also tested for other Reynolds numbers, di/do and do/D.

Table 4.5

Mesh independence test for Re= 0.359475, do/D=0.33 and di/do=0.7. Experimental value =276.18

No. of Elements	No. of Nodes	C_D
19521	91470	241.24
26343	126083	248.11
39069	192224	257.14
43978	218656	266.88
48847	245460	275.14
51792	261788	275.54

4.5.5. Discussion of the Predicted results

The experimental terminal velocity is used as the inlet velocity of the working fluid. The simulation results for all the channel inclinations are compared successfully with the experimentally obtained drag coefficients in Fig.4.4. Fore and aft symmetry is observed in Fig.4.9 for both the vertical and inclined channels. It confirms the laminar flow behavior of fluid flow over the hollow frustum and it accords the experimental laminar flow regime according to the Reynolds number. The prediction of drag coefficient with negligible errors confirms the viability and applicability of the numerical models available in the Ansys Fluentv15.0 for both the vertical and inclined flow channels.

(A)   **(B)**
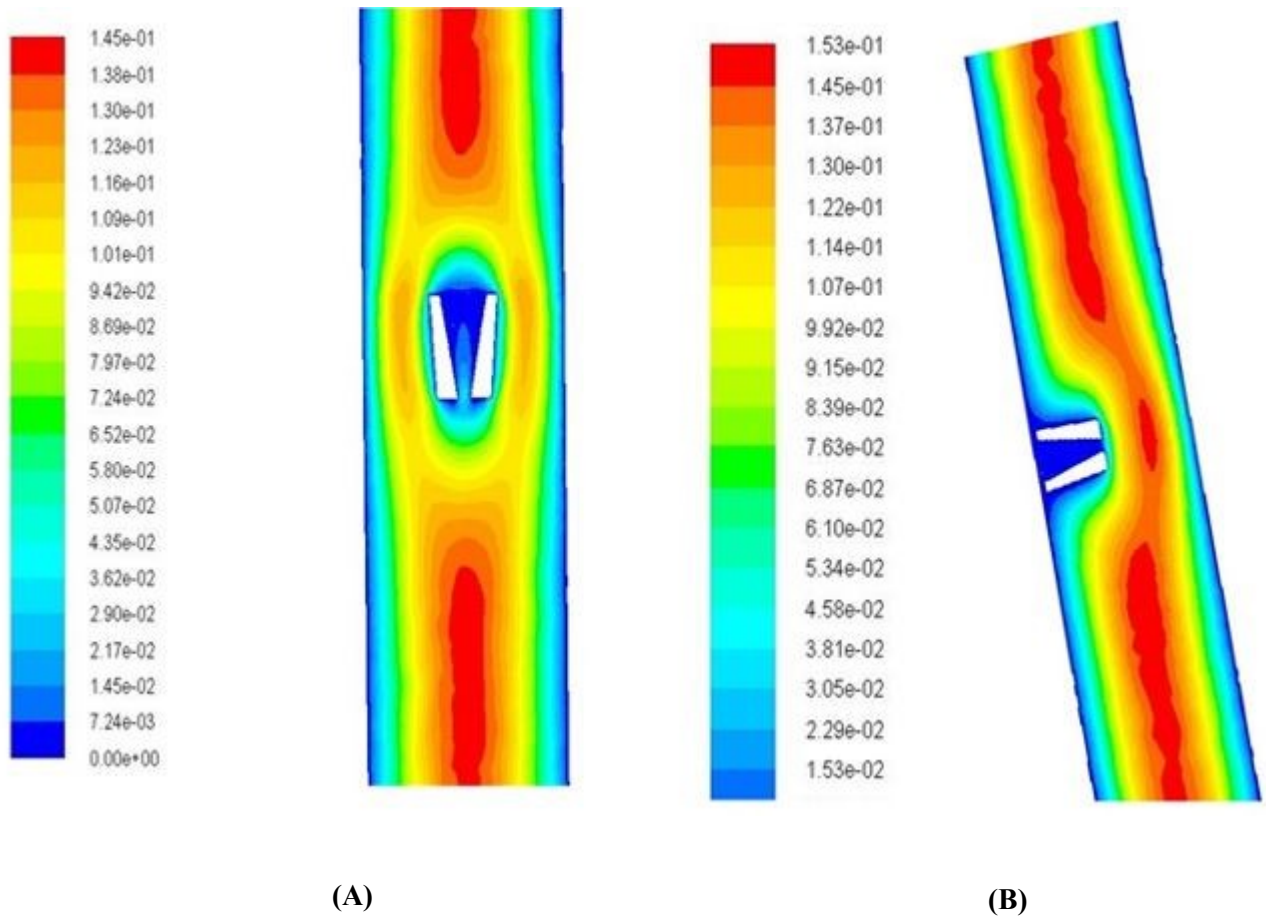
Fig.4.8. Velocity distribution around hollow frustum in (A) vertical and (B) inclined plane

4.6. Conclusions

The through experimental study on Newtonian flow over hollow frustum for terminal velocity and drag coefficient reveals that, at any particular *di/do*, the terminal velocity has been increased monotonically with the ratio of the frustum outer diameter and channel diameter, *do/D*. The increasing trend is just opposite of the decreasing trend of the drag coefficient of the regular shaped solid particles. The terminal velocity of the hollow frustum has been increased with decreasing the *di/do* ratio, for a constant *do/D*. The terminal velocity of the frustum has also been increased due to increasing the downward body force with increasing the angle of inclination. The drag

experienced by the hollow frustum for the inclined channel has been reported in the form of the drag coefficient, C_D estimated for $0.13 \leq Re \leq 8.41, 0.19 \leq d_o/D \leq 0.33, \; 0.22 \leq d_i/d_o \leq 0.83$ and $40^o \leq \theta \leq 90^o$. The C_D values have shown increasing trend with decreasing the angle of inclination of the channel. Appropriate predictive correlation for C_D as a function of *Re, di/do, do/D* and θ has been developed using the least square method. The angle of inclination and fluid viscosity sensitive $C_D Re$ term has shown a declining trend with the *do/D* ratio. The variation of C_D with 1/*Re* has shown linear variation at lower angles of inclinations.

CHAPTER 5

EXPERIMENTAL FINDINGS AND ANALYSIS OF TERMINAL VELOCITY AND DRAG COEFFICIENT OF HOLLOW CYLINDER IN VERTICAL AND INCLINED PLANE

Introduction

In the case of a hollow cylinder, the wetted surface area is more than the solid cylinder. A larger resistance is therefore expected to be experienced by the hollow cylinder while falling through a confined fluid. In spite of abundant available literature on the hydrodynamics of fluid flow over solid particle, no attempts were made earlier in regards to the estimation and reporting of the terminal velocity and drag coefficient of any hollow object. Hence, it is thus safe to claim the novelty of the present work where hollow cylinder is taken as an obstacle, and the pure glycerin and its aqueous solutions are used as flow media. The following objectives are undertaken for this study to fill the void and to accessorize the literature.

- To show the effect of the angle of inclination, outer diameter to inner diameter ratio (di/do) of the hollow cylinder and the outer diameter of the hollow cylinder to the flow channel diameter ratio (do/D) on measured terminal velocity and drag coefficient, C_D.

- Prediction of drag coefficient with the developed correlation of it as a function of $Re, di/do$, do/D and θ.

- Prediction of Drag coefficient using numerical model available in Ansys Fluent v15.

5.1. Physics around particle

The forces acting on a moving hollow cylinder in an inclined channel as shown in Fig. 5.1 are drag force, F_D, sine component of the body weight force $(F_B \sin \theta)$, solid–solid resistance (F_R) and the weight of the hollow cylinder (W). The rolling resistance is negligible here for the smooth plane. The force balance equation at equilibrium is

$$F_B Sin\theta = F_D + F_R \tag{5.1}$$

The expression of drag force is

$$F_D = \frac{1}{2} C_D \rho_F V^2 A \tag{5.2}$$

Substitution of Eq. 2 in Eq. 1 gives the following expression for C_D

$$C_D = \frac{mg(1-\frac{\rho_F}{\rho_p})}{0.5AV^2\rho_F} sin\theta \tag{5.3}$$

For vertical plane consideration Eq. 3 is reduced to

$$C_D = \frac{mg(1-\frac{\rho_F}{\rho_p})}{0.5AV^2\rho_F} \tag{5.4}$$

In general, C_D is a function of the Reynolds number, diameter ratios (*di/do* and *do/D*) and angle of inclination. Mathematically,

$C_D = f\,(Re,\, do/D,\, di/do, \theta)$

Where Reynolds number is $Re = \rho_F(d_O - d_i)V/\mu$.
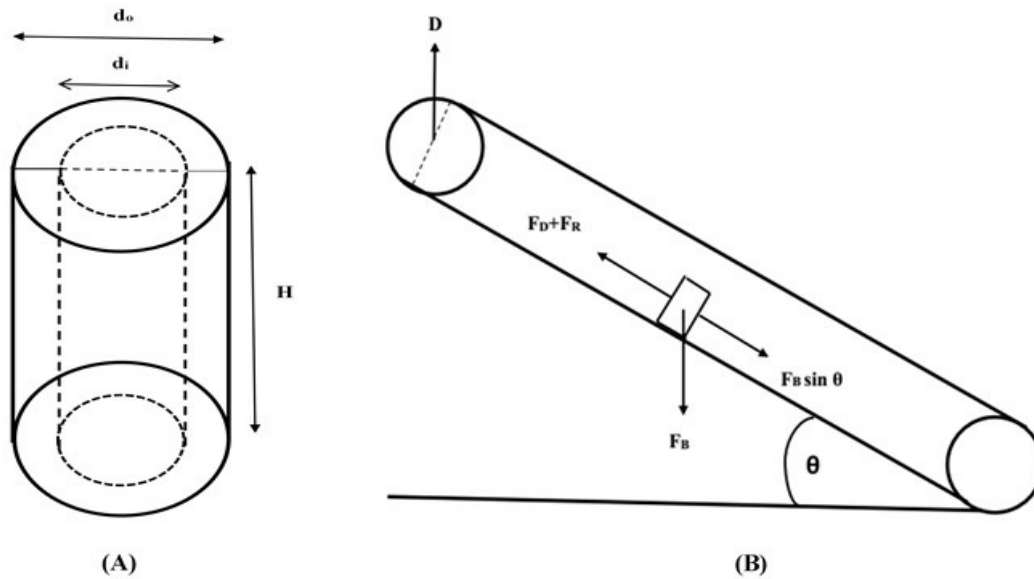
Fig.5.1. Schematic representation of flow over hollow cylinder in (A) vertical and (B) in inclined channel

5.2. Experimental

Hollow cylinders (SS 304L) of density 7859.56 kg/m^3 are machined in wire EDM (Electrical discharge machining) to use as hollow obstacles in 30.1×1200 mm circular Perspex tube. The sizes of the hollow cylinders are listed in Table 5.1. The rheological properties of test fluids are listed in Table 5.2. Rheometer (RheolabQC, Anton Parr, Germany,) is used to measure the viscosity of the fluids, and densities are measured by the pycnometer.

Table 5.1

Physical dimensions (all are in mm) of hollow cylinder

Sl. No.	d_o	d_i	H
1	10	7	
2	10	5	
3	10	3	
4	9	7	
5	9	5	12
6	9	2	

7	6	5	
8	6	3	
9	6	2	

Table 5.2

Physical properties of test fluids

Soln. No.	Fluid	Temperature (K)	Density (kg/m^{-3})	Viscosity (Pa.s)
1	100% Glycerin	298	1257.09	0.7533
2	98% Glycerin	298	1251.906	0.5378
3	96% Glycerin	298	1246.723	0.4025
4	94% Glycerin	298	1241.539	0.3054
5	92% Glycerin	298	1236.356	0.2606
6	90% Glycerin	298	1231.172	0.2094

The Perspex tube is supported on a plywood frame. The angles (90^0-40^0) are measured from a fixed end, and the hooks are clamped at every angular position. The movable end is shifted from one angle to other for different tube inclinations. The schematic representation is shown in Fig. 5.1 (B). The test fluids were loaded 24hrs before to make the fluid bubble free [17, 18]. The test location is taken sufficiently away from the inlet to avoid the entrance effect on the terminal velocity. The hollow cylinders are released by forceps and stopwatch is used to measure settling time. Every experiment is repeated for five times and mean settling time is taken for the calculation of terminal velocity.

5.3. Result and Discussion

5.3.1. Variation of Terminal Velocity

The initial manifesto of the work is to understand the variation of terminal velocity with *di/do* and *do/D*. For this objective, the variation of it is shown in Fig. 5.2 for both the diameter ratios. At any particular *do/D*, it shows an increasing trend with decreasing *di/do*. The thickness

of the hollow cylinder increases with decreasing *di/do*, which increases the body weight and results in higher terminal velocity. In this work, the channel diameter is kept fixed; hence, the *do/D* is varied by altering only the outer diameter of the hollow cylinder. Fig. 5.2 also shows an increasing trend of velocity with increasing the *do/D*. The studies in [7, 14] showed a decreasing trend of velocity with increasing the diameter ratio (*d/D*) for the cylindrical and conical object. Thus the present study contended their observations. A reason may be drawn in respect of this deviation is, in previous studies, the channel diameter, *D* was varied while the obstacle diameter was fixed, hence for higher *d/D* an additional retardation force was applied on the flow path due to the wall, thus lesser velocity was obtained. However, in the current study, the diameter ratio *do/D* is varied due to changing of *do* keeping *D* fixed. As a result of increasing the weight of the hollow cylinder, the terminal velocity increases with *do/D* ratio. The effect of angle of inclination, θ on terminal velocity is shown in Fig. 5.3 for pure glycerin. The terminal velocity gradually increases with increasing the θ because of the increase of the downward body weight component $F_B sin\theta$. The same states of results are observed for other working fluid.
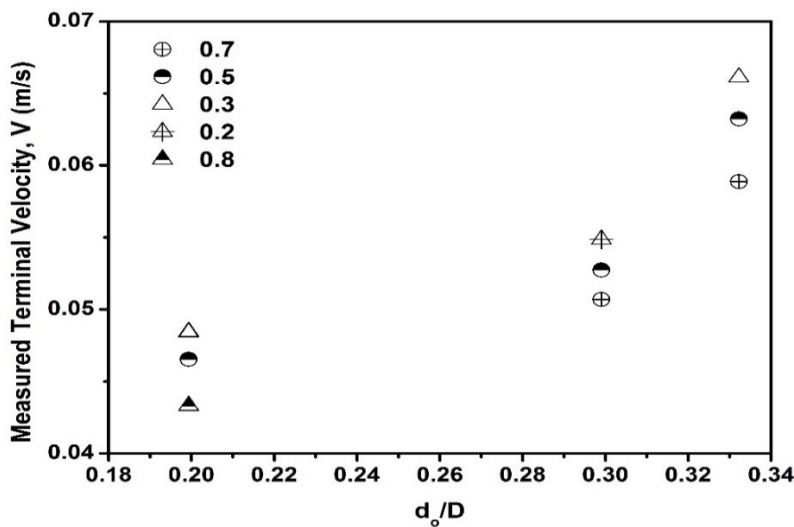
Fig.5.2. Variation of terminal velocity with *di/do* and *do/D* in pure glycerin for vertical channel
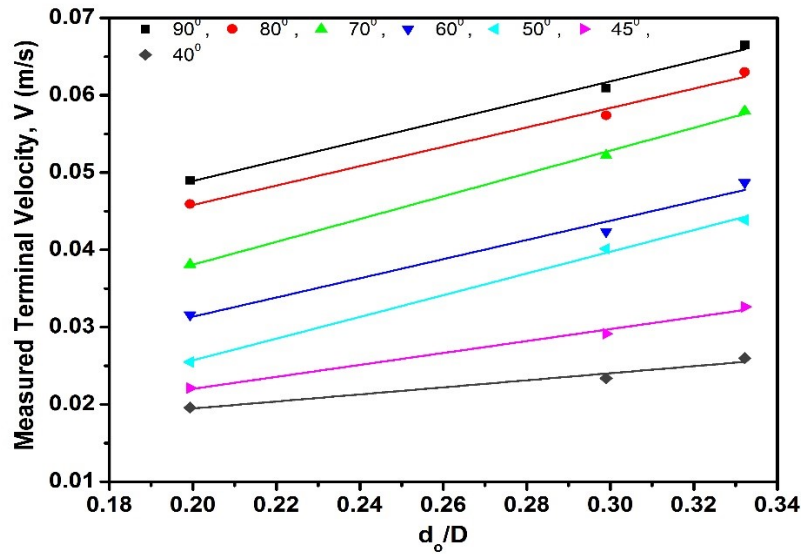
Fig.5.3. Variation of terminal velocity with *do/D* and tube inclination in pure glycerin (R^2 >0.98)

5.3.2. C_D – Re Relationship

The obtained C_D and *Re* from the fundamental properties of a hollow cylinder and test fluid are plotted in Fig.5.4.The test fluids are high viscous. Hence the expected linear decreasing trend of C_D with the Reynolds number is observed. The orientation of the hollow cylinder in Fig. 5.1(A) is vertical for the vertical flow channel, which gives lesser projected area but high terminal velocity with maximum C_D. Having horizontal orientation of the hollow cylinder shown in Fig. 5.1 (B), the other flow channel inclinations produce higher projected area and also lesser downward body force. The decreasing trend of the terminal velocity leads to an increasing trend of the drag coefficient as tube inclinations decreases from 80º to 40º.

Hasan [44] developed a correlation for the estimation C_D, under the scope of *d/D* < 0.707, $C_D Re =$ 15.717$\{1 - (d/D)\}^{-2.5}$ (5.5)
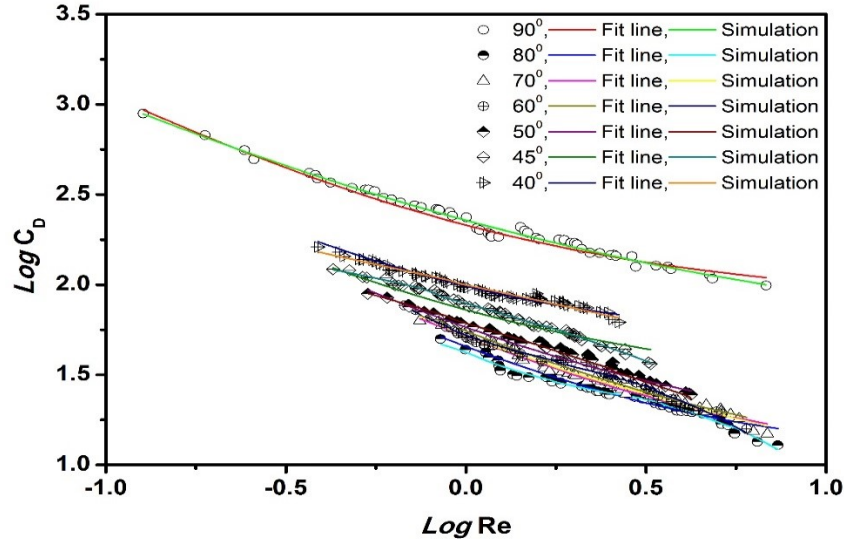
Fig.5.4. C_D-*Re* relationship

In Eq. (5.5) Hasan [44] did not include the effect of angle of inclination. Hence, in this work, a correlation in the form of Eq. (5.6) Is proposed as a function of *di/do*, *do/D* and *Re* for individual tube inclination. An iterative least square method is employed to obtain the coefficients *A*, *B*, *C*, *E* and *F* of Eq. (5.6) for any arbitrary selection of *n*, *m,* and *k*. The best values of the parameter to achieve regression coefficient $R^2 \geq 0.98$ are given in Table 5.3. The R^2 values confirm the reliability and viability of the proposed correlations. The flow channel inclination dependent expressions of the coefficients are given in Table 5.4. The estimated very less magnitude of *E* and *F* as compared to *A* and B confirms quite less dependence of the drag coefficient on *di/do* and *do/D* ratios than the Reynolds number. This analysis agrees with the conclusion drawn by Chhabra et al. [18].

$$C_D = A + BRe^{-1} + CRe^n + E\left(\frac{d_i}{d_o}\right)^m + F\left(\frac{d_o}{D}\right)^k \tag{5.6}$$

Table 5.3

Obtained coefficients of Eq. (5.6) for a different angle of inclination, θ

θ	A	B	C	E	F	n	m	k	R^2
90	0.0075638	-113.766366	105.3304	1.120224	1.12248416	-0.3	-0.01	-0.7	0.995
80	0.134166	-40.599092	10.17856	0.01344	0.172592	-0.1	-0.05	-0.1	0.981
70	0.128502	-44.327188	12.506928	0.001232	0.578704	-0.1	-0.8	-0.4	0.994
60	0.148798	-53.938516	13.634768	0.1232	0.13272	-0.3	-0.6	-0.3	0.986
50	0.132632	-48.952956	22.383648	0.251552	0.438368	-0.01	-0.8	-0.4	0.991
45	0.198358	-57.501293	38.305232	0.068432	0.108304	-0.7	-0.1	-0.8	0.986
40	0.007198	-53.495556	47.20632	0.012432	0.619024	-0.01	-0.01	-0.3	0.993

Table 5.4 Relationships among the coefficients of Eq. (5.6) and angle of inclination, θ

Coefficient	Fitting line equation
A	$0.5869e^{\left(-((\theta-47.21)/1.836)^2\right)} + 0.1344e^{\left(-((\theta+67.5)/18.36)^2\right)}$
B	$-49.11e^{\left(-((\theta-51.11)/33)^2\right)} - 7.32 \times 10^{16}e^{\left(-((\theta-504.2)/70.69)^2\right)}$
C	$1.544 \times 10^{42}e^{\left(-((\theta-750.3)/68.61)^2\right)} - 5.976 \times 10^{26}e^{\left(-((\theta+1954)/262)^2\right)}$
E	$1.532e^{\left(-((\theta-94.22)/6.47)^2\right)} - 0.2072e^{\left(-((\theta+53.37)/6.773)^2\right)}$
F	$2.539 \times 10^6 - 3.366 \times 10^6 \cos(0.001679\theta) - 3.614 \times 10^5 \sin(0.001679\theta) + 8.273 \times 10^5 \cos(0.001679\theta) + 1.797 \times 10^5 \sin(0.001679\theta)$
n	$-7.243 \times 10^7 + 9.656 \times 10^7 \cos(-0.0003535\theta) - 1.729 \times 10^6 \sin(-0.0003535\theta) - 2.413 \times 10^7 \cos(-0.0003535\theta) + 8.646 \times 10^5 \sin(-0.0003535\theta)$
m	$3.827 \times 10^9 - 5.102 \times 10^9 \cos(0.0002293\theta) - 8.04 \times 10^7 \sin(0.0002293\theta) + 1.275 \times 10^9 \cos(0.0002293\theta) + 4.019 \times 10^7 \sin(0.0002293\theta)$
k	$1.146sin(0.04752 \times \theta + 0.7786) + 0.7248sin(0.08552 \times \theta + 1.001)$

According to Eq. (5.5), $C_D Re$ is a function of d/D ratio. In order to verify this for 90^0 and 40^0; the variation of $C_D Re$ with do/D is shown in Fig. 5.5. A decreasing trend of $C_D Re$ is observed with increasing fluid viscosity. The variation of C_D with the inverse of Reynolds number, $1/Re$ is shown in Fig.5.6, which shows a linear profile for all tube inclination. The range of $1/Re$ confirms the collected data are in the laminar region of Newtonian flow.
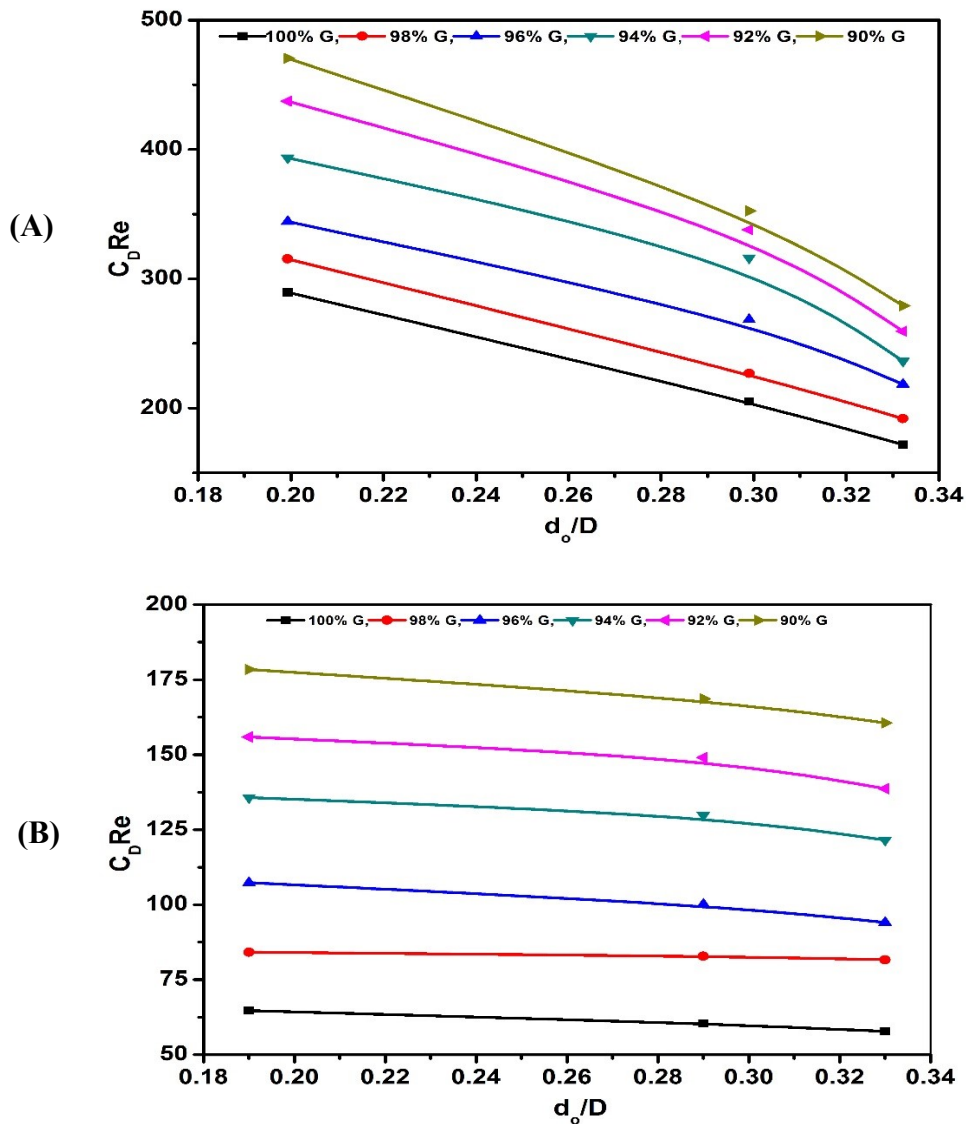
Fig.4.5. Dependency of $C_D Re$ on do/D and the viscosity of fluid for (A) 90^0 and (B) 40^0 angle of inclination at di/do=0.4
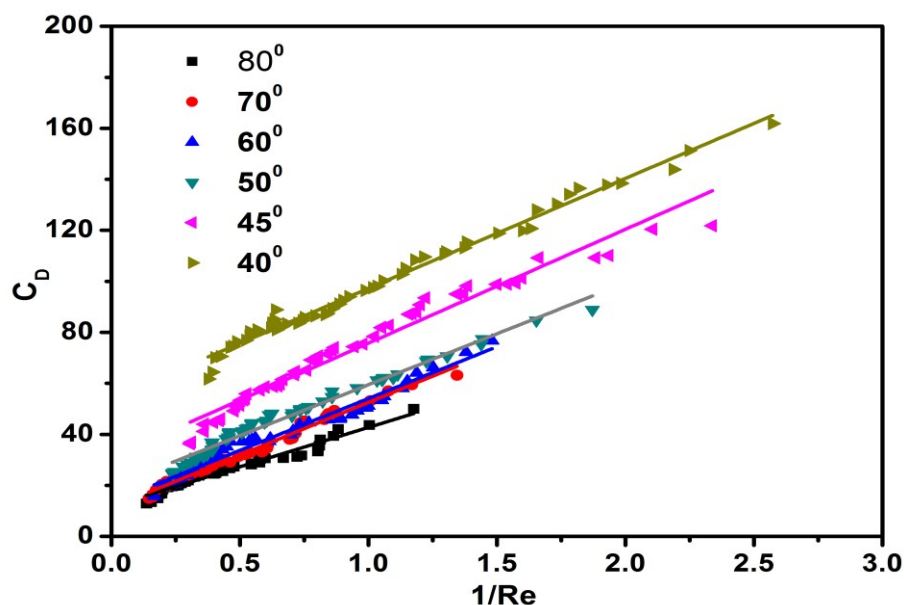
Fig.5.6. Inverse relationship of *Re* with C_D

5.4. Comparison with solid circular cylinder

Unnikrishnan and Chhabra [7] developed an empirical equation for the estimation of drag coefficient of solid circular cylindrical particle, which is

$$C_D = \frac{17.5}{Re} \left(1 + 0.68 Re^{0.43}\right) \tag{5.7}$$

To compare the drag coefficients of hollow and solid cylinder for the vertical channel orientation, Eq. 5.7 is employed to find the C_D for the solid cylinder at any particular *Re*. The comparison is shown in Fig. 5.7. The figure depicts that the C_D values are higher for hollow cylinder than solid cylinder at any particular Re owing to lesser projected area and lesser body weight, which results in lesser terminal velocity. Also, due to the higher wetted surface area, the hollow cylinder experiences higher resistance during free falling than the solid cylinder, hence, the drag coefficient for the hollow cylinder is higher than the solid cylinder.
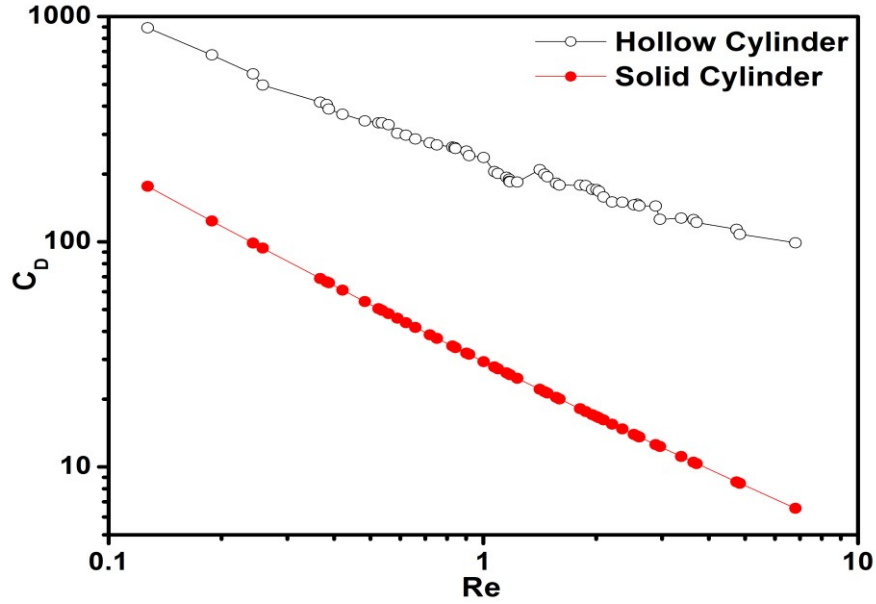
Fig.5.7. Comparison of drag coefficient between hollow cylinder and solid cylinder Unnikrishnan and Chhabr [13]

5.5. Prediction of Drag Coefficient through Numerical Approximation

5.5.1. Model Equations and Geometry

In the present study, the experimental data of the drag coefficient are predicted by Ansys Fluent v15.0. The following steady state model equations are used for the incompressible Newtonian fluids under consideration in the present study.

$$\nabla.(\rho u) = 0 \tag{5.8}$$

$$\nabla.(\rho uu) = -\nabla P + \nabla \tau + \rho_F g \tag{5.9}$$

Where ρ_F is the fluid density, u is the velocity of the fluid, P is the pressure, τ is the stress tensor and, g is the acceleration due to gravity.

(A)

(B)
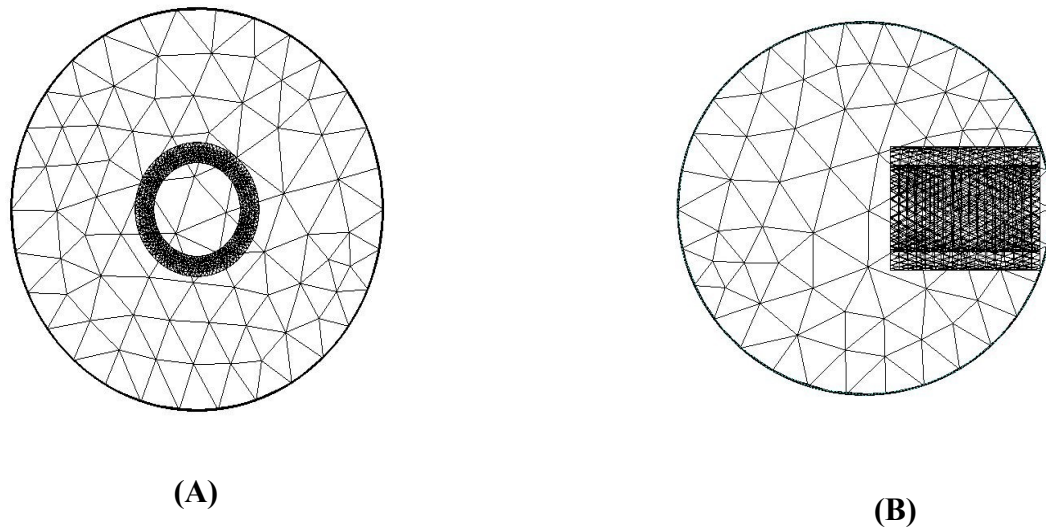
Fig.5.8. Top view of the generated mesh for (A) vertical plane and (B) inclined plane

The meshed geometries prepared in Ansys Workbench are shown in Fig. 5.8 (A) and (B) for the vertical and inclined flow channels, respectively. In the vertical channel, the vertically oriented hollow cylinder is placed symmetrically at the center of the channel. But for the inclined channel, the horizontal cylinder is placed off-centered at the mid-height of the channel. The exact off-centered location of the hollow cylinder is determined by adjusting its position to match the experimental data. In the present study, at all the channel inclinations and diameter ratios, the hollow cylinder is kept 0.4598 mm away from the wall.

5.5.2. Boundary Conditions

The inlet velocity in the flow direction is specified as the terminal velocity. The surface is opposite to inlet assigned as pressure outlet boundary with specified zero gauge pressure. The no-slip condition is imposed on the channel and hollow cylinder walls. For inclined channel, the acceleration due to gravity is used as *gsinθ*.

5.5.3. Solution Methods

The experimental results are in the range of laminar and early transition zone, hence to achieve the best and consistent results over the ranges of *Re*, various models including laminar flow model available in Ansys Fluent are tested. Up to Reynolds number 1.81, both the laminar and Reynolds Stress Model (RSM) models predict the experimental drag coefficient equally well, but RSM is found as a better model for higher Reynolds number. Overall, the predicted drag coefficient using RSM is presented in this work. The default values of the RSM parameters are used in the present study. SIMPLE algorithm and the second order upwind scheme are chosen for the faster convergence and higher accuracy. The convergence criteria are kept 0.00001 for all the flow variables.

5.5.4. Mesh Independency Test

Meshing is very important for the solution purpose and the sensitivity on the mesh quality and quantity affect largely the results. The triangular meshes with fine relevance center and high smoothing are chosen. In order to get fine mesh quality, an additional feature i.e. the *Relevance* is increased with a periodic increase of 10 for automatic refinement of the existing mesh. After 80-relevance center, no further improvements in the results are noticed. The number of nodes and elements are varied along with the diameter ratio. The mesh independency tests are carried out for the optimum grid. In Table 5.5 the changes of C_D values with grid is given for *Re* = 1.380161, *do/D*= 0.33 and *di/do*=0.7. This schema is also tested for other Reynolds numbers, *di/do* and *do/D*.

Table 5.5 Mesh independence test for *Re*= 1.38, *do/D*= 0.33 and *di/do*=0.7, Experimental value 84.83

No. of Elements	No. of Nodes	C_D
217001	41007	80.07
235369	44487	81.19
259687	49256	82.16
316613	59728	83.50
394993	73796	84.68
450802	83586	84.74

5.5.5. Discussion of the Predicted results

The experimental terminal velocity is used as the inlet velocity of the working fluid. The simulation results for all the channel inclinations are compared successfully with the experimentally obtained drag coefficients in Fig.5.4. Fore and aft symmetry is observed in Fig.5.9 for both the vertical and inclined channels. It confirms the laminar flow behavior of fluid flow over the hollow cylinder, and it accords the experimental laminar flow regime according to the Reynolds number. The prediction of drag coefficient with negligible errors confirms the viability and applicability of the numerical models available in the Ansys Fluentv15.0 for both the vertical and inclined flow channels.

(A)

(B)
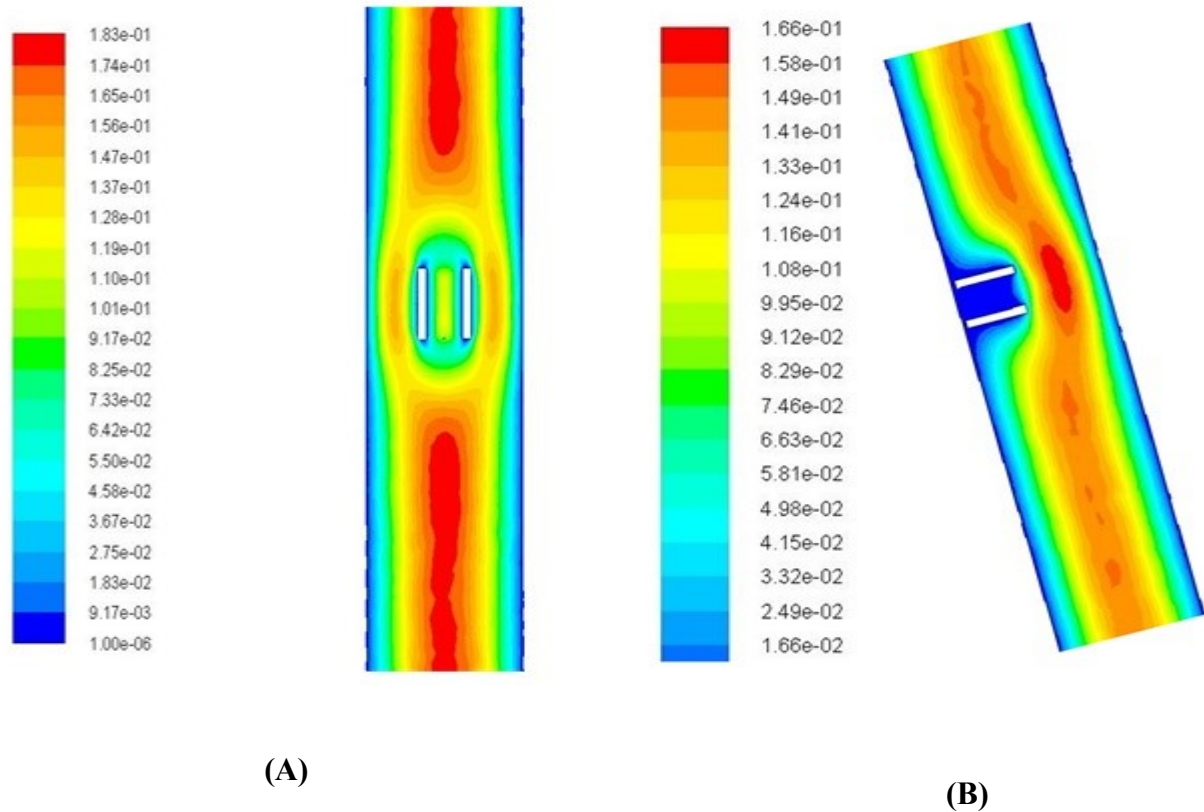
Fig.5.9. A generalized axial view of velocity distribution over hollow cylinder in (A) vertical channel and (B) inclined channel

5.6. Conclusions

The terminal velocity and drag coefficient of hollow cylinder flowing through Newtonian fluids in vertical and inclined channels are estimated experimentally. The correlations for the drag coefficient are developed for individual tube inclination as a function of *di/do*, *do/D* and *Re* using iterative least square method. The effect of system parameters like Reynolds number, diameter ratios and angle of inclination on the terminal velocity and drag coefficient are exhibited. The terminal velocity, *V* of the hollow cylinder increases with decreasing *di/do*. The increasing trend of *V* with *do/D* ratio for the hollow cylinder is opposite of the trend obtained for cone and cylinder object. Owing to increase of the downward body force component, the hollow cylinder terminal

velocity increases with increasing the angle of inclination, θ. The drag coefficient of the hollow cylinder decreases linearly with Re, which agrees with the trend of the other regular shaped object available in the open literature. This study confirms the lesser effect of di/do and do/D on C_D, for the scope of $0.19 \leq di/do \leq 0.33$ and $0.22 \leq do/D \leq 0.83$ than Reynolds number. The product of C_D and Re decreases with the viscosity of the working liquids and increases with the angle of inclination. The linear C_D vs. $1/Re$ plot confirms the expected trend in the laminar flow state. The Reynolds Stress Model available in Ansys Fluent predicts excellently the drag coefficient for both the vertical and inclined flow channels.

CHAPTER 6

A NUMERICAL STUDY OF THE WALL EFFECTS FOR NEWTONIAN FLUID FLOW OVER A CONE

Introduction

The through literature survey showed that, the availability of both the experimental and numerical results for the wall effect study of the regular shaped particles like a sphere, cylinder, spheroids, disk, etc. The studies predict the experimental data and also explain the effect of the Reynolds number, particle to flow channel diameter ratio and the non-Newtonian power law models parameter on the drag coefficient. Experimental results of the wall effect of the cone shaped particles are available in Sharma and Chhabra [14], but to the best of the authors' knowledge, no one has yet predicted these useful experimental data.

The aim of the present work is to fill the void in the literature. It predicts the effect of the Reynolds number and cone to flow channel diameter ratio on the wall factor due to flow over the cone. The effects of blockage ratio on the drag coefficient and wall factor are shown at the given values of unconfined Reynolds number (Re_∞). The validity of the $C_D\,Re^2{=}Constant$ relation is proved for the cone shaped body. The relative effects of the particle to channel diameter ratio of the sphere, cylinder and cone shaped particles on the drag coefficients, wall factors, velocity contours, recirculation length and angle of separation are found in the present work. The root cause of the variation of the drag coefficient and wall factors are also analyzed with the help of velocity contour plots.

6.1. Description of Physical System

In the present simulation study, the hydrodynamic behaviors of Newtonian fluid flow over the submerged cone shaped body are studied in terms of the finding the drag coefficient and wall effect. The geometry of cone shaped particles is the same to (Sharma and Chhabra [14]). The detailed physical specifications and properties of the cone and fluids are given in Table 6.1 and Table 6.2. The geometrical details of cylindrical (Unnikrishnan and Chhabra, [7]) and spherical (Ullhar and Chhabra, [6]) particles are also included in the table. The schematic representations of fluid flow over the particles of each shape are shown in Fig. 6.1. To vary the diameter ratio, the outer diameter i.e. flow domain diameter is changed with maintaining constant particle diameter. In this work, the solid particle will remain in static condition, while the fluid medium flows over the particle.

Table 6.1

Dimensions of cone, cylinder, and sphere

Material	d (mm)	L (mm)
Cone2 and Cone5 [14]		
Perspex (ρ_S =1204 kgm^{-3})	15.05	Cone2:17.31 Cone5: 7.10
Cylinder [7]		
Perspex (ρ_S =1204 kgm^{-3})	10	20,10,5,2.5
Glass (ρ_S =2409 kgm^{-3})	8	6,4.5
	6	3,2
Sphere [6]		
Perspex (ρ_S =1204 kgm^{-3})	15.05	

Table 6.2

Physical properties of working fluid

Material	Density (kg/m³)	Viscosity Pa. s
Cone [14]		
40% Corn Syrup+ Water	1136.4	0.003727
42.5 % Corn Syrup + Water	1147.0	0.00519
45 % Corn Syrup + Water	1153.5	0.005325
Castrol Oil	964.5	0.4008
Cylinder [7]		
100% Glycerin	1245.2	0.4903
Castrol Oil	964.5	0.406
Sphere [6]		
90% Glycerin	1233.6	0.2819
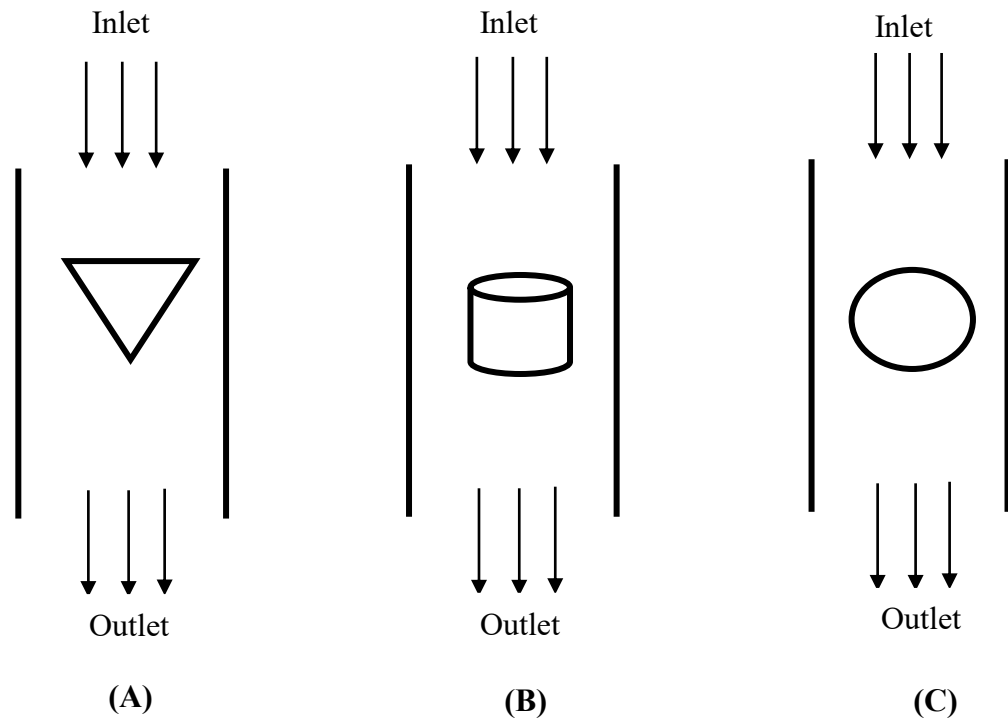
Fig. 6.1. Schematic diagrams of flow over **(A)** cone, **(B)** cylinder and **(C)** sphere

<p align="center">**(A)**   **(B)**   **(C)**</p>
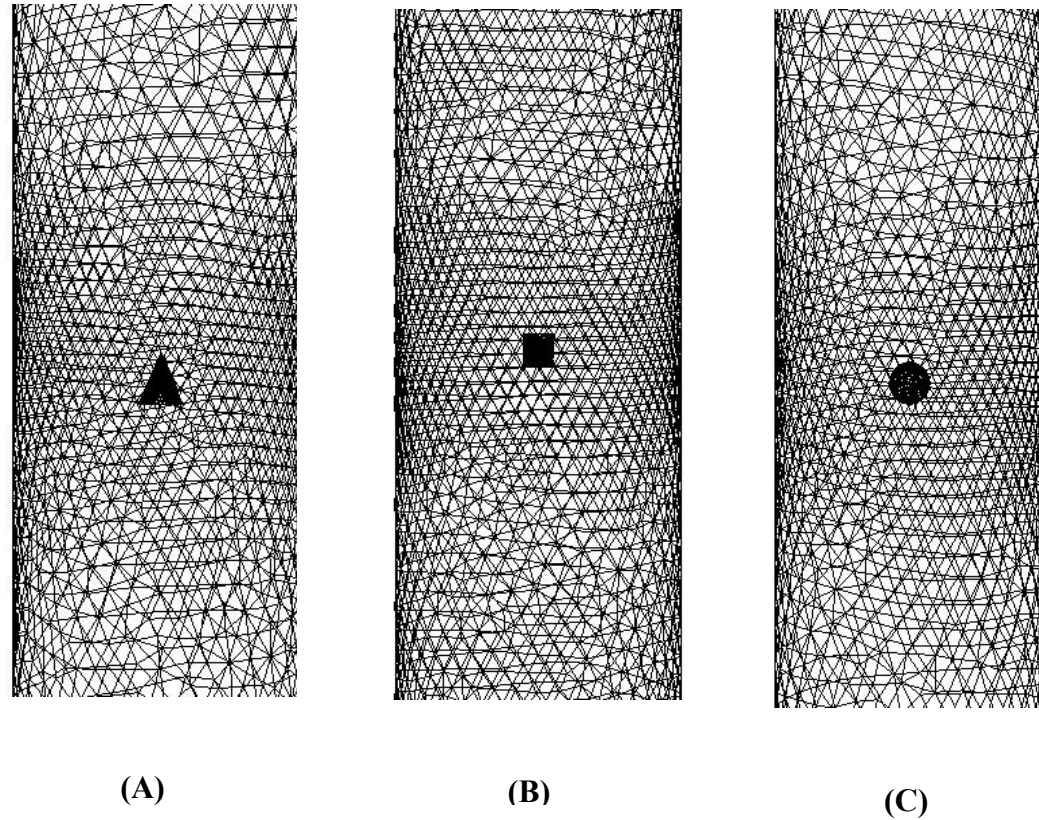
Fig. 6.2. Generated mesh for **(A)** cone, **(B)** cylinder and **(C)** sphere located axially in a cylindrical channel

The geometries of the cone, cylinder, sphere and flow domain are created using Design Modular (DM) of ANSYS Workbench. After defining the geometry, the meshing is important for the solution purpose. The element size, number of node and mesh are changed with the geometry and size of the submerged body, and body to flow channel diameter ratio. The display of mesh for the cone, cylinder, and sphere are presented in Fig. 6.2.

6.1.1. Model Equations

A steady and incompressible fluid flow of Newtonian fluid is considered over the submerged object. The equation of continuity and momentum equations are solved together to obtain the velocity and pressure fields. Based on the computed velocity and pressure fields the

drag coefficient is calculated using Eq. (1.3). The general form the continuity and momentum equations are

$$\nabla.(\rho u) = 0 \tag{6.1}$$

$$\nabla.(\rho uu) = -\nabla P + \nabla \tau + \rho g \tag{6.2}$$

where ρ is the fluid density, u is the velocity of the fluid, P is the pressure, τ is the stress tensor and, g is the acceleration due to gravity.

6.1.2. Boundary Condition and Solution Method

Steady state - pressure based solver of ANSYS Fluent is used herein. The gravitational force is made active in the direction of flow. The cell zone condition consists of either solid or liquid in the respective zone. The no-slip condition is used for boundary wall and solid particle. The inlet velocity is calculated from the Reynolds number equation and specified at the inlet of geometry. The gauge pressure at the outlet is taken as zero. All the available viscous models in FLUENT are tested to validate the experimental results. However, the most accurate and consistency results are obtained with Reynolds Stress Model (RSM) with the default values of $C_\mu = 0.09$, $C_{1\varepsilon} = 1.44$ and $C_{2\varepsilon} = 1.92$. SIMPLE algorithm is used as the simulation algorithm. The pressure gradient is discretized by the least square cell based scheme. The turbulent kinetic energy, turbulent dissipation rate and Reynolds stress are discretized by the second order upwind scheme for the iterative simulation. The default values of the under-relaxation factors are used in the present work. The convergence criteria are kept as 0.0001 for the residuals and drag coefficient calculation.

6.1.3. Mesh Independency Test

Meshing is very important for the solution purpose and the sensitivity of mesh quality and quantity affect largely on the results. The triangular mesh with fine relevance center and high smoothing are chosen. The generalized view of the mesh is given in Fig. 6.2. In order to get fine mesh quality, the relevance is increased for automatic refinement of the existing mesh. The number of node and elements are varied along with the blockage ratio. The mesh independency test is important before presenting the simulated results. In Table 6.3 the effect of a number of element and nodes on the drag coefficient are presented for Re = 0.8 at *d/D* = 0.015 for cone 2. The observation form the table shows that a small change in the value of the drag coefficient occurs for the finest grid (915674 elements) than the fifth grid with a number of elements 627842. However, the CPU time increased significantly with further increasing the number of elements. Thus, the fifth grid in the table is considered. Similar kind of study was carried out for other Reynolds number, and *d/D* ratio, and also for other geometries and the same optimum number of the grid is observed. All the simulations are performed in Intel i7, 4 GB RAM, and Windows 10 intergraded computer.

Table 6.3

Mesh independence test for cone 2 at Re = 0.8 and *d/D* = 0.015

| No. of Elements	No. of Nodes	C_D
246111	45912	22.09
312048	57791	22.88
398858	73194	23.20
533667	96785	23.79
627842	113066	24.56
915674	162402	24.61

6.2. Results and Discussions

6.2.1. Validation of Results

In the present study, the values of drag coefficients, C_D have been calculated for a wide range of Reynolds numbers and *d/D* ratios (0.01 <Re<30000 and 0.0015 < *d/D* <0.9) to find computationally the effect of *Re* and *d/D* on the drag coefficients of the cone. Before going to analyze and portray the new results, it is necessary to validate the computed drag coefficients. The current research work has presented the simulated data of the cones at the given conditions in Sharma and Chhabra [14]. Sharma and Chhabra [14] had compared the experimentally obtained $C_{D\infty}$ with the sphere $C_{D\infty}$ values in Eq. (6.3) Obtained by data fitting procedure. They found a good agreement between these two. In the same line, the computed $C_{D\infty}$ obtained with *d/D* = 0.0015 (low enough to consider $d/D \rightarrow 0$) for both the cones are compared in Fig. 6.3 and 6.4 for all the Newtonian fluids. The figures show that the correspondence is excellent for 40% corn syrup. The closeness of these curves with Eq. (6.3) results increases with decreasing the viscosity of the process fluid especially at higher *d/D* ratio. It may require decreasing the *d/D* further for the higher viscous fluids.

$$C_{D\infty} = \frac{17}{Re_\infty}(1 + Re_\infty^{0.806}) \tag{6.3}$$
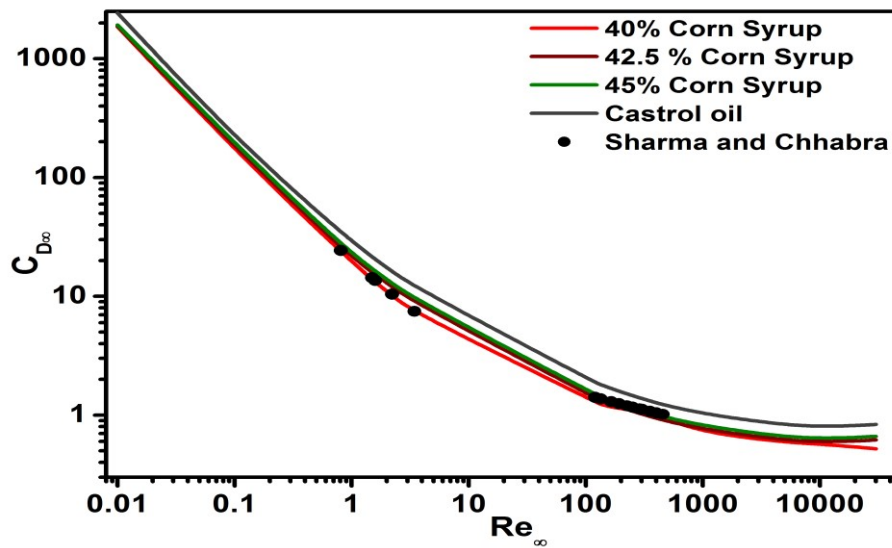
Fig. 6.3. Variation of drag coefficient with Reynolds number in unbounded flow (d/D=0.0015) for cone 2 in Newtonian fluid
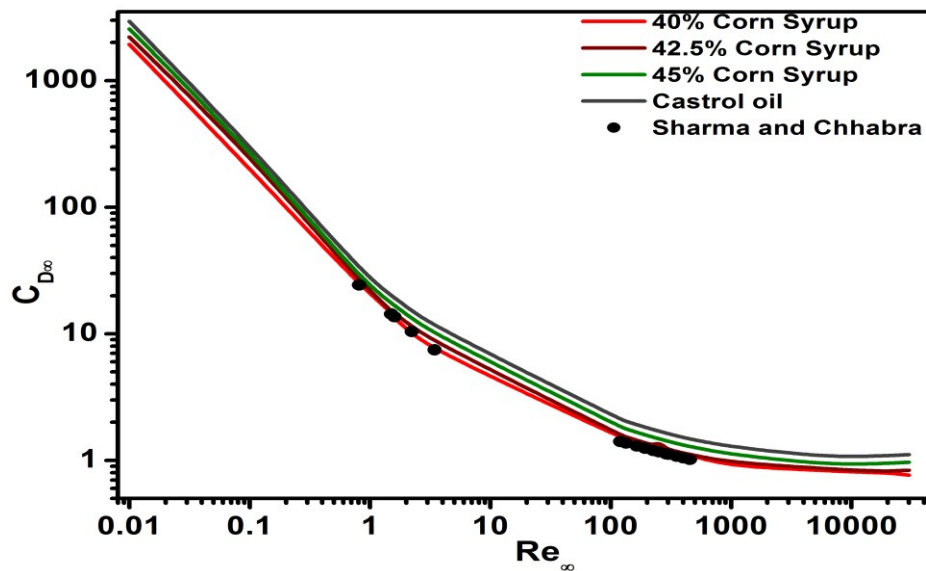
Fig. 6.4. Variation of drag coefficient with Reynolds number in unbounded flow (d/D=0.0015) for cone 5 in Newtonian fluid

6.2.2. Effect of Diameter Ratio and Reynolds Number on Drag Coefficient

To study the variations of C_D with the diameter ratio, the flow domain diameter is adjusted keeping the cone diameter constant. Eight *d/D* ratios i.e. 0.0015, 0.015, 0.03, 0.1, 0.15, 0.4, 0.6 and 0.9 are used for 40% corn syrup-water as the working fluid. The combined effects of the Reynolds number and *d/D* ratio on the drag coefficient are presented in Fig. 6.5 and 6.6. Similar trends are observed for other working fluids. The effect of Reynolds number on C_D is usual which follows the observations of Chhabra & Uhlherr [6] for Newtonian fluid flow over a sphere. The figures show higher drag coefficients at higher *d/D* ratio. These also show that below a certain *d/D* (say 0.015) the drag coefficient values are not significantly changing for further reduction (say 0.0015) of it. The flow area between the cone and the channel wall decreases, and simultaneously, the pressure drop across the cone increases with increasing the blockage ratio, *d/D*. The higher pressure drop produces higher frictional loss i.e. higher drag coefficient.

The computed drag coefficients and Reynolds number at the given settling velocity of cones Sharma and Chhabra [14] are placed in Fig. 6.5 and 6.6 which show that all the C_D – *Re* points, for a particular working fluid, lie on the same straight lines [fit Eq. (2.2)] having a slope of -2 Uhlherr and Chhabra [6]. Thus the C_D – *Re* data satisfy the theoretical relation given in Eq. (2.2).
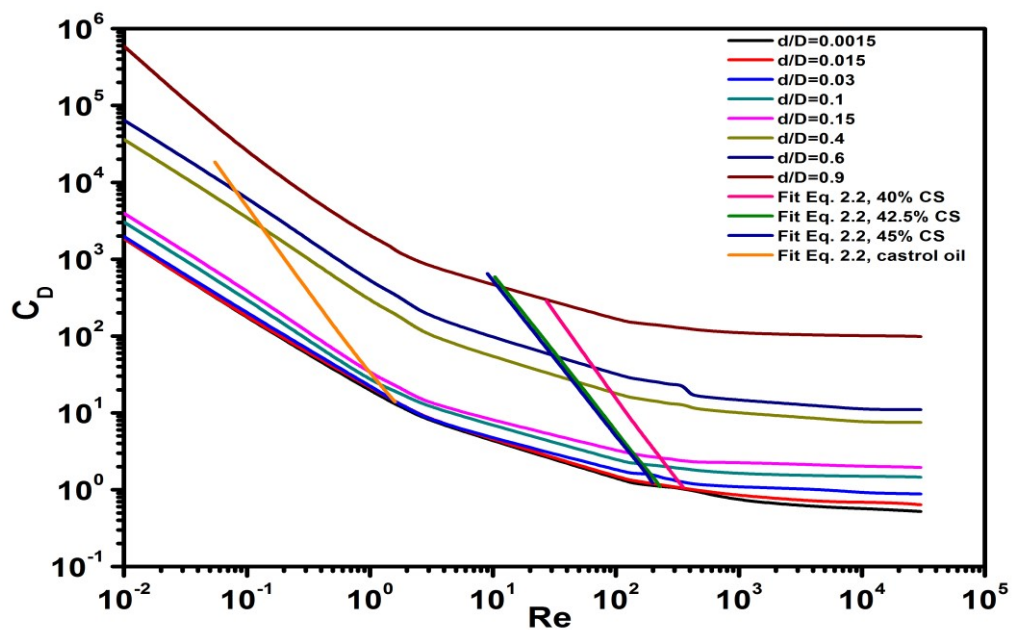
Fig. 6.5. Variation of drag coefficient with Reynolds number and diameter ratio in 40% CS for cone 2
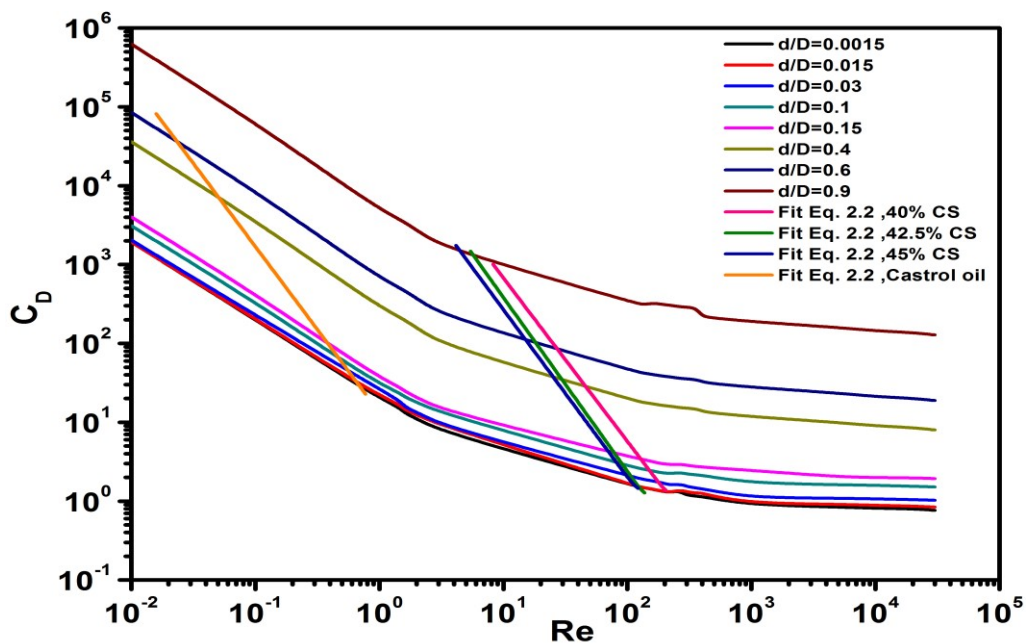

**Fig. 6.6.** Variation of drag coefficient with Reynolds number and diameter ratio in 40% CS for cone 5

6.2.3. Effect of Reynolds Number and Blockage Ratio, d/D on the Velocity Contours

The two-dimensional velocity contours depicted in Fig. 6.7-6.10 give some very important insights. The velocity profiles in Fig. 6.7 and 6.9 show that the flow is symmetric and potential, and there is no separation around the cone at very low Reynolds number (Re = 0.01). The drag force is all due to skin or frictional drag at Re = 0.01. As Reynolds number increases, separation of boundary layer occurs, and thus the total drag coefficient decreases due to a decrease of the skin friction and increase of inertial force. At very high Reynolds number (Re = 1000), an asymmetric flow is observed in Fig. 6.8 and more in the Fig. 6.10.

The figures also present the effect of d/D ratio on the velocity contours. At low d/D, more symmetric flow around the cones is observed where the flow streams around the cones remain unaffected by the boundary layer on the channel wall. Since the cone reaches closer to the channel wall at higher d/D = 0.4, there is an interaction between the flow stream of a cone with the boundary layer of the channel wall. It provides an extra retardation force to the flow of fluid. Thus, the drag coefficient increases with the d/D ratio.
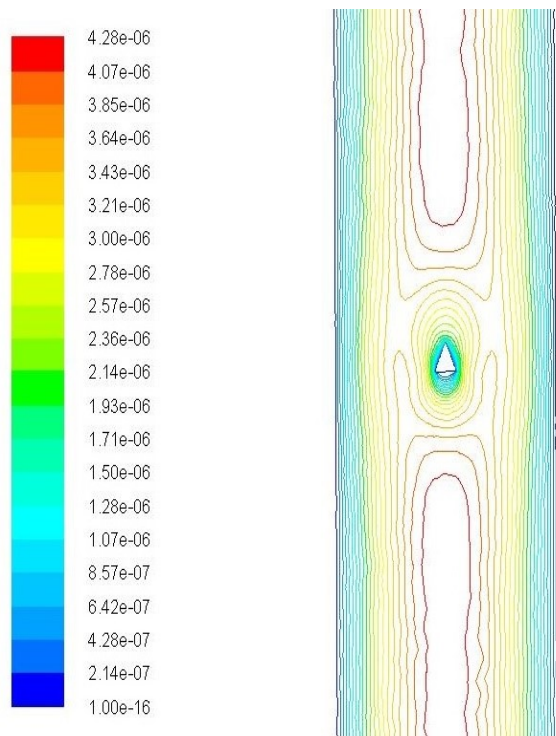
Fig. 6.7. Contours plot of axial velocity for *Re* = 0.01 at d/D = 0.1
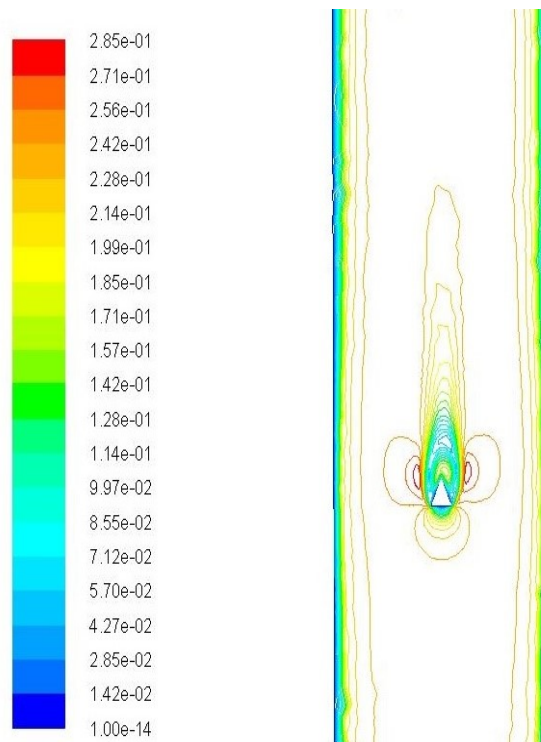
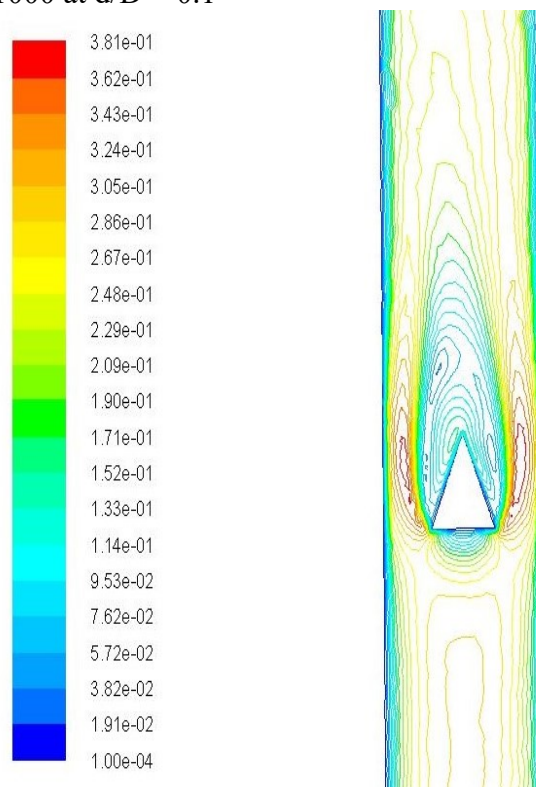**Fig. 6.8.** Contours plot of axial velocity for Re = 1000 at d/D = 0.1
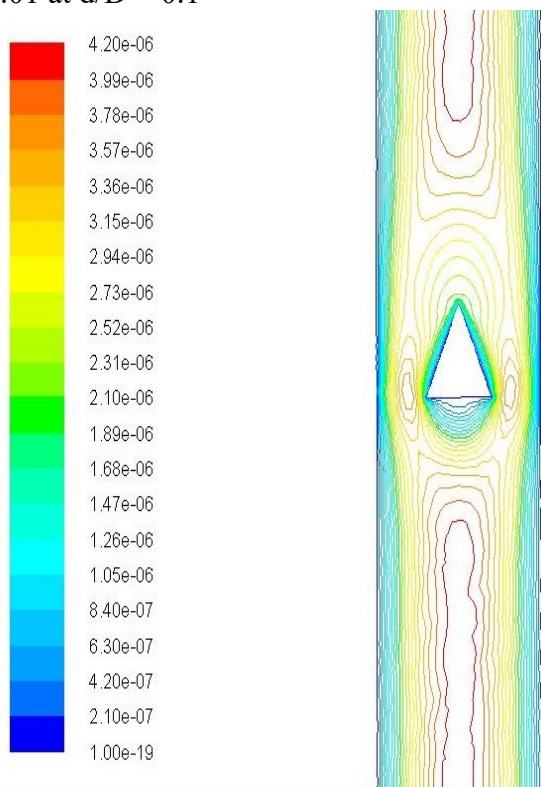
Fig. 6.9. Contours plot of axial velocity for Re = 0.01 at d/D = 0.4

Fig. 6.10. Contours plot of axial velocity for Re = 1000 at d/D = 0.4

6.2.4. Variation of the Wall Factors With Reynolds Number and Blockage Ratio

Sharma and Chhabra [14] had shown graphically the effect of the blockage ratio (maximum *d/D* = 0.4343) on the wall factor for *Re* < 1.0. However, their experiment covered a wide range of Reynolds number to find the terminal velocity distributions with *d/D*. In the present work, the wall factor, *f* is calculated from the given terminal velocities, and then the computed wall factors are compared with experimental values. An excellent agreement is observed between these two in Fig. 6.11. It also confirms the linear decreasing trend of the wall factor with *d/D* ratios. All the curves are intersecting at *f* = 1.0, which other way proves the accuracy of the predicted unconfined terminal velocity, V_∞. Closeness between the calculated and experimental V_∞ given in Sharma and Chhabra [14] is depicted in Fig. 6.12.

The wall factor, *f* are calculated from Fig. 6.5 and 6.6 along with the help of Eq. (2.1) and (2.2) at any chosen *d/D* ratio and Re_∞ (Reynolds number at V_∞). The method requires the C_D vs. *Re* plot of the unconfined flow. According to Fig. 6.5 and 6.6, there is no significant change in drag coefficient due to change of *d/D* from 0.015 to 0.0015, and hence, the C_D vs. *Re* curve for *d/D* 0.0015 is taken as the required $C_{D\infty} vs. Re_\infty$ curve for the unconfined flow. *V* and V_∞ are calculated from *Re* and Re_∞; substituting those in Eq. (2.2) gives the wall factor *f*. The variation of *f* with *d/D* using Re_∞ as the parameter is shown in Fig. 6.13. It shows the usual decreasing trend of *f* with *d/D*. The rate of change of *f* with *d/D* is higher at lower Re_∞, and the width of the variation of *f* becomes higher at higher *d*/D ratio.
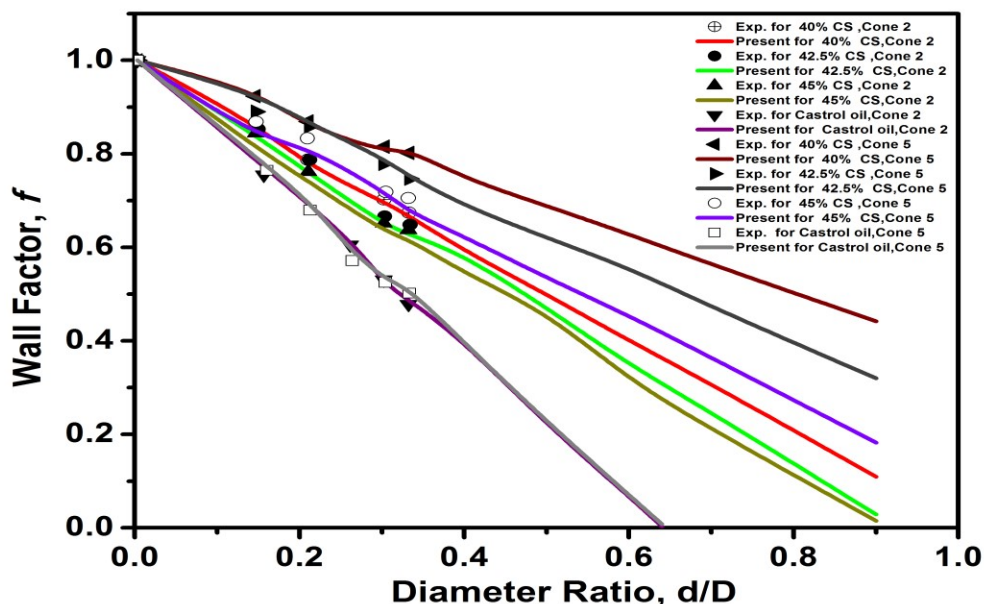
Fig. 6.11. Comparison between experimental (acquired from experimental velocity) and simulated (obtained from simulated velocity) wall factor with diameter ratio
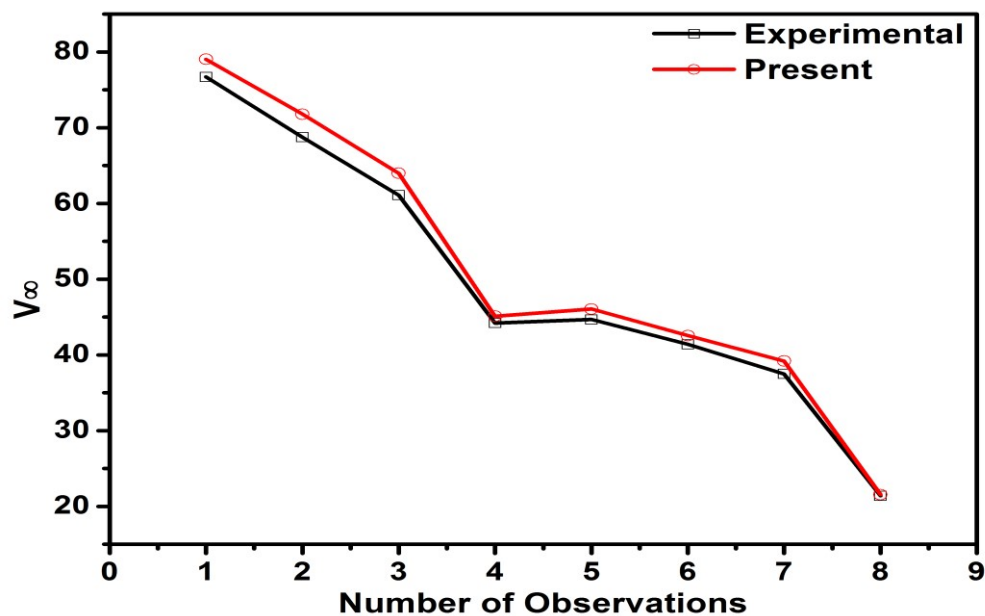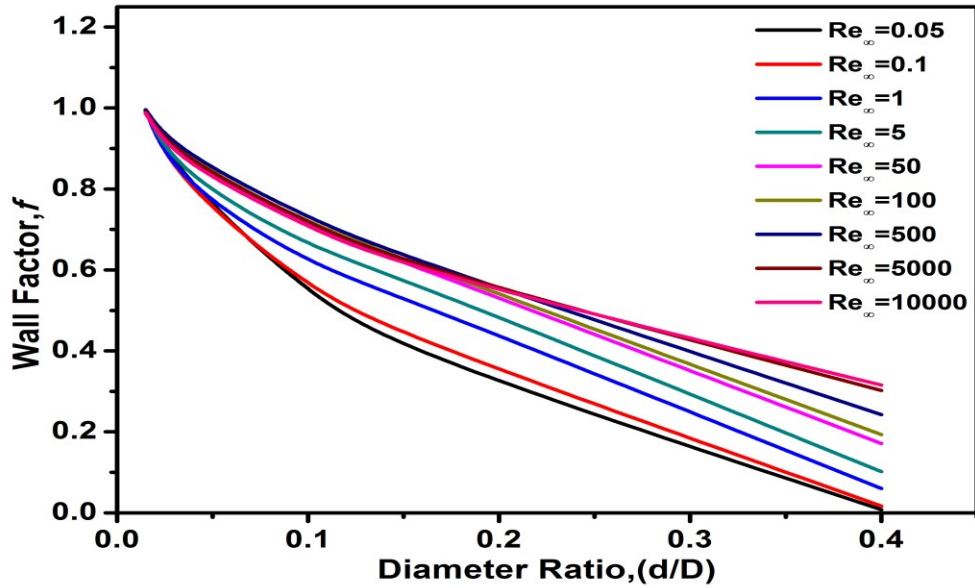

Fig. 6.12. Comparison between the experimental and simulated V_∞

Fig. 6.13. Variation of the wall factors with the diameter ratio and Re_∞ obtained from Fig. 6.5 by using Eq.(2.2)

6.2.5. Comparative Study of the Wall Factors of the Cone, Sphere, and Cylinder

The wall factor is also a function of the shape of submerged object. A comparative study of the wall factors of the spherical, cylindrical and cone-shaped particles are carried out at different *d/D* ratios in Fig. 6.14 – 6.16. All the figures show that *f* increases with Reynolds number in low *Re* region, finally reaching a constant value at higher *Re*. The trends are in accordance with the observations recorded by Sharma and Chhabra [14] for cone and Unnikrishnan and Chhabra [7] for the cylinder. The order of wall factor is cylinder > cone > sphere. The physical explanations of the order are given below.

The velocity contour plots in Fig. 6.17-6.19 at high Reynolds number, 100 shows an early separation of boundary layer for both the cylinder and cones as compared to the spherical body.

It results in the lowest C_D, and hence, the lowest f values for the sphere. Having relatively more streamlined shape, the cone produces less separation and less vortex (Fig. 6.19) than cylinder in Fig. 6.18. The cylinder, therefore, gives the maximum drag coefficient and simultaneously the wall factor.
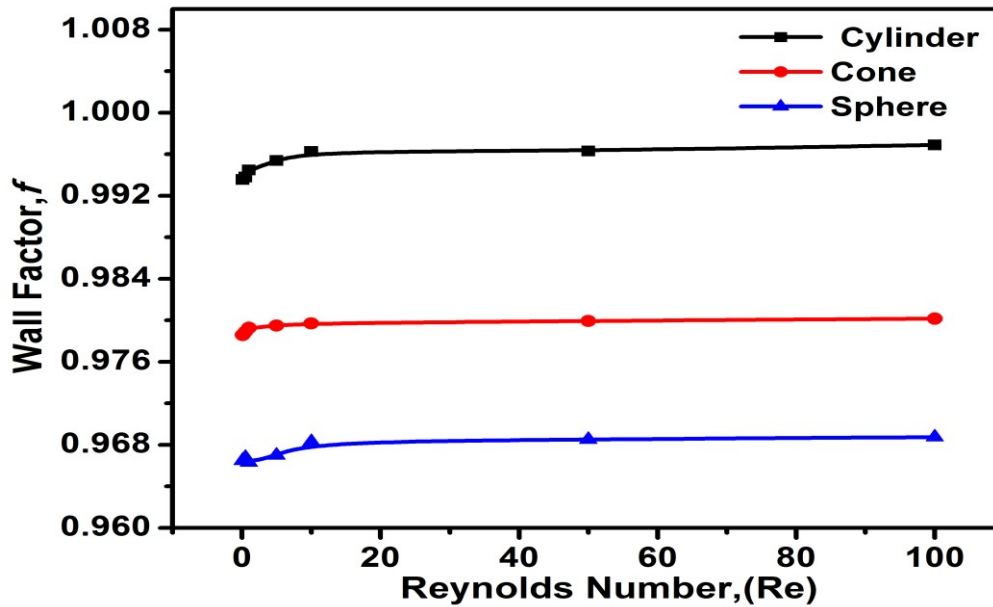
Fig. 6.14. Comparison of wall factors at d/D = 0.015 of cylinder, cone and sphere at different Reynolds number
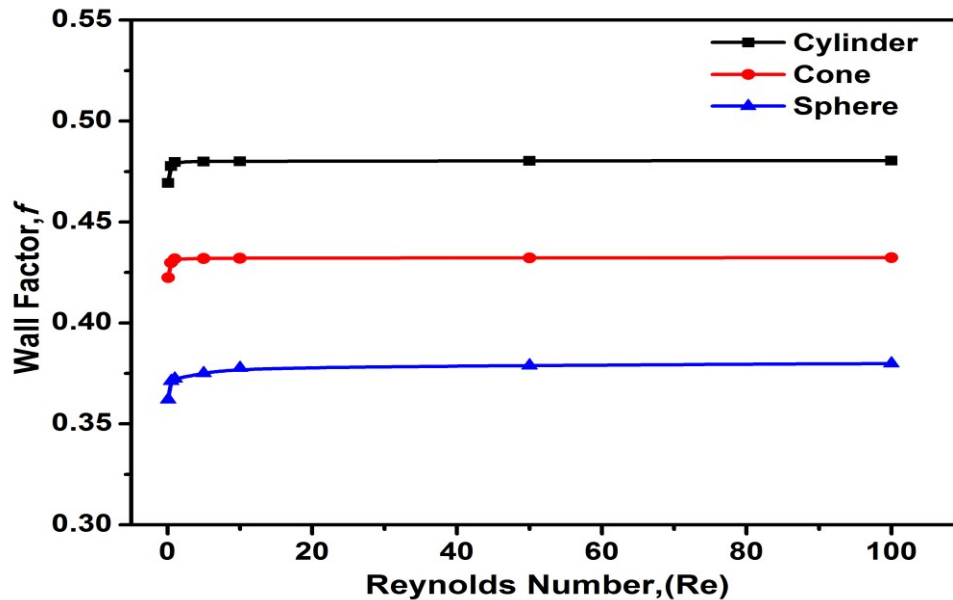
Fig. 6.15. Comparison of wall factors at d/D = 0.5 of cylinder, cone and sphere at different Reynolds number
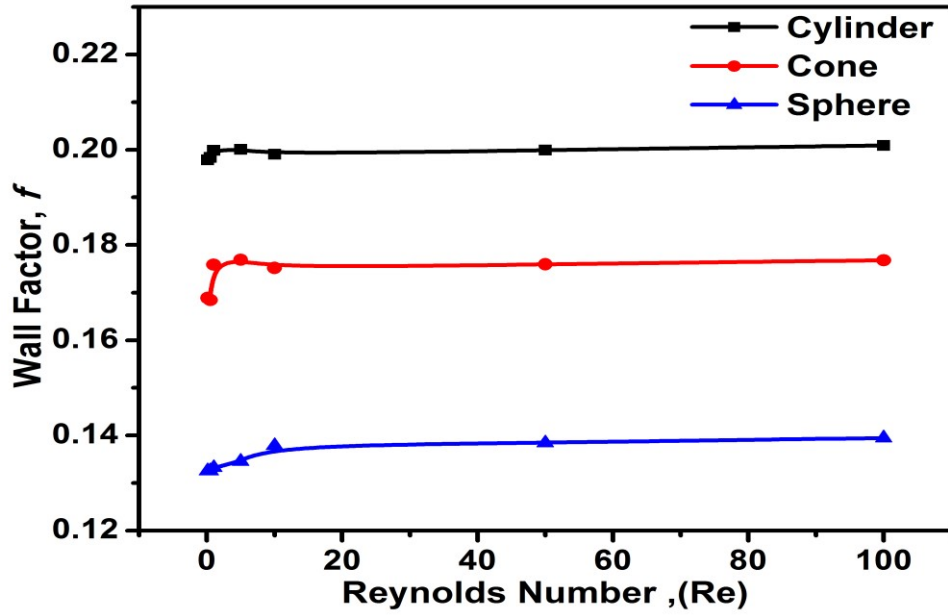
Fig. 6.16. Comparison of wall factors at d/D = 0.8 of cylinder, cone and sphere at different Reynolds number

Fig. 6.17. Contour plot of axial velocity for sphere at d/D = 0.015 and Re = 100
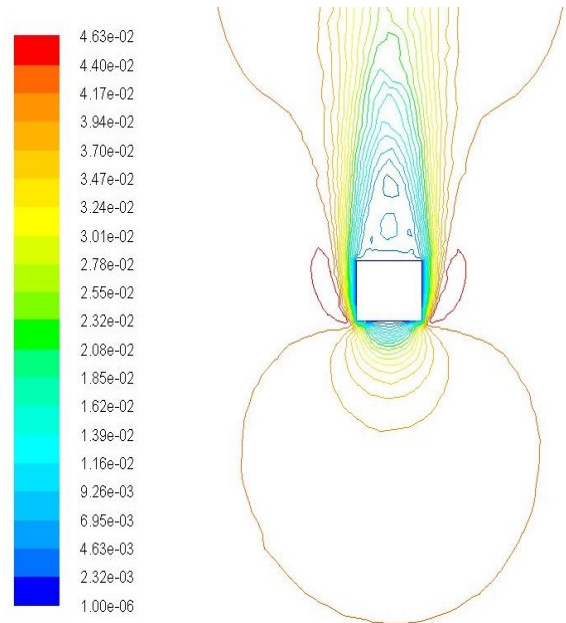
Fig. 6.18. Contour plot of axial velocity for cylinder at d/D = 0.015 and Re = 100
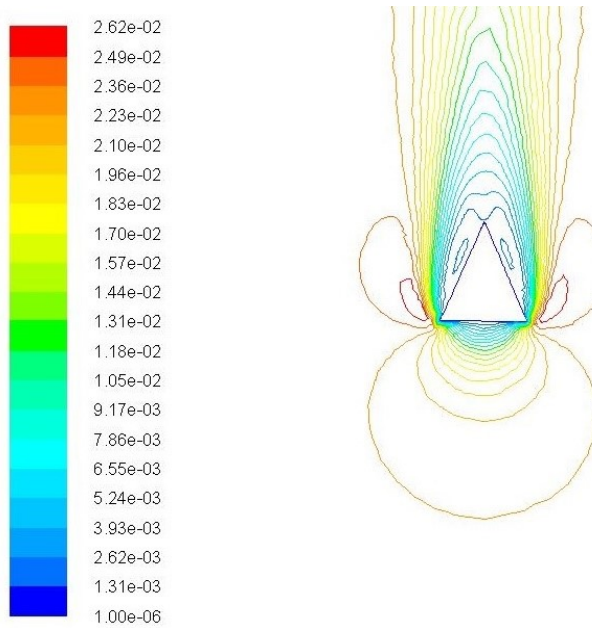
Fig. 6.19. Contour plot of axial velocity for cone 2 at d/D = 0.015 and Re = 100

6.2.6. Re-circulation Length and Angle of Separation

The re-circulation lengths (i.e. the length of the maximum size vortex) for the sphere, cone, and

cylinder at different Reynolds number are compared in Fig. 6.20 for the *d/D* ratio of 0.015, 0.5

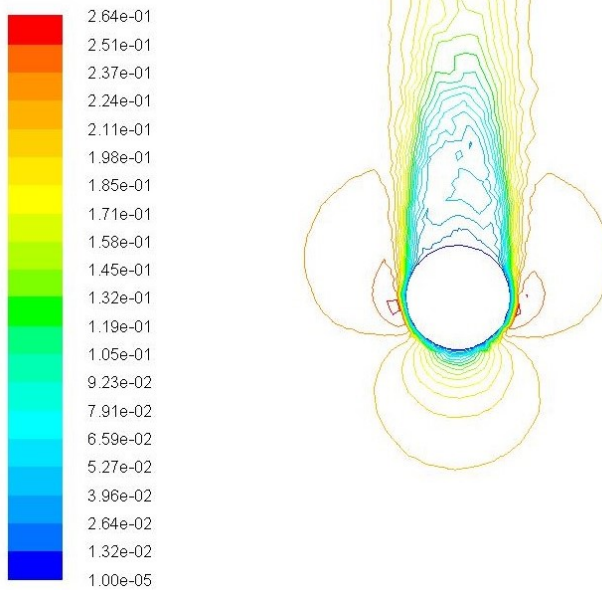and 0.8. As expected, the re-circulation length gradually increases with the Reynolds number due

to comparatively higher inertial force than viscous force. The same observations were reported

by Nitin & Chhabra [11] for a circular disk. The figure shows that the recirculation length

decreases with increasing the *d/D* ratio due to the additional restrictive force from the flow

channel wall on the wake circulation. The figure also depicts that irrespective of the Reynolds

number the order of the re-circulation lengths is sphere > cone > cylinder. The increase of

boundary layer separation with the recirculation length helps to reduce the frictional loss. Thus,

the minimum drag coefficient and wall effect for the sphere, intermediate for cone and the highest for cylinder obtained in the present study are justified.
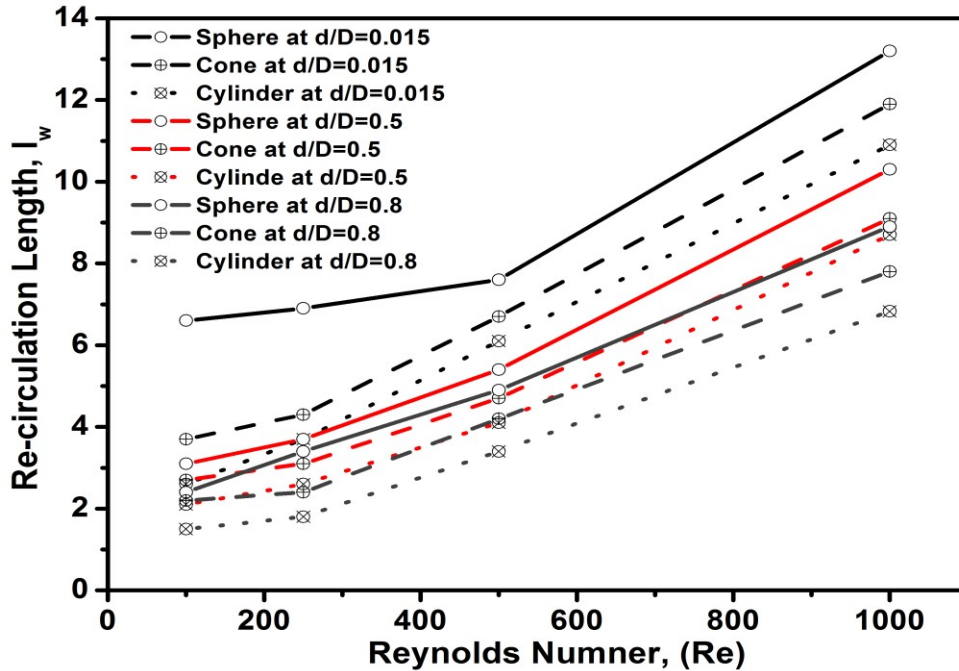
Fig. 6.20. Dependence of Re-circulation lengths on Reynolds number and d/D ratios for sphere, cone

Owing to the possible asymmetry in the flow field, the angles of separation are determined on both the edge 1 and edge 2 of Fig. 6.21. The separation angle with Reynolds number, *Re* at different *d/D* ratios is shown in Fig. 22 and in Table 6.4. These show an exponential decrease of the separation angles on both the edges. At any particular *Re*, a higher separation angle is obtained for higher *d/D* ratio due to delay in separation in the presence of the influence of the wall. In spite of the delay of the separation, the drag coefficient becomes higher for higher *d/D* ratio (Fig. 6.5 and 6.6) due to an increase of the form drag. For the cone, a large decrease of the separation angle occurs due to a small increase of the Reynolds number in its low region, which is unlike of the sphere and cylinder body. It happens due to the sudden change of

the shape of the cone behind the edge 3 as compared to the sphere and cylinder where a smooth

surface transition occurs in the flow direction.
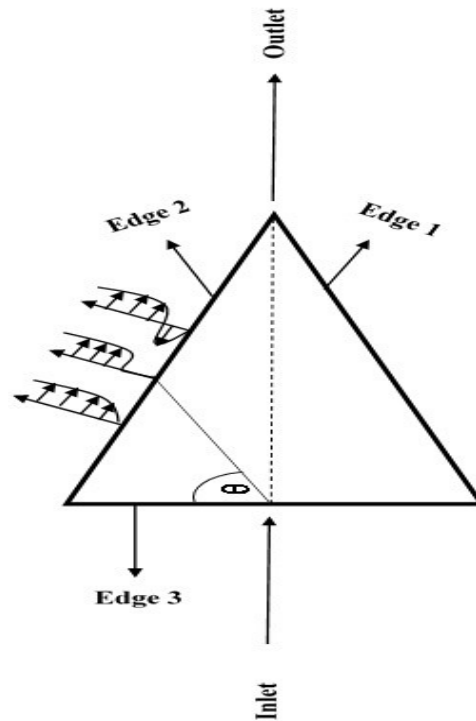
Fig. 6.21. Schematic diagram to display angle of separation

Table 6.4

Angle of separation at different Re for d/D=0.15 and 0.4

Re	d/D=0.4		d/D=0.15	
	Edge-1	Edge-2	Edge-1	Edge-2
70	90	89.997972	80.6786	78.6786
80	17.32	16.14	14.71	10.87
90	18.36	13.6	13.51	10.05
100	11.85	13.23	10.91	8.96
150	9.64	9.53	8.99	8.15
302	12.87	7.83	7.78	7.74
401	12.1	7.54	7.5	6.03
500	7.92	7.45	7.51	5.76
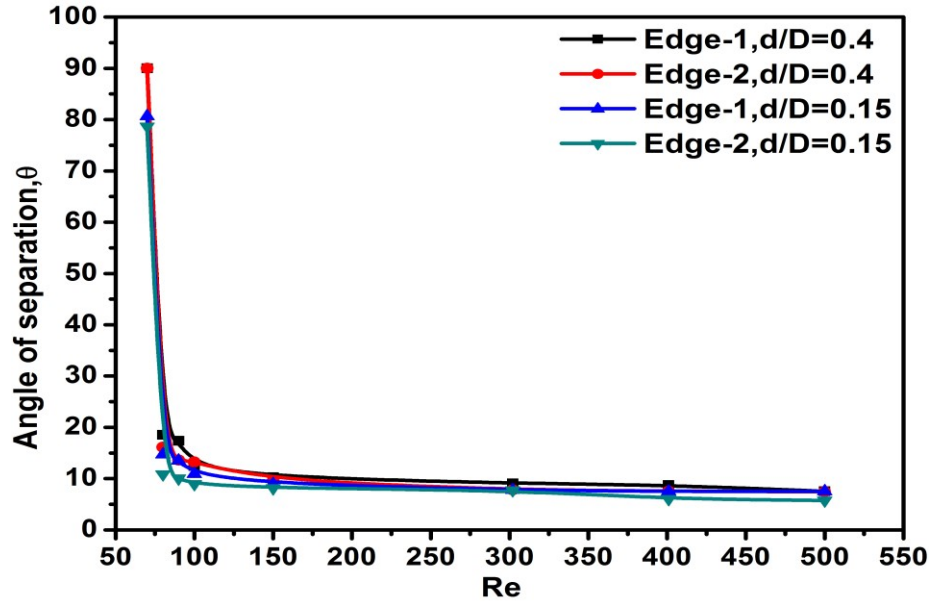
Fig. 6.22. Variation of angle of separation (θ) with Reynolds number for edge 1 &2 at d/D 0.1 and 0.4

6.3.7. Velocity Distribution around Submerged Body

The drag is mostly affected by the hydrodynamics of the flowing fluid especially by the slope of the velocity nearby the submerged body. To understand the effect, the flow direction component velocity is plotted in Fig. 6.23 – 6.27 against the non-dimensional radial distance. The radial distance is taken between the flow channel wall and the vertex of the edge 3 of the cone/the surface of the sphere and cylinder. The Reynolds number is used as the parameter. The Fig. 6.23- 6.25 include the radial velocity distributions individually for the cone, cylinder, and sphere respectively. The relative comparison among the velocity distributions is made in Fig. 6.26 and 6.27 at low and high Reynolds number. The figures show that the velocity gradient nearby cone/sphere/cylinder surface is higher at higher Reynolds number. This occurs due to a decrease of the boundary layer thickness with *Re*. Even with higher velocity gradient, the drag coefficient decreases with Re due to a substantial increase of inertial force as compared to the wall shear

91

stress, and also as seen in the figure more amount fluid is affected and put resistance to the movement of the solid body. The profile is a function of the shape of the submerged object at low Reynolds number; the dependency reduces gradually until it becomes invariant of Re of higher magnitude. The observed order of drag coefficient in Fig. 6.26 and 6.27 i.e. cylinder > cone > sphere follows the similar explanations given for Fig. 6.23 – 6.25.
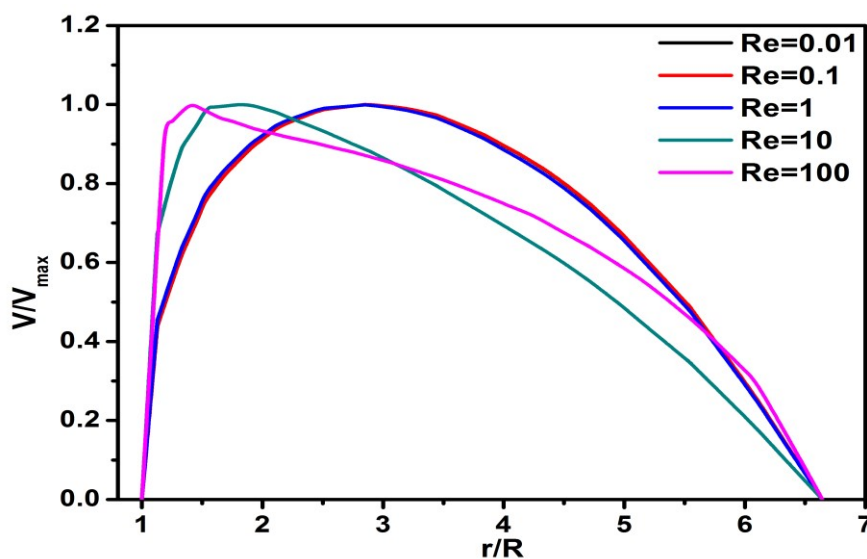
Fig. 6.23. Effect of Reynolds number on the velocity profiles for cone2 at d/D = 0.15
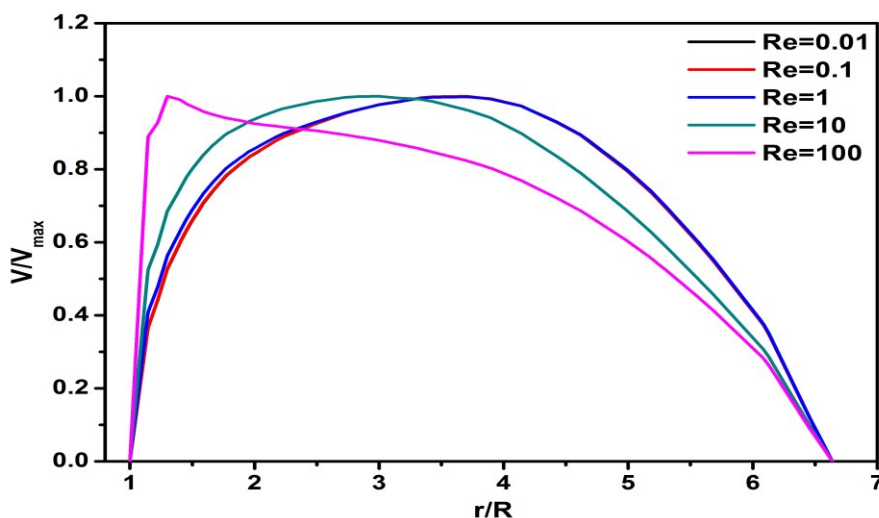
Fig. 6.24. Effect of Reynolds number on the velocity profiles for cylinder at d/D = 0.15
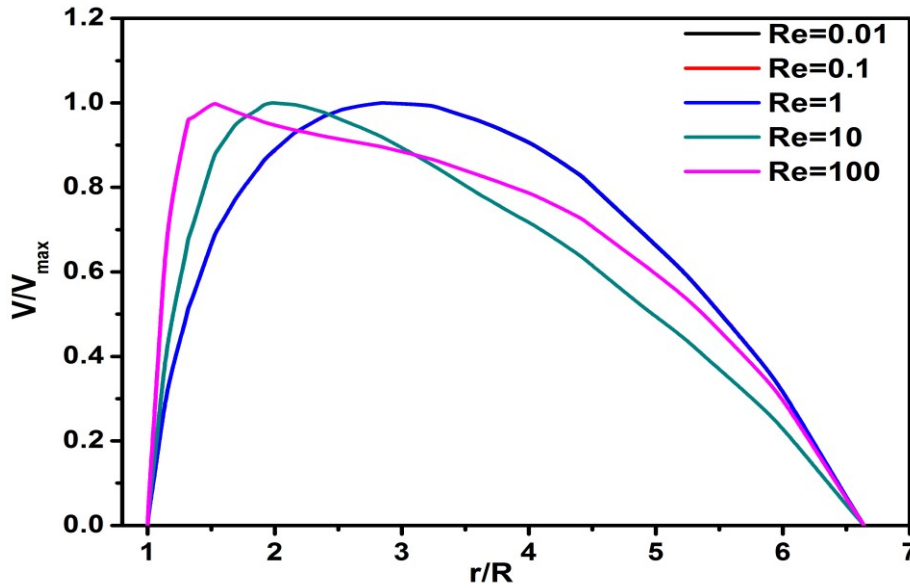
Fig. 6.25. Effect of Reynolds number on the velocity profiles for sphere at d/D = 0.15
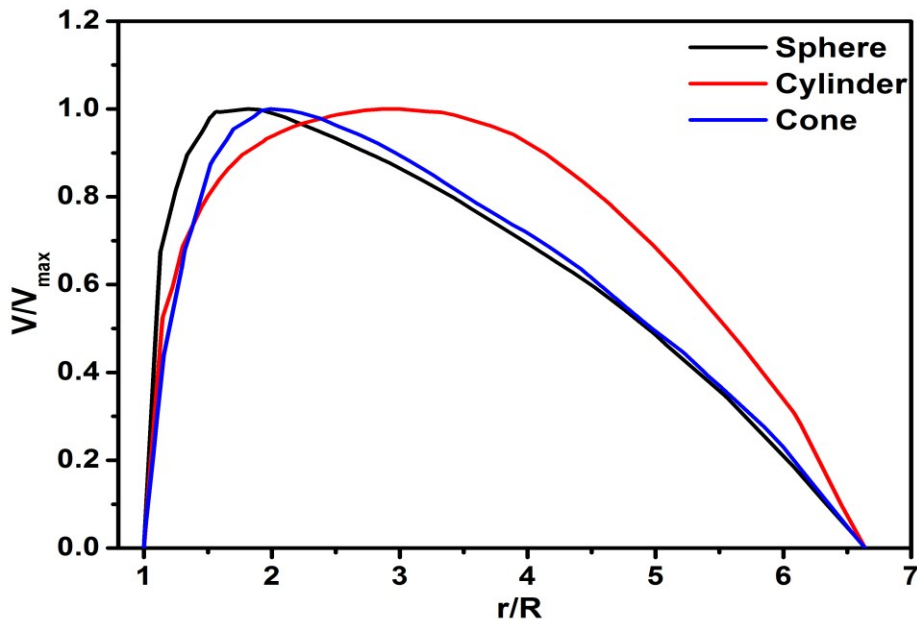
Fig. 6.26. Comparison of velocity profiles of cone, cylinder and sphere at Re = 10 and d/D = 0.15
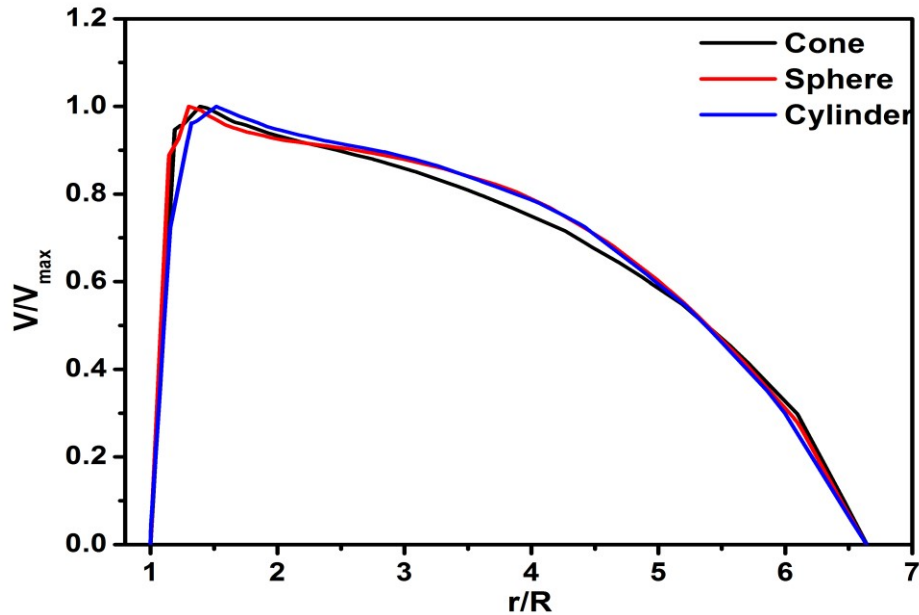
Fig. 6.27. Comparison of velocity profiles of cone, cylinder and sphere at Re=100 and d/D=0.15

The effect of *d/D* ratio on the radial distribution of the velocity profiles of the cone at low and high Reynolds number are depicted in Fig. 6.28 and 6.29. The velocity gradients both at the cone and flow channel wall surface shown in Fig. 6.28 at *Re* = 0.01 increases with the *d/D* ratio. Thus the viscous force acting on the surfaces increases simultaneously with the *d/D*. It is responsible for the delay in the boundary wall separation and to produce the higher drag coefficient at higher blockage ratio. The gradient eventually approaches a *d/D* ratio independent value at higher Reynolds number shown in Fig. 6.29. The viscous drag coefficient, therefore, becomes independent of the *d/D* at higher Reynolds number.
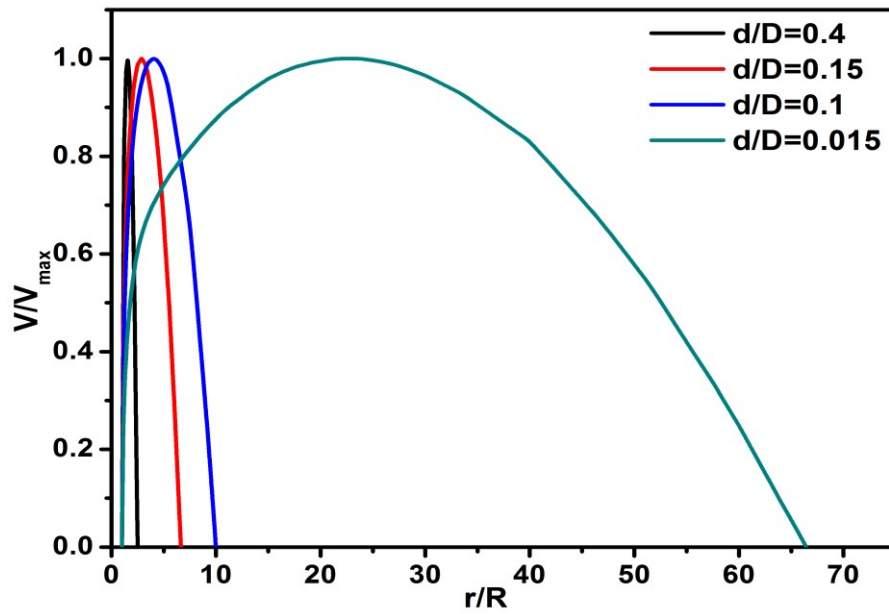
Fig. 6.28. Effect of diameter ratio on the radial distributions of the velocity profiles for cone at Re = 0.01
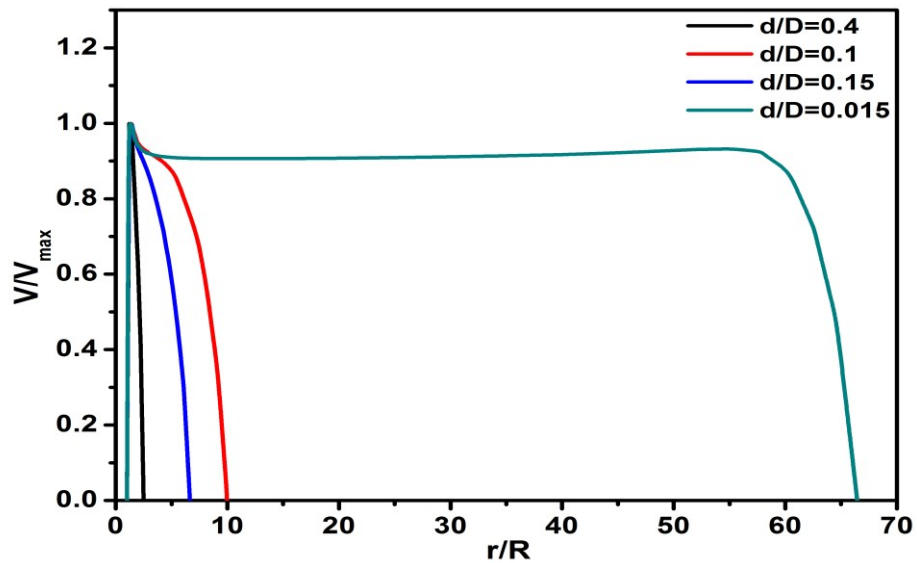
Fig. 6.29. Effect of diameter ratio on the radial distributions of the velocity profiles for cone at Re = 100

6.3. Numerical Study of Drag Coefficient for Newtonian Fluid Flow over Cone-To-Cylinder Body

Literature review in Chapter 2 reveals that, the flow behavior study around the solid geometry under the transition from a conical to cylinder shape has not been studied either experimentally or theoretically. The present study encompasses the effect of Reynolds number and the ratio of top radius to bottom radius of the cone (r/R) on the drag coefficients using computational fluid dynamics (CFD) tools. The radius ratio, r/R for the cone is zero, and it increases gradually to 1.0 for the circular cylinder. The unbounded drag coefficient is calculated and analyzed in the current study. The effect of the interactions between the solid body and fluid medium on the drag coefficient is investigated with the help of velocity contour plots. The schematic diagram and meshed geometries are shown in Fig. 6.30.

(A)   (B)   (C)   (D)
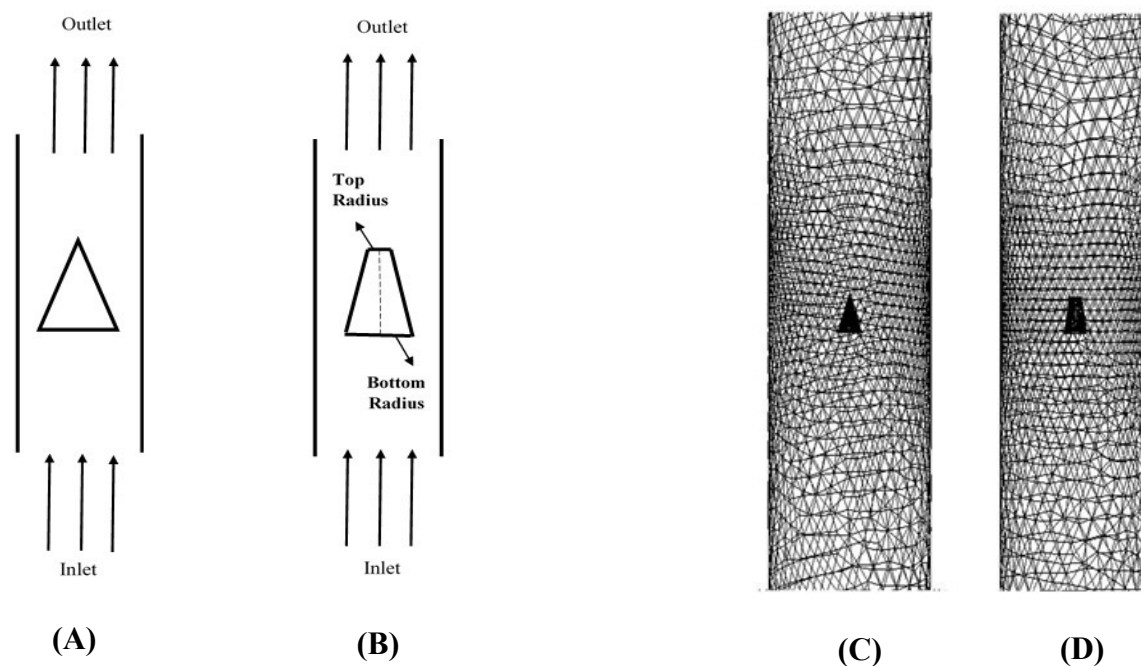
Fig. 6.30. The schematic representation of flow over conical object of (A) r/R=0 and (B) r/R>0, (C) and (D) are the generalized view of generated mesh for (A) and (B) respectively.

6.3.1. Effects of Radius Ratio, r/R on the Drag Coefficient

The radius ratio, r/R gradually changes from 0.0 for the cone to 1.0 for the circular cylindrical body. Ten different radius ratios i.e. 0.06, 0.13, 0.26, 0.39, 0.46, 0.53, 0.66, 0.73, 0.86 and 0.99 are chosen to study the changes of drag coefficient in the transition of cone to cylinder geometry at different Reynolds number for 40% CS. The mutual impacts of both *Re* and *r/R* on drag coefficient are shown in Fig. 6.31. No effective changes in drag coefficients are seen till $r/R \leq 0.13$, but it gradually increases for higher *r/R* ratios. The trend of the C_D-*Re* relationship is the same to the reported trends in Uhlherr and Chhabra [6] for sphere in Newtonian flow media. The drag coefficient is observed to increase with the increase in the top to bottom radius ratio. It occurs due to increase in the resistance to fluid flow with the radius ratio.
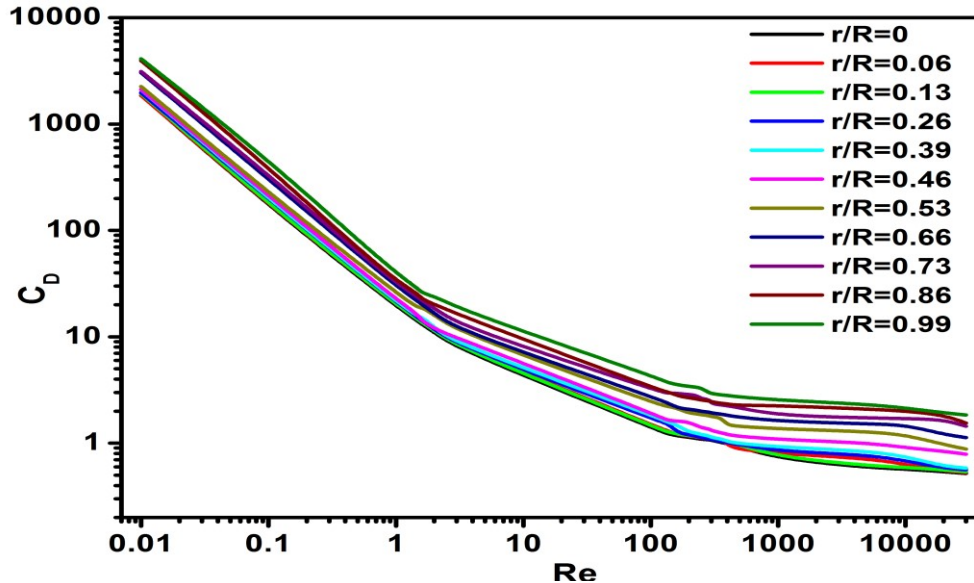
Fig. 6.31. Drag coefficient against Reynolds number plot for cone 2 at different radius ratio (*r/R*) in 40% CS.

6.3.2. Radius Ratio (r/R) Effect on Velocity Magnitude Distribution (Contour) Plot

The axial velocity contour plots at Re 0.01 and 100 are shown in Figures 6.32, 6.33 and 6.34 for the *r/R* 0.00, 0.26 and 0.66. The surface area of the solid body increases with increasing the *r/R*. The larger surface area at higher *r/R* thus creates larger viscous drag. The contours of velocity distributions for all *r/R* at low Reynolds number are symmetric, and no separation is observed in downstream flow for the pure cone. However, as the top radius increases, the flow produces a greater vortex in the downstream, and thus, the increase of the pressure drop with *r/R* ratio increases the drag coefficient even at very low Reynolds number. The same observations are also made at higher Reynolds number. The drag coefficient, therefore, increases with *r/R* ratio.

(A)   **(B)**
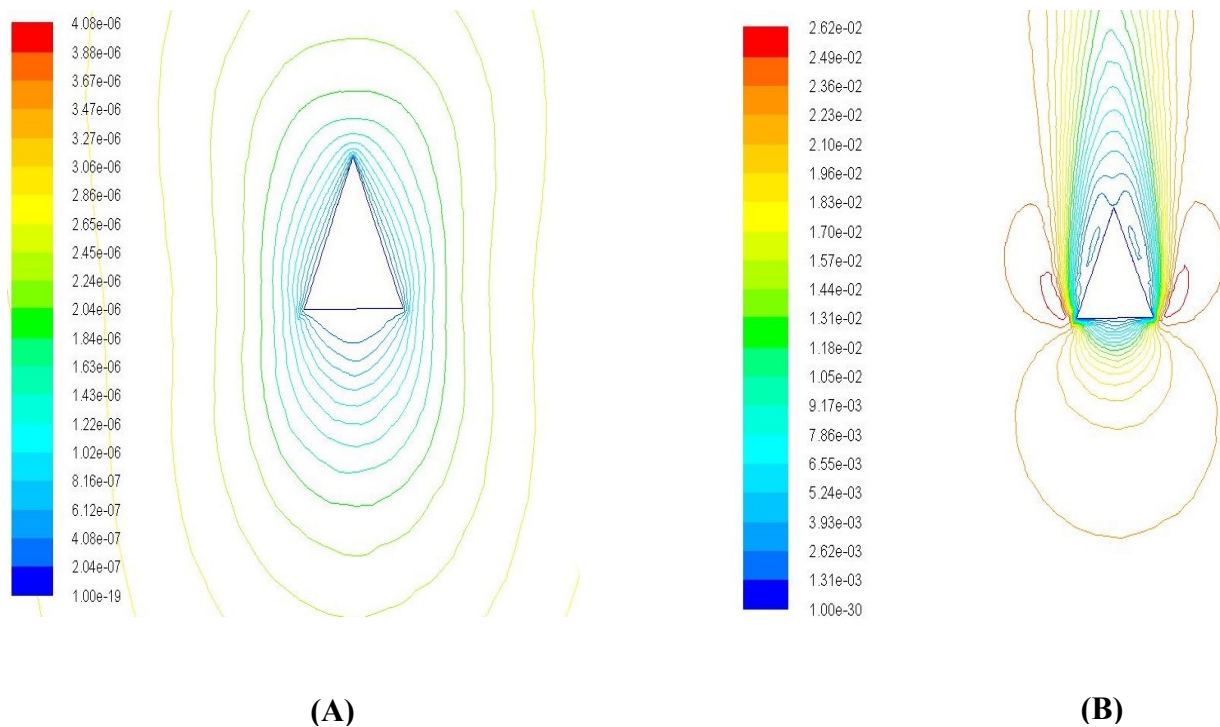
Fig. 6.32 Velocity contour plot for (A) Re = 0.01 and (B) Re = 100 at r/R = 0

(A)

(B)

Fig. 6.33. Velocity contour plot for (A) Re = 0.01 and (B) Re = 100 at r/R = 0.26

(A)

(B)
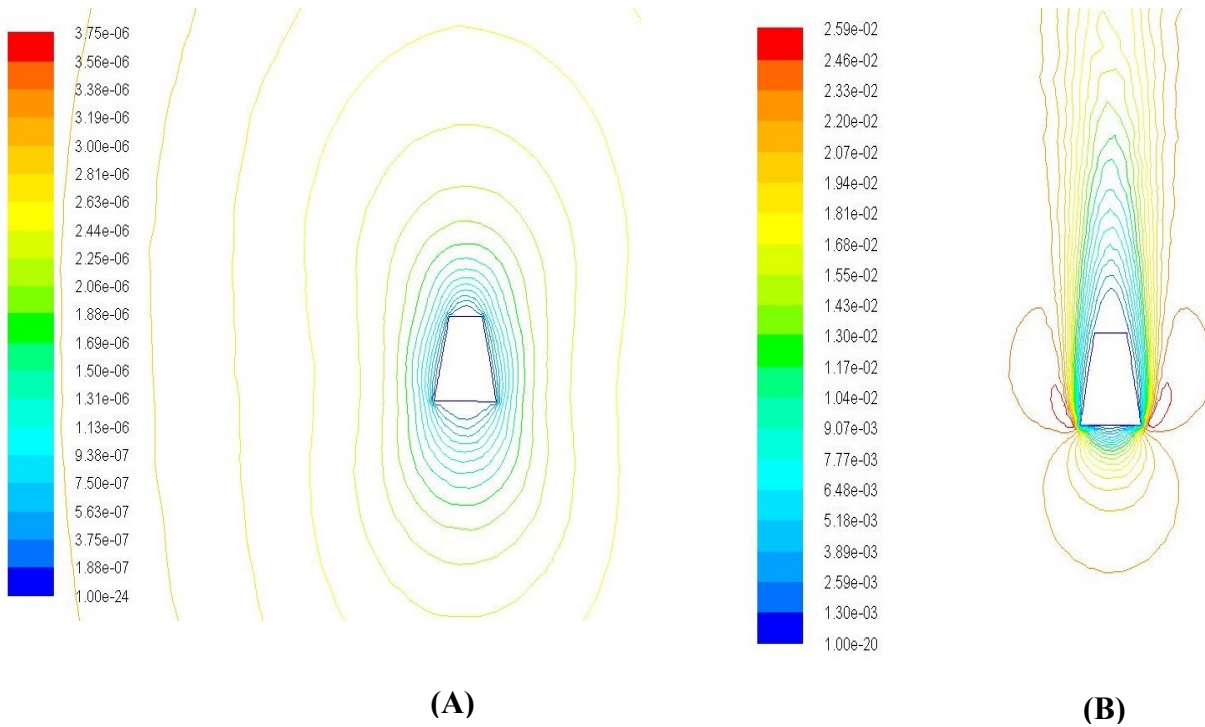
Fig. 6.34. Velocity contour plot for (A) Re = 0.01 and (B) Re = 100 at r/R = 0.66

6.4. Conclusion

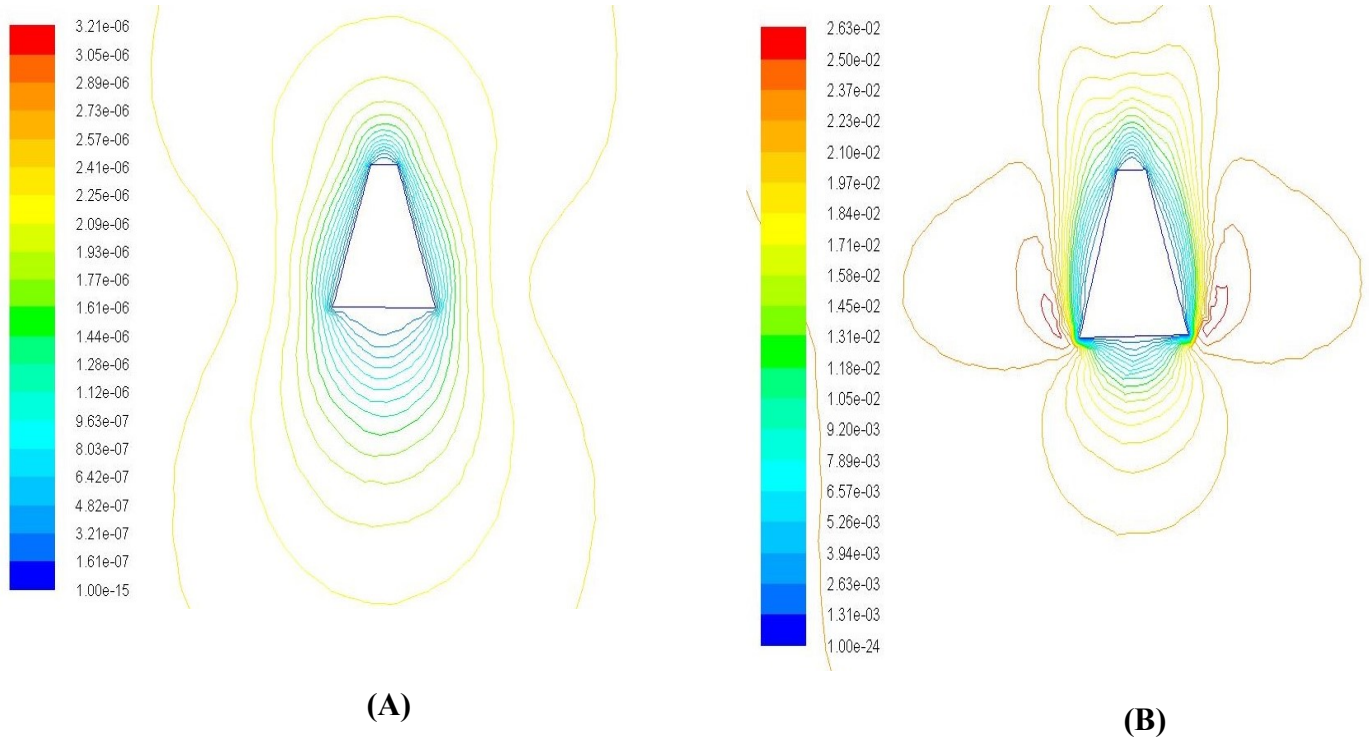The three-dimensional CFD simulations were executed to examine the impact of Reynolds number and diameter ratio on the drag coefficient and wall factor of the cone. The drag coefficient is increased with increasing the diameter ratio; the impact was found more in low Reynolds number region than high. The experimental wall factor (acquired from experimental settling velocity available in the open literature) and computed wall factors in the present study were observed in excellent matching. The relation is given by Eq. (2.2), proposed by Ullher and Chhabra [6] was satisfied by the current computed C_D-Re data for the cone. Like sphere and cylinder, a decreasing trend of the wall factor with the blockage ratio was observed for a cone. The comparative study showed the order of the wall factor as cylinder > cone > circle. The velocity gradients at the surface of the drag bodies were invariant with the Reynolds number at its high values. The estimated recirculation length increased with the Reynolds number and obtained as the highest for the sphere, intermediate for cone and the lowest for the cylinder. It was increased with decreasing the blockage ratio. The angle of separation at various Re on the opposite edges of the cone for d/D = 0.1 and 0.4 were evaluated. The angle of separation is increased with increasing *d/D* ratio due to delay in boundary layer separation at higher blockage ratio. The reported velocity profiles at various Re and *d/D* ratio for the cone, circle, and cylinder showed that the slope of velocity curve increased with both Re and *d/D*.

The variation of drag coefficient under the transition of cone geometry to the cylinder geometry i.e. the theoretical analysis and C_D-Re relationship for the taper-shaped object (0<*r/R*<1) were discussed. The drag coefficient values were gradually increased with the *r/R* ratio due to an additional opposing force applied by the top surface on the downstream flow. The

development and distribution of velocity contour plots around the solid object were found, and

the effects of the Reynolds number and radius ratio on the drag coefficients were explained.

CHAPTER 7

CONCLUSION AND FUTURE SCOPE

Conclusions

Flow past an object (may be solid or hollow) is subject of intense research since many decades. Extensive application of this study in industries encounters a wealth of published article, where experimental, physical and analytical findings were accorded for various flow circumstances. However, as said in Chapter 1, while discussing the origin of the work, some critical issues were never addressed before our work. It is believed that much work should require filling the gaps in the literature. Henceforth, to cater the issues, experimental and theoretical studies are executed. The overall conclusion of this study is texted below.

In Chapter 3, the terminal velocity and drag coefficient of the spherical particle are discussed for a wide range of diameter ratio and angle of inclination. The following conclusions are made from this study.

- The terminal velocity of the falling sphere trend was increased with increasing the d/D ratio of the sphere and flow channel. The increasing trend is just opposite of the decreasing trend the drag coefficient of the sphere with increasing the d/D ratio.

- The terminal velocity was increased with increasing the angle of inclination due to increasing the downward body force with the flow channel inclination.

- The estimated diameter of the sphere for zero terminal velocity showed dependency on both θ and d/D ratio.

- The drag experienced by the sphere for the inclined channel was represented by the drag coefficient, which was estimated for $0.08 \leq Re \leq 5504$, $0.09 \leq d/D \leq 0.37$ and $10^o \leq \theta \leq 90^o$.

- The C_D values were higher for a lower angle of inclination.

- Appropriate prediction equations for C_D as a function of Re, d/D and θ were developed by the least square method.

- The product of $C_D Re$ showed its dependency on both the angle of inclination and fluid viscosity. It showed a declining trend with the viscosity of solution.

- The linear variation of C_D with $1/Re$ showed the collected experimental data are in laminar and early transition flow regions.

- Reynolds Stress Model (RSM) predicts the experimental drag coefficient with good accuracy for both vertical and inclined plane consideration.+

Based on the experimental analysis of flow over hollow frustum in Newtonian flow media for both vertical and inclined plane, the following observations are made.

- At any particular *di/do*, the terminal velocity has been increased monotonically with the ratio of the frustum outer diameter and channel diameter, *do/D*. The increasing trend is just opposite of the decreasing trend of the drag coefficient of the regular shaped solid particles.

- The terminal velocity of the hollow frustum has been increased with decreasing the *di/do* ratio, for a constant *do/D*.

- The terminal velocity of the frustum has also been increased due to increasing the downward body force with increasing the angle of inclination.

- The drag experienced by the hollow frustum for the inclined channel has been reported in the form of the drag coefficient, C_D estimated for $0.13 \leq Re \leq 8.41, 0.19 \leq d_o/D \leq 0.33, \ 0.22 \leq d_i/d_o \leq 0.83$ and $40^o \leq \theta \leq 90^o$.

- The C_D values have shown increasing trend with decreasing the angle of inclination of the channel.

- The appropriate predictive correlation for C_D as a function of *Re*, *di/do, do/D* and *θ* has been developed using the least square method.

- The angle of inclination and fluid viscosity sensitive $C_D Re$ term has shown a declining trend with the *do/D* ratio.

- The variation of C_D with 1/*Re* has shown linear variation at lower angles of inclinations.

In Chapter 5, the flow over hollow cylinder is discussed for terminal velocity and drag coefficient in the vertical and inclined plane. The followings are concluded from the study.

- The terminal velocity, *V* of the hollow cylinder increases with decreasing *di/do*.

- The increasing trend of *V* with *do/D* ratio for the hollow cylinder is opposite of the trend obtained for cone and cylinder object.

- Owing to increase of the downward body force component, the hollow cylinder terminal velocity increases with increasing the angle of inclination, *θ*.

- The drag coefficient of the hollow cylinder decreases linearly with *Re*, which agrees with the trend of the other regular shaped object available in the open literature.

- This study confirms the lesser effect of *di/do* and *do/D* on C_D, for the scope of $0.19 \leq di/do \leq 0.33$ and $0.22 \leq do/D \leq 0.83$ than Reynolds number.

- The product of C_D and *Re* decreases with the viscosity of the working liquids and increases with the angle of inclination.

- The linear C_D vs. *1/Re* plot confirms the expected trend in the laminar flow state.

- The Reynolds Stress Model available in Ansys Fluent predicts excellently the drag coefficient for both the vertical and inclined flow channels.

In Chapter 6, the numerical analysis of flow over conical particle is studied, and the comparison of flow parameters are made among sphere, cylinder, and cone. In addition to this, the variation of drag coefficient for transition of solid geometry from cone to cylinder also studied.The conclusions are

- The drag coefficient is increased with increasing the diameter ratio; the impact was found more in low Reynolds number region than high.

- The experimental wall factor (acquired from experimental settling velocity available in the open literature) and computed wall factors in the present study were observed in excellent matching.

- The relation is given in Eq. (2.2), proposed by Ullher and Chhabra [15] was satisfied by the current computed C_D-*Re* data for the cone. Like sphere and cylinder, a decreasing trend of the wall factor with the blockage ratio was observed for a cone.

- The comparative study showed the order of the wall factor as cylinder > cone > circle. The velocity gradients at the surface of the drag bodies were invariant with the Reynolds number at its high values.

- The estimated recirculation length increased with the Reynolds number and obtained as the highest for the sphere, intermediate for cone and the lowest for the cylinder. It was increased with decreasing the blockage ratio.

- The angle of separation at various *Re* on the opposite edges of the cone for d/D = 0.1 and 0.4 were evaluated. The angle of separation is increased with increasing *d/D* ratio due to

105

delay in boundary layer separation at higher blockage ratio. The reported velocity profiles at various *Re* and *d/D* ratio for the cone, circle, and cylinder showed that the slope of velocity curve increased with both *Re* and *d/D*.

- The variation of drag coefficient under the transition of cone geometry to the cylinder geometry i.e. the theoretical analysis and C_D-*Re* relationship for the taper-shaped object (0<*r/R*<1) were discussed.

- The drag coefficient values were gradually increased with the *r/R* ratio due to an additional opposing force applied by the top surface on the downstream flow. The development and distribution of velocity contour plots around the solid object were found, and the effects of the Reynolds number and radius ratio on the drag coefficients were explained.

7.1. Future Scope

- Only Newtonian fluid are taken here as working fluid for all the study. Hence this work can be extended for other characteristic fluid i.e. power-law fluid.

- The detail numerical analysis for flow parameters i.e. separation angle, velocity profile and re-circulation length of flow over the sphere, hollow cylinder and frustum can be studied.

- This work can be covered for other hollow object.

References

[1]   R. Clift, J.R. Grace, M.E. Weber, Bubbles, Drops and particles, Academic Press, New York, 1978.

[2]   https://www.coursehero.com/file/7883262/Reynolds-Number-and-Drag

[3]   https://en.wikipedia.org/wiki/Drag_coefficient

[4]   R. P Chhabra, Bubbles, Drops and Particles in Non-Newtonian Fluids, CRC Press, Boca Raton, FL, 1993.

[5]   A.R. Khan, J.F. Richardson, The resistance to motion of a solid sphere in a fluid, Chem. Eng. Commun.62 (1987) 135–150.

[6]   P. H. T. Uhlherr and R.P. Chhabra, Wall effect for the fall of spheres in cylindrical tubes at high Reynolds number, Can. J. Chem. Eng.73 (1995) 918-923.

[7]   A. Unnikrishnan and R.P. Chhabra, An experimental study of motion of cylinders in Newtonian fluids: wall effects and drag coefficient, Can. J. Chem. Eng.69 (1991) 729-735.

[8]   A. Unnikrishnan and R. P. Chhabra, Slow Parallel Motion of Cylinders in Non-Newtonian Media: Wall Effects and Drag Coefficient, Chem. Eng. Process.28 (1990)121-125.

[9]   S. Krishnan and A. Kaman, Effect of Blockage Ratio on Drag and Heat Transfer from Centrally Located Sphere in Pipe Flow, Eng. App. of Comp. Fluid Mech.4:3 (2010) 396-414.

[10]   J. Chakraborty, N. Verma, R.P. Chhabra, Wall effects in flow past a circular cylinder in a plane channel: a numerical study, Chem. Eng. Process.43 (2004) 1529–1537.

[11] S. Nitin and R. P. Chhabra, Wall Effects in Two-Dimensional Axisymmetric Flow Over a Circular Disk Oriented Normal to Flow in a Cylindrical Tube, Can. J. Chem. Eng.83 (2005) 450-457.

[12] B. Munshi, R. P. Chhabra and P. S. Ghoshdastidar, A numerical study of steady incompressible Newtonian fluid flow over a disk at moderate Reynolds numbers, Can. J. Chem. Eng.77 (1999) 113–118.

[13] R.P. Chhabra, Wall effects on free-settling velocity of non-spherical particles in viscous media in cylindrical tubes, Powder Technol.85 (1995) 83-90.

[14] M. K. Sharma and R. P. Chhabra, An experimental study of free fall of cones in Newtonian and non-Newtonian media: drag coefficient and wall effects, Chem. Eng. Process.30 (1991) 61-67.

[15] J. J Carty, C.C. Hox, Wall Effect on Drag in Inclined Plane, Amer. J. of Chem. Eng. (1978) 49-57.

[16] R. J. Garde, S .Sethuraman, Variation of the drag coefficient of a sphere rolling along a boundary, La Houille Blanche 7 (1967) 727-732.

[17] C.D. Jan, J.C. Chen, Movements of a sphere rolling down an inclined plane, J. of. Hydraulic Res. 35 (5) (1997) 689–706.

[18] R.P. Chhabra, J.M. Ferreira, An analytical study of the motion of a sphere rolling down a smooth inclined plane in an incompressible Newtonian fluid, Powder Technol. 104 (1999) 130–138.

[19] R.P. Chhabra, J.M. Ferreira, An analytical study of the motion of a sphere rolling down a smooth inclined plane in an incompressible Newtonian fluid, Powder Technol. 104 (1999) 130–138.

[20] M. Jalaal , D.D. Ganji, An analytical study on motion of a sphere rolling down an inclined plane submerged in a Newtonian fluid, Powder Technol. 198 (2010) 82–92.

[21] N.S Cheng , Comparison of formulas for drag coefficient and settling velocity of spherical particles , Powder Technology, (2009) 395–398.

[22] P.P. Brown and D.F. Lawler, "Sphere drag and settling velocity revisited", Journal of Environmental Engineering, 129 (3) (2003) 222–231

[23] R.L.C. Flemmer, C.L. Banks, On the drag coefficient of a sphere, Powder Technology, 48 (1986) 217–221.

[24]   R. Turton, O. Levenspiel, A short note on the drag correlation of spheres, Powder Technology, 47 (1986) 83–86.

[25] F. Engelund, E. Hansen, Monograph on Sediment Transport in Alluvial Streams, Monograpsh Denmark Technical University, Hydraulic Lab, Denmark, 1967.

[26] R. Clift, W.H. Gauvin, The motion of particles in turbulent gas streams, Proc. Chemeca, 70, 1970, pp. 14–28.

[27] S. Singha, K.P. Sinhamahapatra, Flow past a circular cylinder between parallel walls at low Reynolds numbers, Ocean Eng.37 (2010) 757–769.

[28] R.P. Chhabra, S. Agarwal and K. Chaudhary, A note on wall effect on the terminal falling velocity of a sphere in quiescent Newtonian media in cylindrical tubes, Powder Technol.129 (2003) 53–58.

[29] R.P. Chhabra, C. Tiu and P.H.T. Uhlherr, A study of wall effects on the motion of a sphere in viscoelastic fluids, Can. J. Chem. Eng.59 (I981) 771-775.

[30]   D.D. Atapattu, R.P. Chhabra and P.H.T. Uhlherr, Wall effect for spheres falling at small Reynolds number in a viscoplastic medium, J. Non-Newtonian Fluid Mech.38 (1990) 31-42.

[31]   K. H. Dewsbury, A. Tzounakos, D.G. Karamanev and A. Margaritis, Wall Effects for the Free Rise of Solid Spheres in Moderately Viscous Liquids, Can. J. Chem. Eng.80 (2002) 974-978.

[32]   A. Unnikrishnan and R. P. Chhabra, Slow Parallel Motion of Cylinders in Non-Newtonian Media: Wall Effects and Drag Coefficient, Chem. Eng. Process.28 (1990)121-125.

[33]   P.Y. Huang, J. Feng, Wall effects on the flow of viscoelastic fluids around a circular cylinder, J. Non-Newtonian Fluid Mech.60 (1995) 179-198.

[34]   J.F. Stalnaker and R.G. Hussey, Wall effect on cylinder drag at low Reynolds number, Phy. of Fluid.22 (1979) 603-613.

[35]   C. D. Jan, H. W. Shen, Drag coefficients for a sphere rolling down an inclined channel, J. of Chin. Inst. of Eng.18 (4) (1995) 493-507.

[36]   C. Oseen, Hydrodynamik, Chapter 10, Akademische Verlagsgesellschaft, Leipzig, 1927.

[37]   N. Lyotard, W.L. Shew, L. Bocquet, J.-F. Pinton, Polymer and surface roughness effects on the drag crisis for falling spheres, Eur. Phys. J. B. 60 (2007) 469–476.

[38]   B.A.Toms , Some observations on the flow of linear polymer solutions through straight tubes at large Reynolds numbers, Proc. of 1st Int. Cong. in Rheology, 2 (1949) 135-141.

[39]   J.L. Lumley, Drag reduction by additives, Annu. Rev. Fluid. Mech., 1 (1) (1969) 367-384.

[40]   J. Drappier, T. Divoux, Y. Amarouchene, F. Bertrand, S. Rodts, O.Cadot, Turbulent drag reduction by surfactants, Euro. Phys. Lett. 74-2 (2006) 362–368.

[41]   M. Vlachogiannis, T. J. Hanratty, Influence of wavy structured surfaces and large scale

polymer structures on drag reduction, Exp. in Fluids, 36 (2004) 685-700.

[42]   Khadom.A, Ali A., Performance of polyacrylamide as drag reduction polymer of crude petroleum flow, Ain Shams Engineering Journal, (2014) 212-218.

[43]   M. Tian, B. Fang, L. Jin, Y. Lu, X. Qiu, H. Jin, K. Li, Rheological and drag reduction properties of hydroxypropyl xanthan gum solutions, Powder Technology, (2015) 16-22.

[44]   M.A. Hasan, Wall effects on the motion of a rolling sphere in a closely fitting tube, Chem. Eng. Journal, 33 (1986) 97 – 101.

CURRICULUM VITAE

Saroj Kumar Samantaray

Email: samantaray.sarojkumar@gmail.com

Phone: +91 9776095394

Educational Qualifications

- **Master of Technology** in Chemical Engineering, National Institute of Technology Rourkela, India, (CGPA: 9.07 (Scale on 10)) Dissertation submitted – April 2017.

- **Bachelor of Engineering** in Plastic Engineering, Central Institute of Plastics Engineering and Technology Bhubaneswar, India (CGPA: 7.67 (Scale on 10)).

Research Publications:

1. **S. K. Samantaray**, S.N. Makitaya, S. S. Mohapatra and B. Munshi, Wall Effect on the Terminal Velocity and Drag Coefficient for the Newtonian Flow over a Sphere in Inclined Plane: A Reverse Trend, Powder Technology, Manuscript No: POWTEC-D-17-00300, (Under Review)

2. **S. K. Samantaray**, S. S. Mohapatra and B. Munshi, Newtonian Flow past a Hollow Frustum in Vertical and Inclined Plane: An Experimental Observation for Terminal Velocity and Drag Coefficient, Powder Technology, Manuscript No: POWTEC-D-17-00931, (Under Review)

3. **S. K. Samantaray**, S. S. Mohapatra and B. Munshi, Experimental Findings and Analysis of Terminal Velocity and Drag Coefficient of Hollow Cylinder in Vertical and Inclined Channel, Advanced Powder Technology, Manuscript No: CHERD-D-17-00490. (Under Review)

4. **S. K. Samantaray**, S. S. Mohapatra and B. Munshi ,Numerical Study of Drag Coefficient for Newtonian Fluid Flow over Cone-To-Cylinder Body, Alexandria Journal of Engineering (Elsevier), Manuscript No: AEJ-D-17-00525, (Under Review)

5. **S. K. Samantaray**, S. S. Mohapatra and B. Munshi ,Prediction of Drag Coefficient of spherical particle using ANN, ANFIS, Regression and GA Optimization, International Journal of Chemical Sciences, Manuscript No:293,(Accepted)

6. **S. K. Samantaray**, S. S. Mohapatra and B. Munshi ,A Numerical Study of the Wall Effects for Newtonian Fluid Flow over a Cone, Engineering Science and Technology , an International Journal, Manuscript No: JESTCH_2017_625,(Revision under preparation)

7.